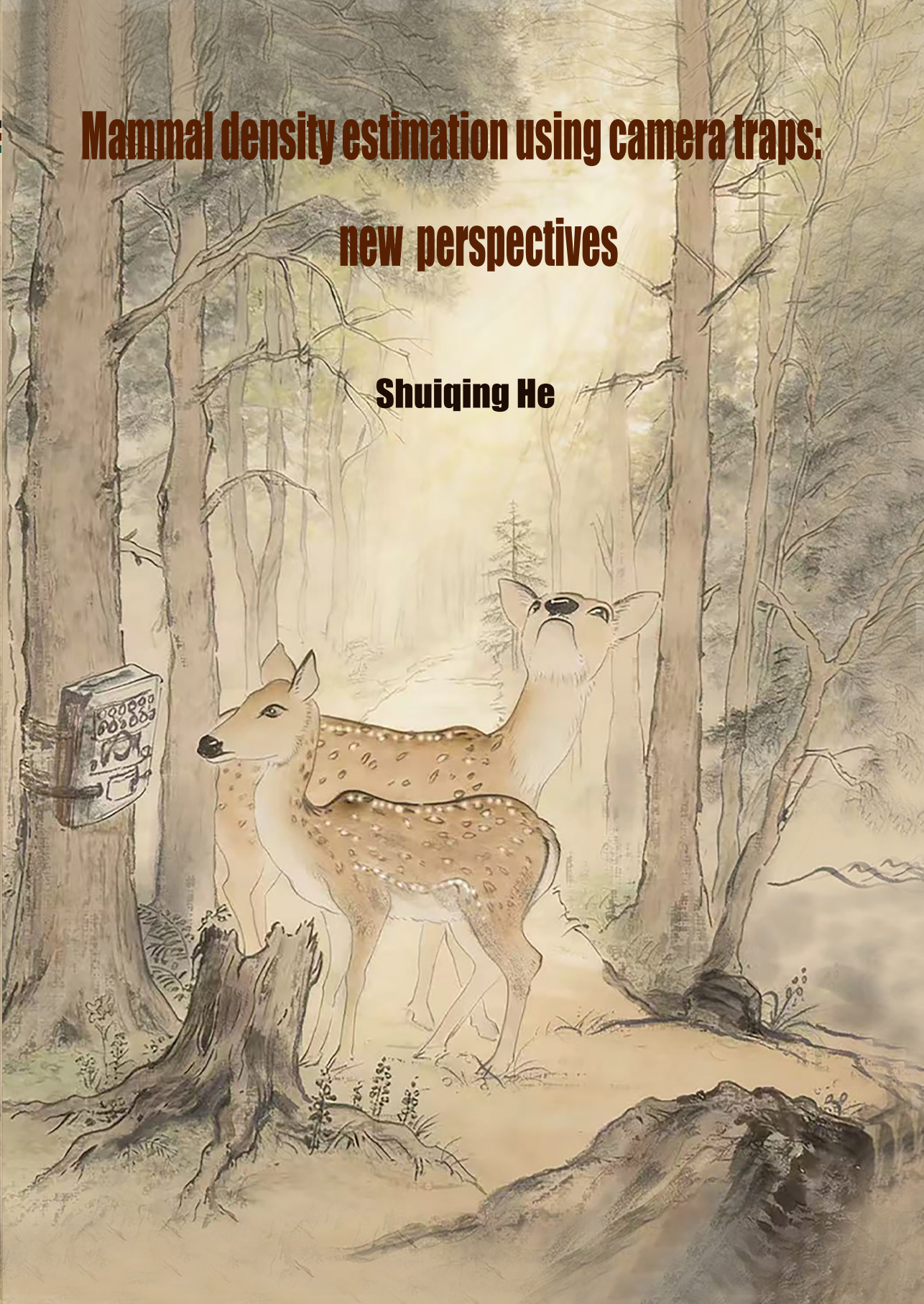
Mammal density estimation using camera traps: new perspectives

Shuiqing He



PROPOSITIONS

1. Independent reference densities used for validation bias assessments of wildlife density estimation methods.
(this thesis)

2. The scientific value of vertical camera trapping for wildlife monitoring is underestimated.
(this thesis)

3. Scientific progress is driven by cumulative contributions rather than single breakthroughs.

4. Site-level studies matter as much as global-scale studies in conservation science.

5. How important something appears depends on the scale used for evaluation.

6. Conservation plans lacking support from social sciences fail during real-world implementation.

Propositions belonging to the thesis, entitled:
“Mammal density estimation using camera traps: new perspectives"

Shuiqing He
Wageningen, 10 June2026

Mammal density estimation using camera traps: new perspectives

Shuiqing He

Thesis committee

Promotors

Prof. Dr Frank van Langevelde

Professor of Wildlife Ecology and Conservation

Wageningen University & Research

Prof. Dr Patrick A. Jansen

Professor of Wildlife Ecology & Nature Restoration

Utrecht University

Co-promotors

Prof. Dr Chris Carbone

Professor in Ecology

Zoological Society of London, UK

Prof. Dr J. Marcus Rowcliffe

Professor in Ecology

Zoological Society of London, UK

Other members

Prof. Dr Douglas Sheil, Wageningen University & Research

Dr W. Daniel Kissling, University of Amsterdam

Dr Tim Hofmeester, Swedish University of Agricultural Sciences, Uppsala, Sweden

Dr Monique de Jager, Utrecht University

This research was conducted under the auspices of the Graduate School for Production Ecology & Resource Conservation (PE&RC)

Mammal density estimation using camera traps: new perspectives

Shuiqing He

Thesis

submitted in fulfilment of the requirements for the degree of doctor
at Wageningen University
by the authority of the Rector Magnificus,
Prof. Dr C. Kroeze,
in the presence of the
Thesis Committee appointed by the Academic Board
to be defended in public
on Wedesday 10 June 2026
at 10.30 a.m. in the Omnia Auditorium.

Shuiqing He

Mammal density estimation using camera traps: new perspectives,
120 pages.

PhD thesis, Wageningen University, Wageningen, the Netherlands (2026)
With references, with summary in English
978-94-6534-415-7.

TABLE OF CONTENTES

Chapter 1	General introduction	7
Chapter 2	A Random Encounter Model for wildlife density estimation with vertically oriented camera traps	19
Chapter 3	Wildlife density estimation using the Random Encounter Model: a comparison between horizontal and vertical camera-trap placements	45
Chapter 4	Does controlling for body size and diet improve relative abundance estimates for macroecological studies using camera-trap data?	69
Chapter 5	Synthesis	83
Appendix	Summary	98
	Acknowledgement	109
	Biography	115
	Publication list	116
	Overview of Completed Training Activities	117
	Colophon	119


2024-05-19 08:59:42
M 5/10
26°C
RECONYX

1

General Introduction

1.1 FROM DENSITY ESTIMATION TO CAMERA TRAPS

Animal abundance is a key variable in many ecological and conservation questions; therefore, reliable and accurate estimation is fundamental (Becker et al., 2022; Buckland et al., 2005; Gopalaswamy et al., 2012; Nakashima et al., 2018a). However, obtaining unbiased density estimates remains challenging, particularly for mammals that are nocturnal, elusive, or cryptic (Burton et al., 2015a; Nakashima et al., 2018a). The expansion of motion-activated camera traps over the past three decades has transformed wildlife monitoring in an effective way (Wearn and Glover-Kapfer, 2019). Camera trapping provides a practical, non-invasive approach for monitoring animal occurrence, behaviour, and community structure, and for estimating the abundance of terrestrial mammals. As a result, camera traps have been widely adopted in wildlife and biodiversity research across broad spatial and temporal scales (Burton et al., 2015; Gilbert et al., 2021; Pfeffer et al., 2018; Sanderson and Trolle, 2005). Large-scale initiatives such as TEAM, eMammal, Snapshot USA, and MammalWeb has generated millions of images annually, creating unprecedented opportunities for large-scale ecological, macroecological, and biogeographical analyses (Ahumada et al., 2011; Hsing et al., 2022; McShea et al., 2016; Shamon et al., 2024).

1.2 PRINCIPLES OF CAMERA-TRAP OPERATION

Camera traps can be triggered using several mechanisms, including time-lapse schedules, microwave sensors, mechanical triggers, active infrared (AIR) beams, and passive infrared (PIR) sensors. Despite this diversity, PIR sensors are most commonly used in wildlife monitoring because they offer a practical balance between energy efficiency, sensitivity, and reliability under field conditions (Wearn and Glover-Kapfer, 2017; Welbourne et al., 2016). PIR sensors detect changes in infrared radiation emitted from the surfaces of warm-blooded animals as they move through the environment. A PIR trigger consists of two key components: a pyroelectric sensor and a Fresnel lens. The pyroelectric sensor generates an electrical signal when it detects a change in incoming infrared radiation, which occurs when an animal with a surface temperature different from that of the background moves across the sensor's field of sensitivity. The Fresnel lens acts as the optical element that structures this sensitivity in space by dividing the environment into one or multiple detection windows that together define the sensor's detection geometry. Different Fresnel lens designs therefore produce different detection geometries, influencing when and where animals trigger the camera (He et al., 2025; Welbourne et al., 2016).

As a consequence, camera traps are characterised by two distinct but related spatial domains: the detection zone and the filming zone. The detection zone refers to the area within which an animal can trigger the PIR sensor, whereas the filming zone corresponds to the camera's field of view (O'Connell et al., 2011; Rowcliffe et al., 2008; Sheng et al., 2014). The detection zone is commonly conceptualised as a segment defined by a detection radius and angle (Rowcliffe et al., 2008) and may be larger or smaller than the filming zone depending on sensor design, animal characteristics, and environmental conditions such as vegetation structure and thermal environment (Hofmeester et al., 2017; Kelly and Holub, 2008; Rowcliffe et al., 2011; Rowcliffe et al., 2008). Importantly, this separation between detection and filming means that camera-trap observations are not determined solely by animal presence. Instead, whether an animal is recorded depends on the probability that it enters the detection zone and triggers the sensor, a process governed by both biotic and abiotic factors. Detection and detectability therefore form the central principle underlying both the strengths and limitations of camera traps for wildlife monitoring.

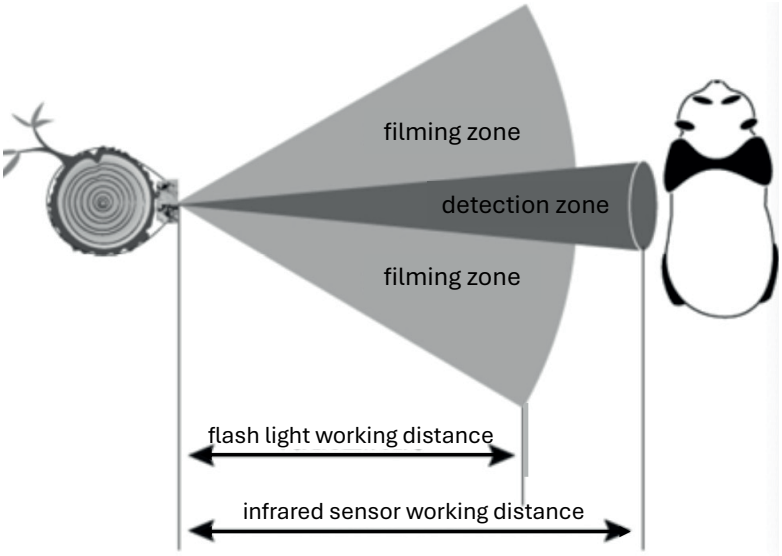


Figure 1.1 Conceptual illustration of the detection zone and filming zone of a PIR camera trap as an animal passes through the field of view. The original figure was published in Chinese and is reproduced here in translated form (Li et al., 2014).

1.3 STRENGTHS AND LIMITATIONS OF DENSITY ESTIMATION USING CAMERA TRAPS

Camera traps are widely used for monitoring wildlife and estimating population density, especially for medium- to large-sized mammals (Burton et al., 2015; O'Connell et al., 2011; Tobler et al., 2008). Early camera-trap studies focused on species with individually identifiable markings, enabling abundance estimates through capture–recapture methods (Karanth and Nichols, 1998.; O'Brien et al., 2003). However, for the majority of mammal species that are unmarked, robust density estimation remains challenging (Chandler and Royle, 2013; Rowcliffe et al., 2008). Despite a rapid increase in camera-trap data in recent decades (Steenweg et al., 2017; Wearn and Glover-Kapfer, 2019), most studies rely on relative abundance indices (RAIs) as proxies for true abundance (Carbone et al., 2001; O'Brien et al., 2003). However, capture rates do not account for detection probability, which can vary with species traits, environmental conditions, and camera setup (Carbone et al., 2005; MacKenzie et al., 2002; Rowcliffe et al., 2011; McNab, 1980; Sollmann et al., 2013). Larger animals passing in front of camera traps are more likely to be detected as they emit more heat (Rowcliffe et al., 2011; McNab, 1980). Moreover, species with longer daily travel distances and bigger home range, are more likely to pass in front of camera traps (Carbone et al., 2005; Sollman et al., 2013). Specific responses from different species to trap setup can also bias RAIs (Sollman et al., 2013). Consequently, RAIs may not reliably reflect true abundance because detection probability varies among species and environmental conditions, highlighting the importance of incorporating detectability into abundance estimation.

Camera traps also represent a substantial financial investment, and commonly used horizontally oriented deployments are prone to theft, vandalism, fire, and damage by wildlife (He et al., 2025; Meek et al., 2019, 2016; Smith and Coulson, 2012). Mid-range camera models suitable for scientific monitoring typically cost around 300–500 USD (Wearn & Glover-Kapfer, 2017). In multiple field studies, including those in this thesis, large mammals such as elephants frequently displaced or destroyed horizontally deployed cameras, leading to data loss and increased costs. These challenges have led to growing interest in vertically oriented camera traps, which are mounted above ground and face downward to reduce the risk of damage or theft (Smith & Coulson, 2012; Meek et al., 2016; He et al., 2025). However, changes in deployment orientation affect not only camera placement but also detection processes. Vertical setups alter the geometry of the detection zone, influencing the probability that an animal triggers the sensor. As a result, capture rates from different deployment strategies are

not directly comparable unless differences in detection probability are clearly understood and accounted for.

Together, these limitations indicate that both methodological challenges in estimating abundance for unmarked species and practical constraints in camera deployment are rooted in variation in detection. Understanding the way of detection and detectability is therefore essential for interpreting camera-trap data and for improving density estimation across species, environments, and deployment strategies.

1.4 DENSITY ESTIMATION MODELS USING CAMERA TRAPS

In recent years, several methodological advances have enabled density estimation for individually unmarked species. Chandler and Royle (2013) developed the spatial count model (SCM), which estimates density from spatially correlated counts collected at closely spaced sampling sites. Moeller et al. (2018) proposed the time-to-event (TTE) model, which requires independent estimates of animal movement rates. Howe et al. (2017) introduced distance sampling with camera traps (CT-DS) by adapting conventional distance-sampling methods to camera-trap data. The Time in Front of the Camera (TIFC) method estimates animal density by relating the total time animals spend within the camera detection zone to encounter processes (Becker et al., 2021). Among these approaches, the random encounter model (REM) has become widely used (He et al., 2025; Palencia et al., 2022; Pettigrew et al., 2021; Rowcliffe et al., 2008). REM estimates animal density by correcting camera-trap capture rates for key biological parameters, including average group size, movement speed, and activity level, characteristics of camera sensors, as well as the environment (Rowcliffe et al., 2008). This framework was later extended by Nakashima et al. (2018) to the random encounter and staying time (REST) model.

The Random Encounter Model (REM) is one widely used approaches for estimating population density of unmarked animals from camera-trap data (Palencia et al., 2022; Schaus et al., 2020). Originally developed by Rowcliffe et al. (2008), REM is based on the two-dimensional ideal gas model, where encounter rates depend on random movement through space (Hutchinson and Waser, 2007). REM links camera-trap detections to animal density by incorporating animal movement speed (day range), activity level, group size, and the effective detection zone of the camera. A key assumption of the model is that animal movement is random and independent of camera placement. REM has been applied across

a broad range of taxa, ecosystems, and spatial scales from single-species studies to community-level and regional monitoring. When core parameters such as movement speed, activity, and detection distance are well estimated, REM can yield reliable density estimates without requiring individual identification (Palencia et al., 2022; Schaus et al., 2020; Rowcliffe et al., 2011). Like most camera-based density estimation frameworks, REM has been developed for horizontally oriented, forward-facing cameras, where the detection zone is modeled as a sector defined by a radius and angle (Rowcliffe et al., 2008). Applying REM to vertically oriented cameras requires a better understanding of detection geometry that differs from horizontal setups.

1.5 THESIS OUTLINE

The aim of this thesis is to improve the estimation of wildlife density from camera-trap data, with a focus on unmarked terrestrial mammals. Although camera traps are widely used in biodiversity monitoring, density estimation for unmarked species remains challenging because capture rates depend not only on animal density but also on detectability, which is influenced by both biotic and abiotic factors (Burton et al., 2015; Nakashima et al., 2017; Rowcliffe et al., 2008). If variation in detection is not explicitly accounted for, inference on animal abundance may be biased. In recent years, several new approaches for density estimation have been proposed, but these methods typically require additional biological or observational parameters that are not available for most collected camera-trap data. In contrast, decades of accumulated camera-trap data largely consist of capture-rate information alone, limiting their direct use for robust density estimation. At the same time, camera traps are costly monitoring tools, and commonly used horizontally oriented deployments are vulnerable to vandalism, fire, and damage by wildlife. In systems where such risks are high, alternative deployment strategies can be adopted to reduce equipment loss and protect data quality and long-term monitoring investment (Meek et al., 2016; Smith & Coulson, 2012; He et al., 2025). However, alternative deployment strategies also alter detection geometry and detectability. This raises a key methodological question: how detection and detectability should be understood and incorporated into modelling frameworks when adapting orientation from conventional horizontal setups.

This thesis adopts the Random Encounter Model (REM) as an analytical framework to address these challenges. Across the chapters, REM was used to (i) adapt density estimation to an alternative camera orientation, (ii) quantify how deployment orientation influences detection processes and density estimates,

and (iii) develop approaches that allow capture rates, which constitute the majority of existing camera-trap data, to better reflect underlying wildlife density. The thesis progresses from methodological development, through empirical evaluation, to macroecological application, with a focus on understanding detection and detectability in camera-trap surveys.

Chapter 2

A random encounter model for wildlife density estimation with vertically oriented camera traps

Chapter 2 adapts the Random Encounter Model (REM) from conventional horizontal deployments to vertically oriented camera traps. Although vertical deployments are gaining interests in reducing camera damage, theft, and habitat disturbance, their detection geometry differs fundamentally from that of horizontal setups, violating assumptions implicit in REM applications. This chapter formalizes the detection geometry of vertical camera traps, estimates the required biological and detection parameters, and evaluates the vertical REM (vREM) using empirical data from a mammal community with a wide range of body sizes. By comparing the density estimates from vREM with independently estimated densities from formal studies, the chapter demonstrates how REM can be extended to vertical orientations and discusses the conditions under which vREM provides reliable density estimates.

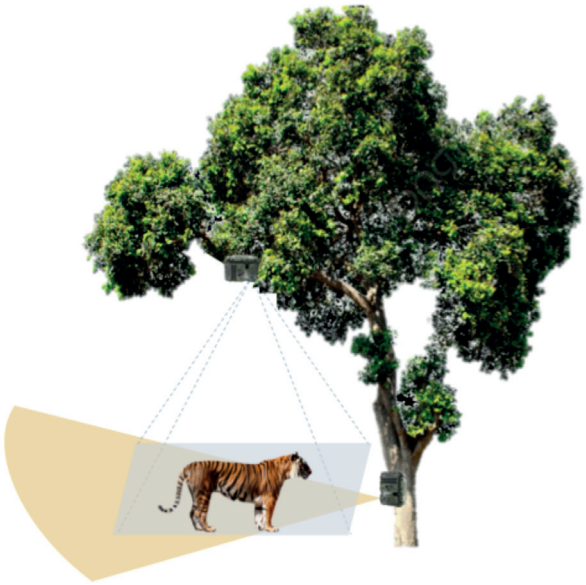


Figure 1.2 Theoretical illustrations for detection zones of horizontal and vertical oriented camera traps.

Chapter 3

Wildlife density estimation using the Random Encounter Model: a comparison between horizontal and vertical camera-trap placements

Although Chapter 2 establishes a theoretical framework for vertical camera traps, the relative performance of vertical and horizontal deployments has not been evaluated under matched field conditions. Chapter 3 addresses this gap through a controlled field study involving simultaneous deployments of paired vertical and horizontal camera traps at 36 sites. This chapter directly compares core parameters, capture rates, and REM-based density estimates between orientations while controlling for environmental variation. It quantifies orientation-specific differences, evaluates how these differences propagate into density estimates, and examines practical constraints associated with horizontal deployments, including camera damage and data loss. By identifying systematic biases linked to camera orientation, this chapter provides empirical guidance on when vertical or horizontal deployments are appropriate for density estimation and highlights limitations that must be considered when applying vertical deployments.

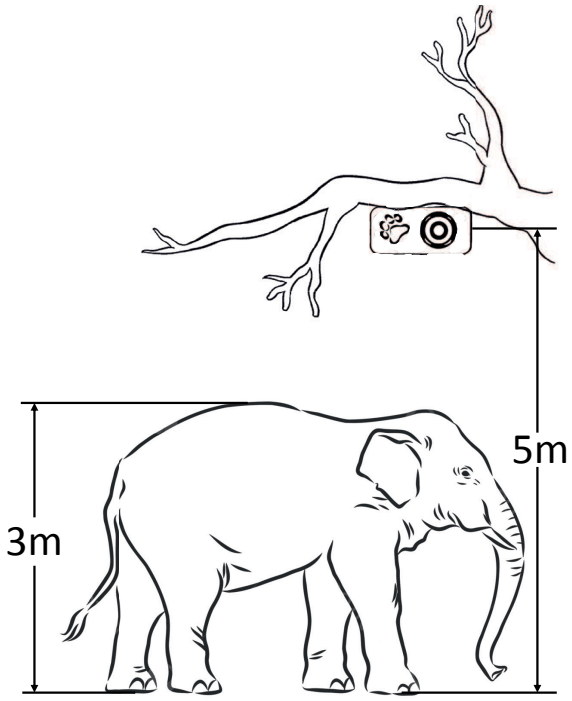


Figure 1.3 Theoretically optimal mounting height for vertically oriented camera traps under an elephant-damage constraint.

Chapter 4

Does controlling for body size and diet improve relative abundance estimates for macroecological studies using camera-trap data?

While Chapters 2 and 3 focus on site-level density estimation, many large-scale camera-trap datasets lack the information required for full REM-based density estimation and therefore rely on capture-rate metrics, which constitute the majority of camera-trap data accumulated over past decades. Chapter 4 addresses this limitation by developing a corrected mass-relative abundance index (mRAI) to improve the interpretability of capture rates for macroecological analyses. This chapter derives scaling relationships between REM parameters, species body mass, and diet, and uses these relationships to adjust capture rates for differences in detectability among species. The performance of mRAI is evaluated with independent density datasets across multiple species. The results demonstrate how biologically informed corrections can improve the correspondence between capture rates and true density, providing a practical tool for comparative studies where direct density estimation is not feasible and enabling better use of existing camera-trap data.

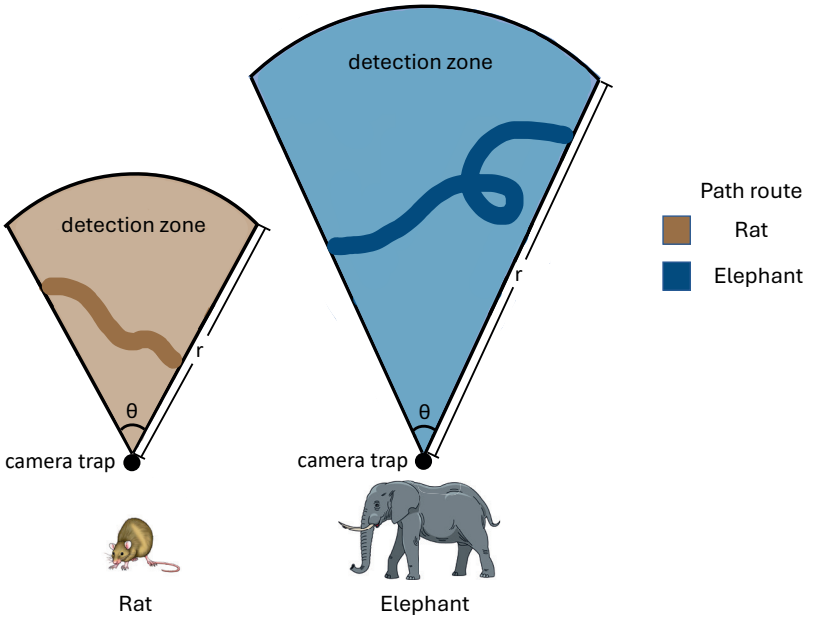


Figure 1.4 Detection zones and movement paths for animals of different body masses. Detection angle is denoted by θ, and r represents the detection radius. The brown curve shows a representative movement path of a rat, and the blue curve shows a representative movement path of an elephant.

1.6 SUMMARY

Together, the chapters of this thesis address key methodological and practical limitations in wildlife density estimation using camera-trap data. By explicitly accounting for detection geometry and detectability, this work extends the Random Encounter Model (REM) to vertically oriented camera traps, evaluates how deployment orientation influences detection processes and resulting density estimates, and develops approaches that improve the interpretation of capture rates for large-scale studies. By adapting density estimation methods to alternative camera deployments, this thesis demonstrates how camera-trap surveys can be designed to reduce equipment loss while maintaining robust inference on wildlife density. In addition, by correcting capture-rate metrics for systematic differences in detectability among species, the thesis enables more effective use of the extensive camera-trap datasets that consist primarily of capture-rate information. Overall, the results provide both theoretical insight into detection processes underlying camera-trap observations and practical guidance for designing, analysing, and interpreting camera-trap surveys across species, environments, and deployment strategies.


2024-06-19 11:02:55 M 3/10 33°C
BNP-09H
RECONYX

2

A Random Encounter Model for wildlife density estimation with vertically oriented camera traps

(1) The Random Encounter Model (REM) estimates animal densities from camera-trap data by correcting capture rates for a set of biological variables of the animals (average group size, speed, and activity level) and characteristics of camera sensors. The REM has been widely used for setups in which cameras are Mounted on trees or other structures aimed parallel to the ground.

(2) Here, we modify the REM formula to accommodate an alternative field of view acquired with vertically oriented camera traps, a type of deployment used to avoid camera theft and damage. We show how the calculations can be adapted to account for a different detection zone with minor modifications. We find that the effective detection area can be close to a rectangle with dimensions influenced by the properties of the Fresnel lens of the camera's motion sensor, the body mass of different species, and the height of the camera. The other REM parameters remain the same.

(3) We tested the modified REM (vREM) by applying it to wildlife data collected with vertically oriented camera traps in Bardia National Park, Nepal. We further validated that the effective detection area for the camera model used was best approximated as a rectangle shape using maximum likelihood estimation. Density estimates obtained broadly matched independent density estimates for nine species from previous studies in Bardia with varying body sizes by four orders of magnitude.

(4) We conclude that these modifications allow the REM to be effectively used for mammal density estimation for species with a wide range of body sizes, with vertically oriented camera traps.

Key words
mammal community; Bardia National Park, Nepal; photogrammetry; detectability

Abstract

2.1 INTRODUCTION

Animal abundance estimates are essential to answer important questions in ecology and conservation biology (Buckland et al., 2005; Gopalaswamy et al., 2012). Camera trapping has become a major method for estimating densities of terrestrial mammals (Gilbert et al., 2021; Meek et al., 2019). Camera-trap surveys are economical, efficient, and non-invasive, as well as providing clear and robust evidence of species occurrence (Pfeffer et al., 2018; Sanderson and Trolle, 2005). However, one of the limitations of this technique is that cameras themselves are expensive, and can be vulnerable to damage or theft, which can bring great financial and data losses (Meek et al., 2016). In sites with poachers or elephants, for example, placements close to the ground have a high risk of theft or destruction (Grassman et al., 2005; Glover-Kapfer et al., 2019).

Vertical orientation of camera traps, in which camera traps are mounted several meters above the ground facing straight down, is an effective solution to minimize the risk of damage from animals like bears or elephants and theft by humans in such situations (Grassman et al., 2005; Meek et al., 2016). Besides the reduced risk of vandalism and theft, a more clearly defined detection zone and reduced habitat disturbance have been put forward as advantages of a vertical orientation (Smith and Coulson, 2012). In addition, mounting off the ground may also make cameras less vulnerable to wildfire, especially in areas with seasonal forest fires.

One common goal of camera trapping is to estimate population densities of mammal species as to inform conservation and management. Among these, the Random Encounter Model (REM) (Rowcliffe et al., 2008) is one of the most reliable and most often used approaches (Palencia et al., 2022; Schaus et al., 2020). REM estimates animal densities from camera-trap data by correcting capture rates for a set of biological variables of the animals (average animal group size, speed, and activity level) and characteristics of camera sensors. Currently, the REM and other approaches for estimating animal density from camera traps are designed for horizontal setups (Howe et al., 2017; Rowcliffe et al., 2008). To apply the REM to vertical setups, modifications are required.

Here, we modify the standard formula of the detection zone of the REM so that it can be used for wildlife density estimation with vertical camera-trap orientations, as vREM. We show how the effective detection area must be calculated as a rectangle, depending on the properties of the lens of the camera's motion sensor. Then, we test the vREM by applying it to wildlife data collected with vertical camera traps in Bardiya National Park, Nepal, a species-rich protected

area, and compare the resulting density estimates for 12 species varying in size over 4 orders of magnitude (3.713 - 3160 kg) with independent estimates from former studies. Our study broadens the application of density estimation using the REM to a novel camera placement strategy.

2.2 METHODS

2.2.1 From horizontal to vertical

The REM was adapted from the classic two-dimensional gas model, in which the expected number of contacts is simply the ratio of area covered by all particles present to the total area (Hutchinson and Waser, 2007). Manipulating this equation and applying it to animals and cameras allows animal density to be estimated from the capture rate (y) for a survey period (t). For horizontal setups, the effective detection area – the contact zone of animals and the camera – is a sector-shaped area, defined by radius r and angle θ, within which the camera's passive infrared motion sensor detects passing animals. The profile ($\overline{p}$) is calculated by the width of the covered path presented to animals by the detection zone averaged across all possible angles of approach (Rowcliffe et al., 2008). The density of an animal species with velocity v, activity level a, and group size g can then be calculated (Formula 1).

$$D = \frac{y}{t} * \frac{\pi g}{v \cdot a \cdot r(2+\theta)} = \frac{y}{t} * \frac{g}{va\overline{p}} \qquad \text{Formula 1}$$

Two key components of any PIR sensor are the pyroelectric sensor and the Fresnel lens. The pyroelectric elements use the pyroelectric effect to generate an electrical current when they are at different temperatures from one another. The Fresnel lens is the optics of the PIR trigger which alters where in the environment the pyroelectric sensor is 'looking'. Fresnel lenses can be either single-zone or multi-zone, containing single or multiple detection windows composing the 'detection zone' of the camera (Welbourne et al., 2016). Based on this, different types of Fresnel lenses can have different shapes of detection zones.

Three camera-trap models were used in this project: Browning BTC-5HDPX, Reconyx HC500 (HYPERFIRE), and Reconyx HYPERFIRE 2 (Table S2.4). From the detection area of their PIR Fresnel lenses (Fig. S2.4 & Fig. S2.5), it seems a priori likely that the effective detection zone in vertical setups is best described by a rectangle with a detection angle of 2π radians, defined by half width and half height of the rectangle, a and b (Fig. 2.1). Based on this assumption, through a coordinate system using the directions of a and b as the x and y axes, the approach profile of the detection zone can be calculated from the transverse line

of the rectangle with the approaching direction of the animal (Formula 2 & 3). Imagine an animal approaching the detection zone from a direction , the profile of the detection zone from this angle of approach should be the perpendicular distance between the two lines (l_1 and l_2) that cut across the diagonal points (A & B) of the rectangle (Fig.2.1). The profile can be derived from two times the distance between the origin (O) and the crosspoint (C) between l_2 and its perpendicular line (Formula 3) that goes through the origin (Formula 4 & Formula 5). The average profile ($\bar{p}$) in this model can then be calculated through trigonometry and integration (Formula 6 & Formula 7). The integration range of g was set between 0 and $\frac{\pi}{2}$ assuming symmetry of rectangle.

$$y = tan\gamma(x - a) - b \qquad \text{Formula 2} \qquad (0 \le a \le b;\ 0 \le \gamma \le \pi/2)$$

$$y = -(1 / \tan\gamma)x \qquad \text{Formula 3}$$

$$tan\gamma(x - a) - b = -\left(\frac{1}{\tan\gamma}\right)x \qquad \text{Formula 4}$$

$$OC = \sqrt{\left(\frac{atan^2\gamma + btan\gamma}{sec^2\gamma}\right)^2 + \left(-\frac{atan\gamma + b}{sec^2\gamma}\right)^2} \qquad \text{Formula 5}$$

$$p = 2OC = 2(asin\gamma + bcos\gamma) \qquad \text{Formula 6}$$

$$\overline{p} = \frac{\int_0^{\frac{\pi}{2}} 2(asin\gamma + bcos\gamma)\, d\gamma}{\frac{\pi}{2}} = \frac{2(a+b)}{\frac{\pi}{2}} = \frac{4(a+b)}{\pi} \qquad \text{Formula 7}$$

2.2.2 Photogrammetry

The width of the field of view on the ground (d) was calculated from field of view angle (α, provided my the manufacturer, Table S2.4) and height of camera (h) using:

$$d = 2h \tan\frac{1}{2}\alpha \qquad \text{Formula 8}$$

Given image width in pixels (W), and the distance of an animal from the image origin (the midpoint of the image) in pixels (w), its real-world distance from the origin can then be calculated as: wd/W.

2.2.3 Animal tracking

Movement paths were tracked by tagging pixels using the same frontmost foot consistently across all images of a group observation (a continuous sequence of photo records of a group of animals with given species passing the camera) as

the tracking point and converting to real-world position as above for estimation of parameters including detection zone and animal movement speed. Only the first individual to trigger the camera within one group observation was tracked for detection zone and speed estimation. Speeds were calculated by dividing the summed distance moved across images by time elapsed, given by the difference between timestamps of the last and first images of the observations.

2.2.4 Detection zone estimates

The half width and height of the rectangle detection zone (a and b in Fig. 2.1) were estimated by fitting detection functions (Buckland et al., 2001) to distances from the origin in the first image of each observation in, respectively, the x and y axes of the image plane. The rectangle dimensions were assumed to potentially differ between camera models, to increase with increasing body mass (Rowcliffe et al., 2011; Schmidt-Nielsen, 1984) , and to increase with increasing height of the camera.

2.3 FIELD TEST

2.3.1 Study site and data collection

To assess the performance of vREM in field conditions, we applied it to data collected in the western part of Bardiya National Park (BNP), located in the Terai lowlands of southwestern Nepal. BNP covers a protected area of 968 km^2 and is comprised by a landscape of sal (*Shorea robusta*) forests, grasslands, mixed forests, and riverine forests (Dinerstein, 1979a; van Lunenburg et al., 2017). BNP is well known as a habitat rich in bird and mammal species with a record of 513 bird species and 62 mammal species including a large range of carnivores, mesoherbivores, and megaherbivores (Kral and van Lunenburg, 2017; DNPWC & DFSC, 2022; BNPO, 2022).

The survey used a 1.4 km x 1.4 km grid of 50 vertically placed camera traps with PIR triggers mounted at heights ranging from 4.5 m to 8.4 m (Fig. 2.2). The camera traps were put on the trees by field staff with ladders or elephant-back and climbing. The heights from camera traps to the ground were measured with tape. Images of the observations were stored in Agouti, an online platform and database for processing and archiving of camera-trap images (Casaer et al., 2019). Animals in the images were identified and annotated using an AI algorithm which has been trained for vertical camera trapping images for over four years of data, combined with manual validation and annotation. No time limit was given to a single observation. If the time gap between two subsequent observations is lower or equal to 2 min, these two observations were then merged

into one. We used a dataset that covers the period between May 10, 2018 and Mar 16, 2022. Deployments with wrong time records due to failures of the internal clocks of the cameras were deleted, including deployments with a wrong starting time and ending time. The total sampling effort in the remaining dataset was 32,144 days. All data analyses and visualizations were done in R version 4.4.0 (R core Team, 2024).

2.3.2 vREM parameter estimates

2.3.2.1 Animal tracking

The minimum sample size for parameter estimation was set at 150 (Rowcliffe et al., 2011; Palencia et al., 2022; Bollen et al., 2023). To meet or exceed this target, we tracked animals in all records for species with fewer than 300 observations. For species with more than 300 observations, 300 observations were randomly selected. For all but one species (golden jackal (*Canis aureus*) speed, n = 63), sample sizes exceeded 100, and the sample sizes of three species fell between 100 and 150 (Indian crested porcupine speed (*Hystrix indica*), n = 104 ; Nepal gray langur (*Semnopithecus schistaceus*), n = 127; Asian elepant, n = 135). The locations were also estimated and marked both inside and outside the view (Fig. 2.3). Similarly, if the front foot was obscured by an animal's body, the foot position was estimated. For greater one-horned rhinoceros (*Rhinoceros unicornis*) and Asian elephants (*Elephas maximus*), in contrast, the central point of the body part shown in the first photo was selected as the tracking point.

2.3.2.2 Detection zone estimates

The number of observations per species used to model the detection zone ranged from 107 (golden jackal) to 594 (chital (Axis axis)) (Table S2.1). To validate the assumption that the detection zone is a rectangle, the first-triggered points of each species were plotted separately (Fig. 2.4) and combined using an empirical distribution with the absolute values of x and y coordinates in meters (Fig. S2.2). Based on the distribution plots of the first triggers, we assumed that the distribution of the x and y axis distances followed a bivariate normal distribution in a rectangle-shaped detection zone, with the midpoint of the image as the origin of the rectangle-shaped detection zone (Fig. 2.4 & Fig. S2.2). The height and length, which together define the sizes and shapes of the rectangles, were then estimated through the maximum likelihood function using height of the camera traps, body mass, and camera types as covariates (Table 2.1).

Three different types of cameras were used in this study, each with a different field of view (Table S2.4). Image metadata included the pixel dimensions of the

image, the position of the tracking points, the deployment ID, the time of the records, and the information of the species.

Maximum Likelihood Estimation was applied using the *mle2* function from the *bbmle* package (Bolker, 2022). The Akaike Information Criterion (AIC) was applied to assess the best-fitting model with different covariates to get half the height and width of the rectangle detection zones through the coefficients result. The estimated profiles of different species in different camera heights and types were then calculated with the major and minor axes through integral (Formula 7). Bootstrap with 1000 resamples of the integral results of the profiles was applied to calculate the standard error with *boot* function from *boot* package (Angelo Canty & Brian Ripley, 2022; Davison & Hinkley, 1997).

2.3.2.3 Movement speed, activity level, and group size

The number of observations per species used to estimate speed varied from 63 (golden jackal) to 312 (chital). Activity level was estimated using all observations, without weighing for group size. Sample size for estimating group size ranged from 108 (golden jackal) to 22,512 (chital) (Table S2.1). The harmonic mean of speed observations was used to estimate the average speed (m/s) through *hmean* function from *sbd* package in R, which serves to reduce the impact of faster speeds on the mean speed since animals are more likely captured while moving faster than while moving slowly (Rowcliffe, 2022; Rowcliffe et al., 2016). Movement paths that included periods of animal inactivity (speed <0.01 m/s) were excluded.

To estimate animal activity level (proportion of time spent active), we used the *fitact* function from the R package *activity*, in which a circular kernel density is fitted to radian time-of-day data to estimate the activity level from the distribution (Rowcliffe et al., 2014; Rowcliffe, 2023). To account for variation in day length during the study, clock time was converted to the solar time before activity level estimation using *solartime* function from *activity* package (Vazquez et al., 2019). Group size (*g*), the mean number of animals per observation, was included in the density calculation as in formula 1 since the unit of photo rate was the group not the individual (Rowcliffe et al., 2008).

2.4 RESULTS

Fifty-eight species were recorded in this survey, including 18 bird species, 1 amphibian species, and 39 mammalian species (Table S2.3). The most recorded species was chital with 23,308 observations, followed by rhesus macaque

(*Macaca mulatta*), Nepal gray langur, and barking deer (*Muntiacus muntjak*). Together, these species encompassed 97.5% of all animal observations.

Among all estimated parameters, group size showed little variation across species (from 1.03 to 2.04). Conversely, activity level displayed slightly greater variability (from 0.29 to 0.75). Average speed while active showed pronounced variation (from 0.09 to 0.39 m/s). The vREM estimates of species density ranged from 0.22 km^{-2} (tiger, *Panthera tigris*) to 155 km^{-2} (chital) (Table 2.3).

To validate the vREM density estimates, we compared them with independent density estimates for nine species, sourced from four published surveys carried out in BNP (Table S2.5). A Wald test on chi-square distribution with 1 degree of freedom was applied to compare the difference between the vREM estimates and reference estimates with standard errors. For rhinoceros, the actual population size was known, hence this density estimate has no standard error. We found a broad match between vREM and independent estimates (Fig. 2.5 & Table 2.2).

2.5 DISCUSSION

In this study, we modified the REM to a vREM to work with vertically oriented camera traps. This involved an alternative way to calculate the effective detection area, which was best described by a rectangle, as well as alternative approaches to calculate the parameters from the images through photogrammetry, and an alternative formulation of the vREM density equation. We tested the method in Bardiya National Park, Nepal on 12 mammal species varying over four orders of magnitude in body mass. We found that the density estimates obtained from our results broadly matched those from previous studies in BNP across nine species for which contemporary independent estimates were available. This suggests that the vREM can be effectively used for mammal density estimation from surveys using vertically oriented camera traps.

Looking in more detail at the comparison of density between vREM estimates and independent estimates, density was similar for three out of nine species (greater one-horned rhinoceros, barking deer, and wild boar, *Sus scrofa*), slightly overestimated for one (Asian elephant), overestimated for two species (chital and tiger), and underestimated for three species (sambar deer, *Rusa unicolor*, Rhesus macaque, and Nepal gray langur) (Fig. 2.5 & Table 2.2). The camera trap capture rate of macaque and langur, which are both semi-arboreal, may be biased by missed captures when they are active in the tree canopy, which might

lead to the underestimation of the density of this species. For this reason, vREM might not work for semi-arboreal species. Time gaps between the reference studies and the present research may also account for some of the discrepancies observed in the estimates.

A second important factor may be a mismatch between the regions covered by the current survey and the comparisons. Our survey covered around an 80 km^2 section of BNP including the buffer zone lying by a perennial river, the Gerwa River, in the western part of BNP containing most of the floodplain and grassland of the whole BNP (Dinerstein, 1979a). In contrast, most comparison densities were derived from the full 968 km^2 park area, which is predominantly covered by sal forest. The riverine grasslands covering much of the camera trapped region particularly attract two species, chital and tiger (Dinerstein, 1979a; Moe and Wegge, 1994; Thapa et al., 2021). Since chital is the most abundant tiger prey species, and also the possible better visibility after the fires during the hot-dry season, tigers tend to be present more in grassland areas as well (Dinerstein, 1980), which can lead to overestimates of these two species. In contrast, sambar (*Rusa unicolor*) favors more continuous climax forests (Dinerstein, 1979b), which mainly occur in the eastern part of BNP outside the research area of this project. As an important help in the forest, domestic elephants were used to assist in camera deploying and checking, which can make the density of this rare species slightly overestimated.

Two species here deserve further discussion, which are rhinoceros and chital. As one of the most endangered species in Nepal, rhinoceros has been the subject of many conservation efforts over the past half a century. In BNP, since 1986, these efforts include translocation, fighting poaching, reintroduction, and very close monitoring (DNPWC, 2017). For this reason, all individuals of rhinoceros within BNP are known and well monitored, while the population size of almost all other species is merely estimated. By 2017, 35 individuals of rhinoceros lived in BNP (DNPWC, 2017). Since rhinoceros are habitat specialists, all the potential habitats of this species are within the riverine area. Therefore, the density estimate of rhinoceros from the reference is within 86 km^2, instead of the whole national park, which includes the Karnali floodplain, community-managed forest, and Khata forest corridor (Subedi et al., 2013). This area also largely overlaps with the study area of this project.

Another species of interest is chital, the most abundant tiger prey-species in BNP with the highest density estimate from vREM. Besides the dominance and habitat selection of chital, some factors can also be responsible for a higher estimate compared with density estimation from the reference. The population

of prey species, especially chital, has been increasing in recent years (DNPWC & DFSC, 2022). The widely used method of distance sampling has been applied to estimate prey density in this area for years (Buckland et al., 2001; DNPWC & DFSC, 2022). However, such a method does not perform well with thick vegetation for disturbance and low visibility (DNPWC & DFSC, 2022). For these reasons, together with personal communication with experienced field technicians who conducted the distance sampling survey, a downward bias for transect-based estimates of chital density can be reasonably expected. This, in combination with our high accuracy in estimating the reference population (i.e., rhinoceros), means that some of our relatively high density estimates may actually be representative. Also, although the AI model in this study performs well overall, misclassifications of similar deer species occur, which may have led to an inflated chital capture rate.

A major challenge in adapting the REM to vREM was to define the best-fit shape of the effective detection area, which theoretically depends on the properties of the Fresnel lens used in PIR sensors. Based on the distribution of the 'windows' of the Fresnel lens (Welbourne et al., 2016), the shape of the distribution of the first triggered points may vary. We reasoned that the shape of the detection area should be better described as a rectangle or an oval based on the distribution of Fresnel lens of camera trap types used in this project (Fig. S2.4 & Fig. S2.5). This choice was further validated through the field test in BNP. Based on a visual examination of the distribution of the first triggers (Fig. 2.4 & Fig. S2.2), a bivariate normal distribution was observed and applied in the maximum likelihood function. A subsequent challenge was to determine the scale (ratio between width and height) and size of the detection zone based on other covariates. We found that the scale varied between camera models, and that detection zone size varied significantly with species body mass and camera height as well as camera model.

One unique feature of our field application is that it yielded density estimates for 12 different species, ranging from small to megafauna, that together formed the bulk of the mammal community in a single protected area. Most REM applications to date concern one or a few species rather than entire communities (Palencia et al., 2022; Schaus et al., 2020; Wearn et al., 2022), and smaller, more cryptic species in mammal communities are often lacking in density estimates. The application in BNP explores the effective use of REM in a wider range of body sizes in a mammal community with a novel camera orientation. However, our density estimates may be less accurate estimates for species with smaller body size. The higher the camera traps go, the lower the detectability will be, especially for small and medium-sized species (Meek et al., 2016). Heights of

the camera traps in this study ranged from 4.5 m to 8.4 m, while the effective detection distance of many small to medium-sized species in horizontal camera placements can be shorter than 4 m (Rowcliffe et al., 2011). Thus, preparatory trials to explore the proper heights of the camera trap for research species to increase the detection probability in future studies are advisable.

In conclusion, this study extends the application of REM from horizontal oriented camera traps to vertically oriented camera traps, which makes it achievable to estimate population density with vertical setups. This prospect may encourage application of vertical oriented camera traps as to protect camera traps from damage, theft, and forest fire. The vREM method has the potential to contribute to the conservation and management of mammals, especially in communities where there is a diverse range of species with varying body mass.

2.6 ACKNOWLEDGEMENTS

We thank Bardiya National Park (BNP), National Trust for Nature Conservation (NTNC), and Department of National Parks and Wildlife Conservation (DNPWC) for their help and support; the Himalayan Tiger Foundation for funding the Bardiya survey, and Chinese Scholarship Council (CSC) for the PhD project; Joost de Jong and Naresh Suebdi for comments; NTNC field technicians, who diligently maintained the camera trap network in BNP, in particular Ram Raj Chaudhary, Khusiram Chaudhary, Phirulala Tharu, Tikaram Tharu, and Kararu Tharu, and Santigali, the elephant field technician of NTNC. Thank you so much for your efforts and commitments to guard this lovely forest in cold winters and extremely dry seasons.

2.7 AUTHORS' CONTRIBUTIONS STATEMENT

CC, MR, PJ, SH, and HL conceived the ideas and designed the methods; HL, MR, SH and YL built the model and analysed the data; HL, SH, YL, ST, and BS collected the data; SH, HL, PJ, CC and MR did the writing.

2.8 DATA ACCESSIBILITY

Part of the codes and related for building and verifying the model are available on github: https://github.com/Shuiqinghe/vertical_REM.

TABLES

Table 2.1 Coefficients from the summary result of the best fit model using *mle2* function: 0.5*width ~ height + body mass + camera type; ratio ~ camera type. 0.5*width was ln-transformed and body mass was power-transformed with an exponent of 2/3 (Schmidt-Nielsen, 1984). The ratio (height/width) defines the shape of the detection zone from different types of camera traps.

Response	Estimate	Std. Error	Z value	Pr(z)
0.5*width intercept: Browning	-0.6156	0.1832	-3.3607	***
0.5*width height (m):	0.1618	0.0245	6.6121	***
0.5*width body mass (kg)	0.0020	0.0002	11.3377	***
0.5*width intercept: Reconyx HC500	-0.9700	0.0521	-6.7980	***
0.5*width intercept: Reconyx Hyperfire 2	-0.8760	0.0367	-7.0963	***
Ratio: Browning	0.3680	0.0084	43.7651	***
Ratio: Reconyx HC500	0.5914	0.0419	5.3297	***
Ratio: Reconyx Hyperfire 2	0.3705	0.0192	0.1335	

Table 2.2 Wald test result between vREM and density estimates from reference studies.

Species	W value	p value
Indian rhinoceros	-	-
Tiger	8.0507	**
Wild boar	1.0604	
Asian elephant	3.2444	.
Rhesus macaque	6.2720	*
Sambar deer	5.6556	*
Barking deer	0.2676	
Chital	20.0683	***
Nepal gray langur	8.8972	**

Table 2.3 12 mammal species in Bardiya National Park and their group size, speed (m/s), activity level, and density (ind/km2) estimated with the vREM. Body mass data were sourced from PHYLACINE 1.2 (Faurby et al., 2018b).

Common Name	Body mass (kg)	Observations	Trap rate (Obs/100d)	Group size	Speed (m/s)	Activity level	Density (ind/km2)
Chital	66.17	23,308	72.51	2.04±0.02	0.09±0.01	0.46±0.00	154.88±23.92
Rhesus macaque	3.71	1,927	6.00	1.74±0.04	0.29±0.04	0.35±0.01	4.49±0.90
Nepal gray langur	17.35	1,144	3.56	1.62±0.05	0.15±0.03	0.32±0.01	6.04±1.22
Barking deer	15.93	709	2.21	1.07±0.01	0.17±0.02	0.39±0.02	1.64±0.35
Wild boar	101.05	630	1.96	1.62±0.06	0.17±0.02	0.46±0.01	1.70±0.32
Sambar deer	180.34	587	1.83	1.17±0.03	0.18±0.02	0.46±0.02	1.25±0.23
Tiger	162.56	436	1.36	1.03±0.01	0.39±0.08	0.75±0.02	0.22±0.05
Indian rhinoceros	1602.33	232	0.73	1.16±0.02	0.24±0.03	0.39±0.02	0.61±0.26
Indian hog deer	34.14	246	0.77	1.10±0.02	0.09±0.01	0.57±0.02	0.80±0.18
Asian elephant	3,16	233	0.73	1.45±0.09	0.31±0.04	0.29±0.00	0.39±0.09
Indian crested porcupine	12.44	117	0.36	1.23±0.04	0.31±0.06	0.33±0.03	0.26±0.06
Golden jackal	10.35	91	0.28	1.13±0.04	0.31±0.08	0.51±0.02	0.45±0.50

FIGURES

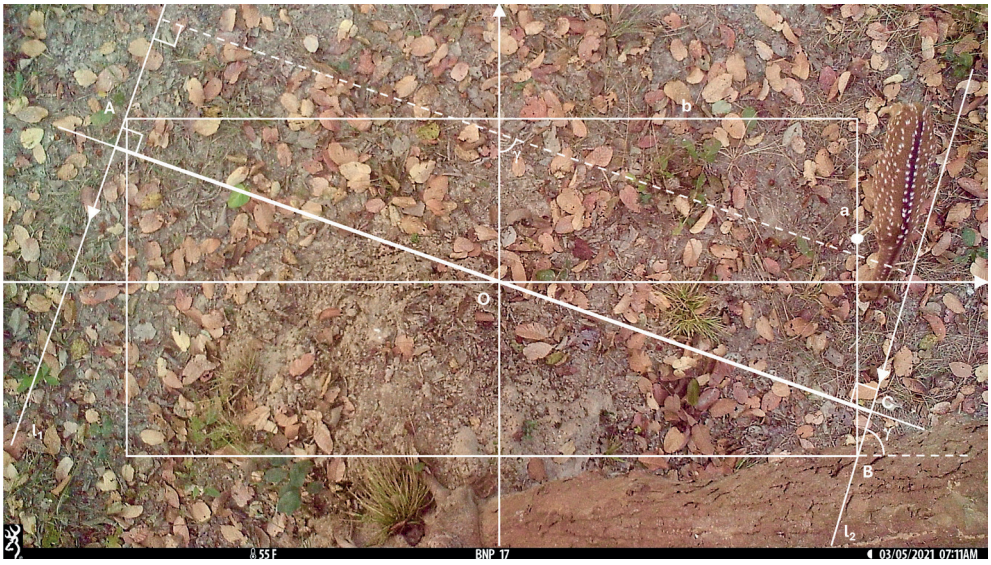


Figure 2.1 Diagram illustrating the profile (bold line) of a rectangle detection zone when an animal is approaching. The rectangle is defined by half the width and height, a and b. l_1 and l_2 go across the diagonal points A and B of the rectangle with orientation reflecting the direction of approach (γ) of the animal.

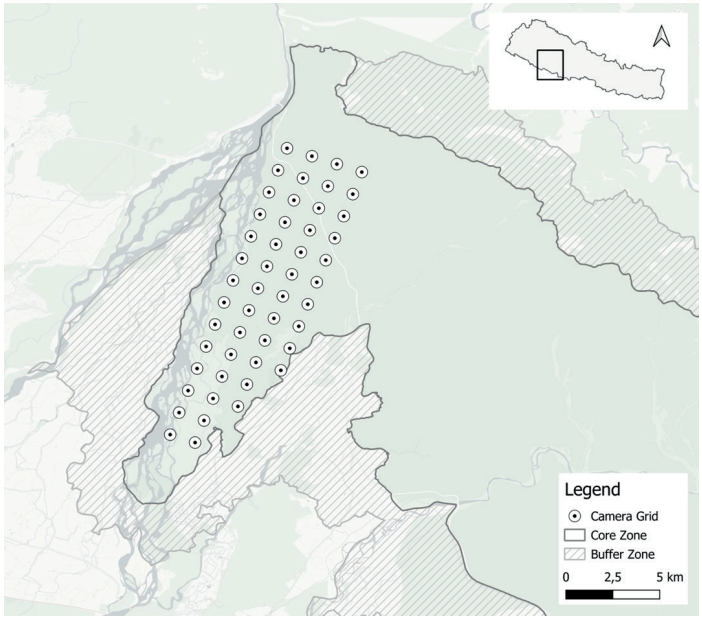


Figure 2.2 Map of the study area within the western part of Bardiya National Park, showing the grid camera traps used in the survey. The inset in the top right of the figure shows the location of Bardiya National Park within Nepal.

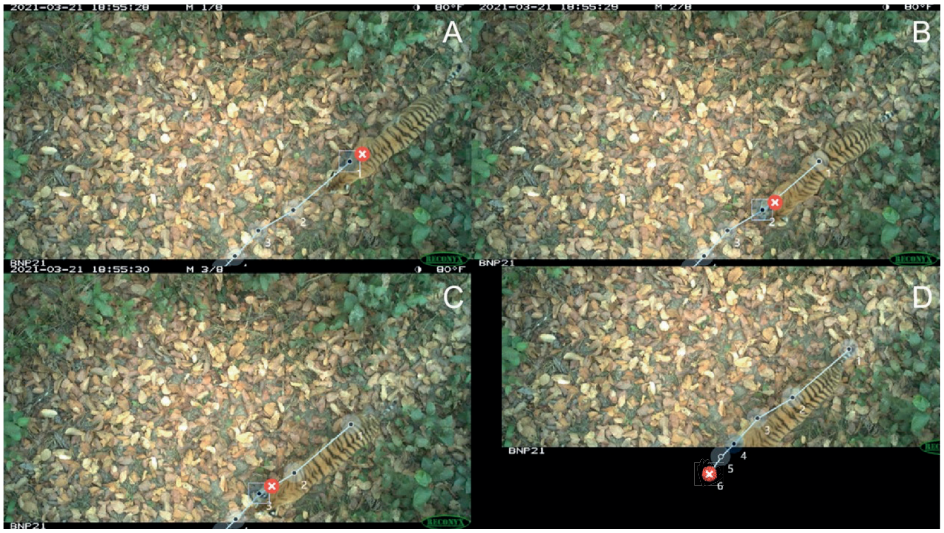


Figure 2.3 Animal tracking in Agouti. Images A to D show the track of a tiger passing through the detection view. Each point was consistently pinned to one of the animal's front feet (in this case the right foot). D shows the situation when the front foot was out of view and the point was therefore approximated outside the image frame.

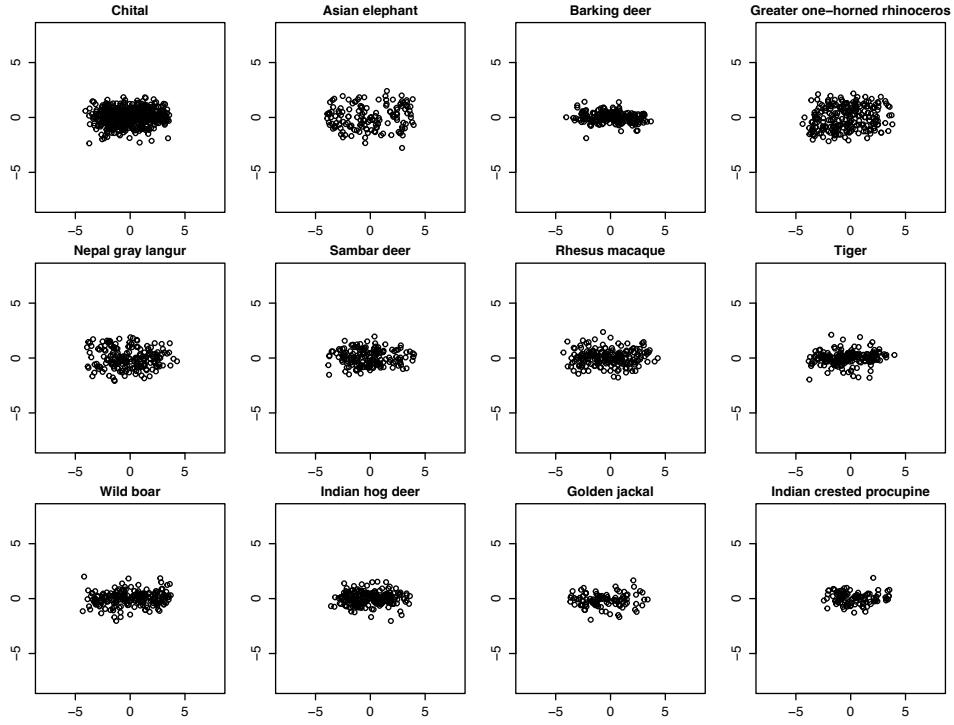


Figure 2.4 First trigger positions of 12 mammal species in Bardiya. The midpoints of the graphs were set as the origins. The unit of the axes is in meters.

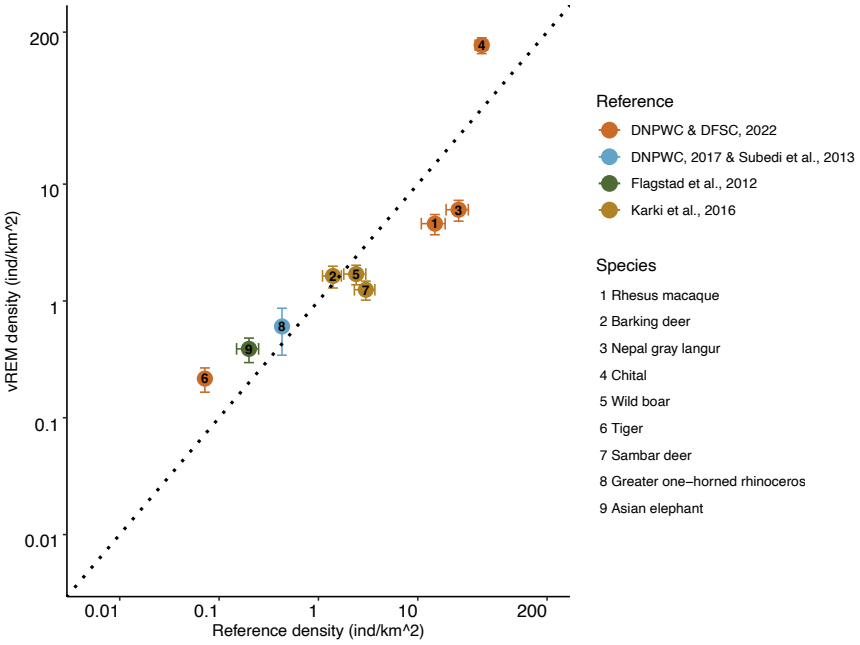


Figure 2.5 Comparison of density estimates from REM using vertical camera traps (y axis) with the result of previous surveys in BNP (x axis). The black dotted line is the identity line (y = x). The closer the point is to this line, the more similar the results of REM are to the previous records. Axes are logarithmic. SE bars show the uncertainty.

SUPPORTING INFORMATION

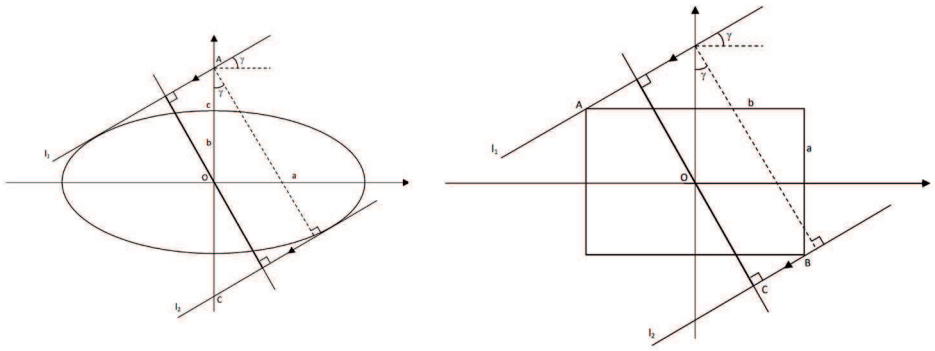


Figure S2.1 Diagram illustrating the profile (bold line) of an oval detection zone when an animal is approaching. The oval is defined by major and minor axes a and b. l_1 and l_2 are tangents to the detection zone parallel to each other with orientation reflecting the direction of approach (g) of the animal (left). Diagram illustrating the profile (bold line) of a rectangle detection zone when an animal is approaching. The rectangle is defined by half the width and height, a and b. l_1 and l_2 go across the diagonal points A and B of the rectangle with orientation reflecting the direction of approach (g) of the animal (right).

$$\frac{x^2}{a^2} + \frac{y^2}{b^2} = 1 \qquad (a > b)$$ Formula 9 (a > b)

$$y = \tan\gamma\, x + c$$ Formula 10

$$(\frac{1}{a^2} + \frac{tan^2\gamma}{b^2})x^2 + (\frac{2c}{b^2} + tan\gamma)x + \frac{c^2}{b^2} - 1 = 0$$ Formula 11

$$c = \sqrt{a^2 tan^2\gamma + b^2}$$ Formula 12

$$p = \cos\gamma AC = \cos\gamma 2c$$ Formula 13

$$\overline{p} = \frac{\int_0^{\frac{\pi}{2}} \cos\gamma 2c\, d\gamma}{\frac{\pi}{2}} = \frac{\int_0^{\frac{\pi}{2}} 2\sqrt{a^2 tan^2\gamma + b^2}\cos\gamma\, d\gamma}{\frac{\pi}{2}} = \frac{4b}{\pi} E(1 - \frac{a^2}{b^2})$$ Formula 14

The process of deducing the oval-shaped detection zone

The oval-shaped detection zone with a detection angle of 2π radians can be defined by the major and minor axes a and b (Formula 9). Based on this assumption, after building a coordination system using the directions of major and minor axes a and b as the x and y axes, the approach profile of the detection zone can be calculated from the transverse line of the oval with the approaching

direction of the animal (Formula 10). Imagine an animal approaching the detection zone from a direction g, the profile of the detection zone from this angle of approach should be the perpendicular distance between the tangents (l_1 and l_2) to the detection zone (Fig.S2.1). The intercept of the tangent (c, giving by line AO or OC) can be derived through formula 11, hence formula 12. The averaged profile ($\overline{p}$) in this model can then be calculated through trigonometry and integration (Formula 13 & 14). The integration range of was set between 0 and $\frac{\pi}{2}$ assuming symmetry of oval, which can be further transformed into complete elliptic integral of the second kind (Formula 14).

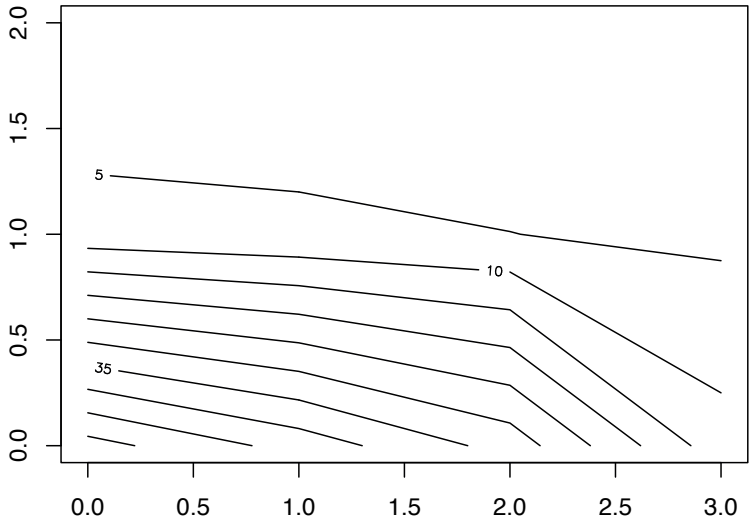


Figure S2.2 Empirical distribution of the first triggered points of 16 species using the absolute values of x and y coordinates in meters. The given values represent the proportion of observations.

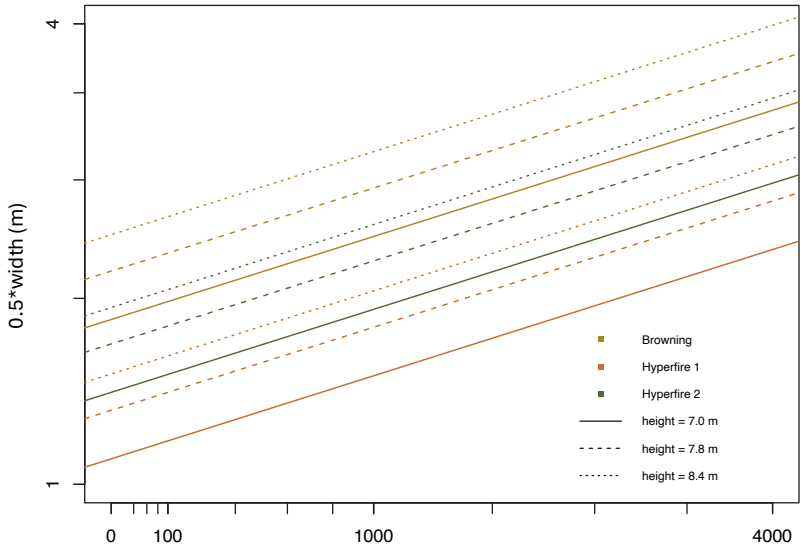


Figure S2.3 Estimated half the width (m) (y axis) distribution of species with different body mass (kg) (x axis). X axis was power-transformed with an exponent of 2/3 and y axis was ln-transformed.

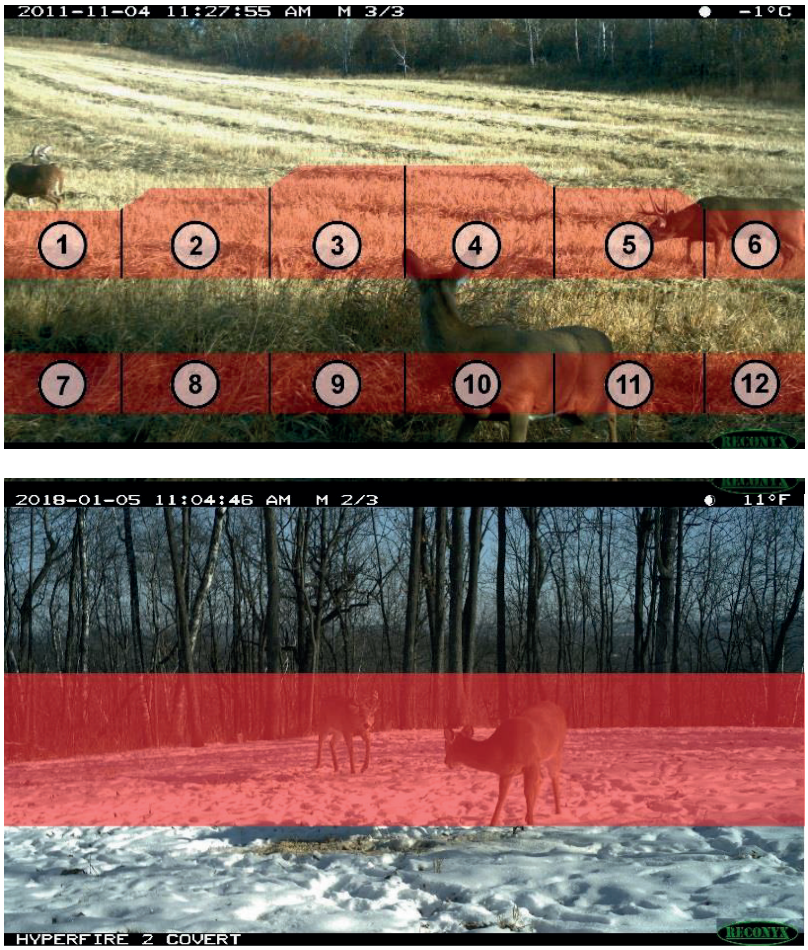


Figure S2.4 Detection area of PIR in Reconyx Hiperfire (up) and Hyperfire 2 (down) from instruction manual.

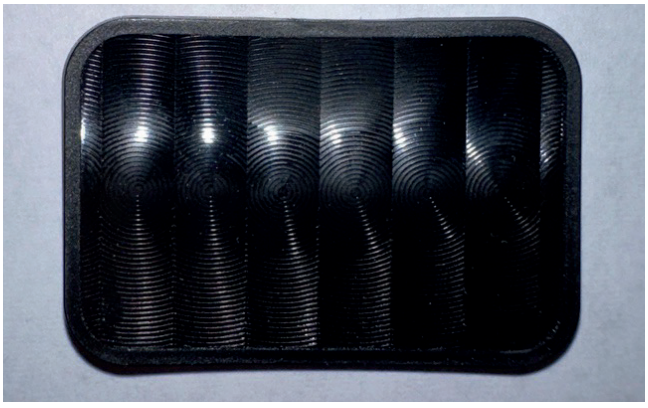


Figure S2.5 Fresnel lens of PIR in Browning BTC-5HDPX from technical support of Browning.

Table S2.1 Sample size for parameter estimation.

Species	Speed	Activity level	Detection zone	Group size
Indian rhinoceros	228	2,966	235	258
Tiger	188	2,926	214	472
Indian hog deer	193	2,643	215	268
Wildboar	171	5,477	207	622
Indian crested porcupine	104	624	107	116
Asian elephant	135	6,492	144	239
Rhesus macaque	175	18,150	211	1,929
Sambar deer	158	7,608	173	622
Barking deer	203	54,56	211	732
Chital	312	273,000	594	22,512
Nepal gray langur	127	13,533	191	1,165
Golden jackal	63	979	107	108

Table S2.2 Comparison between vREM results in oval and rectangle shapes

Species	Oval	Rectangle
Indian rhinoceros	0.73±0.31	0.61±0.26
Tiger	0.26±0.06	0.22±0.05
Indian hog deer	0.97±0.23	0.80±0.18
Wildboar	2.06±0.38	1.70±0.32
Indian crested porcupine	0.32±0.08	0.26±0.06
Asian elephant	0.47±0.11	0.39±0.09
Rhesus macaque	5.55±1.05	4.59±0.90
Sambar deer	1.51±0.30	1.25±0.23
Barking deer	1.99±0.42	1.64±0.35
Chital	187.67±28.76	154.88±23.92
Nepal gray langur	7.31±1.42	6.04±1.22
Golden jackal	0.55±0.60	0.45±0.50

Table S2.3 List of all captured species.

Class	Order	Scientific name	Common name
Aves	Ciconiiformes	*Ciconia episcopus*	Woolly-necked stork
		Leptoptilos javanicus	Lesser adjutant
	Galliformes	*Galloperdix spadicea*	Red spurfowl
		Gallus gallus	Red junglefowl
		Gallus gallus domesticus	Chicken
		Pavo cristatus	Indian peafowl
		Pavo muticus	Green peafowl
	Passeriformes	*Acridotheres tristis*	Common myna
		Copsychus saularis	Oriental magpie-robin
		Dendrocitta vagabunda	Rufous treepie
		Dicrurus macrocercus	Black drongo
		Dicrurus remifer	Lesser racket-tailed drongo
		Passeriformes	Unknown passerine species
		Tephrodornis pondicerianus	Common woodshrike
		Turdus boulboul	Grey-winged blackbird
		Urocissa erythroryncha	Red-billed blue magpie
	Perissodactyla	*Rhinoceros unicornis*	Greater one-horned rhinoceros
	Pholidota	*Manis pentadactyla*	Chinese pangolin
	Piciformes	*Chrysocolaptes guttacristatus*	Greater flameback
		Dinopium benghalense	Black-rumped flameback
	Proboscidea	*Elephas maximus*	Asian elephant
	Scrotifera	*Chiroptera*	Unknown bat species
Mammalia	Artiodactyla	*Axis axis*	Chital
		Axis porcinus	Indian hog deer
		Boselaphus tragocamelus	Nilgai
		Muntiacus muntjak	Barking deer
		Rucervus duvaucelii	Barasingha
		Rusa unicolor	Sambar deer
		Sus scrofa	Wild boar
	Carnivora	*Canis aureus*	Golden jackal
		Canis lupus familiaris	Dog
		Felis chaus	swamp cat
		Herpestes edwardsi	Indian grey mongoose
		Herpestes javanicus	Javan mongoose
		Herpestes smithii	Ruddy mongoose
		Mellivora capensis	Honey badger
		Melursus ursinus	Sloth bear
		Neofelis nebulosa	Clouded leopard
		Panthera pardus	Leopard

Table S2.3 Continued

Class	Order	Scientific name	Common name
		Panthera tigris	Tiger
		Paradoxurus hermaphroditus	Asian palm civet
		Prionailurus bengalensi	Leopard cat
		Viverra zibetha	Large Indian civet
		Viverricula indica	Small Indian civet
		Vulpes bengalensis	Bengal fox
	Lagomorpha	*Caprolagus hispidus*	Hispid hare
		Lepus nigricollis	Indian hare
	Primates	*Macaca mulatta*	Rhesus macaque
		Semnopithecus schistaceus	Nepal gray langur
	Rodentia	*Hystrix indica*	Indian crested porcupine
Reptilia	Squamata	*Varanus bengalensis*	Bengal monitor

Table S2.4 Camera types used in the survey.

Camera type	FOV (°)	Source
Browning BTC-5HDPX	55	Instruction manual
Reconyx HYPERFIRE 2	38	Official support manager
Reconyx HC500 (HYPERFIRE)	42	Official support manager

Table S2.5 Previous density estimates of some mammal species in Bardiya.

Common name	DNPWC, 2017 & Subedi et al., 2013	DNPWC & DFSC, 2022	Flagstad et al., 2012	Karki et al., 2016
Chital		44.05±6.3		
Rhesus macaque		14.86±4		
Nepal gray langur		25.77±6.5		
Barking deer				1.4±0.3
Wild boar		2.4±0.6		
Sambar deer				3±0.7
Tiger		0.072±0.0038		
Indian rhinoceros	0.43			
Asian elephant			0.2±0.05	


N 73 F
BNP 73
12/20/2021 03:31PM

3

Wildlife density estimation using the Random Encounter Model: a comparison between horizontal and vertical camera-trap placements

Background: The random encounter model (REM) provides a robust means to estimate the densities of a wide range of terrestrial mammals from camera-trap data. The REM was developed for surveys that mount camera traps near the ground on vertical structures (trees, posts etc.) with horizontal orientation (hREM), but has recently been adapted to surveys that mount camera traps higher with vertical orientation towards the ground (vREM). Vertical placements have the advantage of reducing the risk of damage by fire, humans, or animals. Whether the methods indeed yield similar density estimates is unknown.

Aim: The aim of this study was to determine whether vertical and horizontal camera-trap orientations produce comparable REM estimates of wildlife density and related parameters.

Methodology: We conducted a field survey where horizontal and vertical camera placements were simultaneously implemented at 36 locations in Bardiya National Park, Nepal (BNP), a protected area that harbours mammals that widely range in body mass, which is helpful given that size influences detectability. We compared capture rate, group size, detection area, activity levels, speed, and REM density estimates between the two setups for seven medium to large-sized mammal species.

Principle findings: hREM and vREM produced comparable parameter estimates for movement speed and activity level. Group size estimates were also consistent between orientations, except for species that occurred in large groups. However, vertical setups showed more variable detection zones and substantially lower capture rates than horizontal setups, particularly at higher mounting positions and among smaller species, resulting in lower density estimates of vREM compared with hREM.

Conclusion: While vertical camera-trap orientation offers advantages in protecting equipment and data, the approach suffered from lower detection rates when mounting heights exceed the effective detection distance of target species without a compensatory reduction in detection zone profile, suggesting an increased tendency to miss animal records and therefore lower density estimates. Further adjustments are needed to correct for these biases.

Key words: abundance estimation; mammal community; camera trapping; detectability

Abstract

3.1 INTRODUCTION

Estimating animal abundance is important for addressing key questions in ecology and conservation biology (Buckland et al., 2005). Camera trapping has become a widely used method for estimating the densities of terrestrial mammals (Burton et al., 2015b; Gilbert et al., 2021). Several methods came out in recent years for estimating population density in non-identifiable species. Chandler and Royle (2013) developed the spatial count model (SCM) with closely spaced sampling sites. Moeller et al. (2018) proposed the time to event (TTE) model with the requirement of independent estimates of animal movement rate. Howe et al. (2017), developed a distance sampling approach with camera traps (CT-DS) to apply distance sampling to camera-trap data, which was extended by Nakashima et al. (2018) to the random encounter and staying time approach (REST). One most widespread approach is the random encounter model (REM; Palencia et al., 2022; Pettigrew et al., 2021; Rowcliffe et al., 2008). REM estimates animal densities from camera-trap data by correcting capture rates for a set of biological variables of the animals (average animal group size, speed, and activity level) and characteristics of camera sensors (Rowcliffe et al., 2008).

Most camera-trap surveys for density estimation with the REM use cameras that are mounted on trees or poles at a low height aimed parallel to the soil surface. A less-used alternative is vertically oriented setups, where cameras are mounted several meters above the ground facing directly downward (De Bondi et al., 2010; He et al., 2025; Meek et al., 2016a). This vertical orientation reduces the risk of damage from large animals such as bears or elephants, lowers the likelihood of theft by humans, and provides a more clearly defined detection zone with less habitat disturbance from dense vegetation (Smith and Coulson, 2012; Meek et al., 2016a). Recently, the vertical Random Encounter Model (vREM) was developed as a modified alternative for density estimation (He et al., 2025). No study has so far compared the performance of the density-estimation models for vertical and horizontal setups.

Horizontal and vertical oriented camera traps differ fundamentally in deployment, detection process, and interactions with animals and the surrounding environment. Horizontally oriented camera traps detect animals within a segment-shaped area defined by a detection angle and radius, whereas vertically oriented cameras detect animals within a rectangular area bounded by the camera's field of view and a fixed detection distance determined by mounting height (Rowcliffe et al., 2008; He et al., 2025). Horizontally oriented camera traps can be influenced by vegetation structure, trail placement, and animal responses to visible devices and the potential damage from them (Smith & Coulson, 2012;

Meek et al., 2016a; Meek et al., 2019). In contrast, vertically oriented camera traps are less affected by vegetation and less likely to be directly encountered, investigated, or damaged by animals (Smith & Coulson, 2012; Taylor et al., 2014). However, vertical orientation also alters the encounter process by restricting detections to animals passing directly beneath the camera. Under horizontal deployments, the majority of detected species, typically medium- to large-bodied terrestrial mammals, enter the field of view from the lower margin as they move across the landscape, whereas under vertical deployments animals can enter the detection area from any direction within the view. At the same time, passive infrared (PIR) sensors, which dominate modern wildlife camera-trap systems and are used in this study, trigger in response to changes in emitted body heat (Wearn & Glover-Kapfer, 2017; Welbourne et al., 2016; He et al., 2025). Under this detection mechanism, vertical deployments can reduce capture rates relative to horizontal deployments, depending on mounting height, species body size, and movement behaviour (Meek et al., 2016a; Moore et al., 2020; Thomas et al., 2020). These differences indicate that density-estimation methods developed for horizontally oriented camera traps cannot be directly transferred to vertical deployments without explicit modification and empirical evaluation To date, aside from He et al. (2025), all the other applications of vertically oriented camera traps have focused on relatively low mounting heights (generally within 3 m above ground) and have primarily targeted small- to medium-sized species (De Bondi et al., 2010; Smith & Coulson, 2012; Taylor et al., 2014; Meek et al., 2016a; Moore et al., 2020; Thomas et al., 2018).

This study aimed to compare REM density estimation between vertical and horizontal camera-trap setups. We conducted a field survey where horizontal and vertical camera placements were simultaneously implemented at 36 locations in Bardiya National Park, Nepal (BNP), a protected area well known as a habitat rich in bird and mammal species. We then compared capture rate, group size, detection area, activity levels, speed, and density estimates between the two setups for the seven mammal species that yielded sufficient observations.

3.2 METHODS

3.2.1 Study area

The study was conducted in the western region of Bardiya National Park (BNP), located in the Terai lowlands of southwestern Nepal. BNP covers a protected area of 968 km² and comprises a landscape of sal (*Shorea robusta*) forests, grasslands, mixed forests, and riverine forests (Dinerstein, 1979; van Lunenburg et al., 2017). The park spans an elevational range from approximately 150 to

1,560 m and includes two main physiographic units: the alluvial Terai plain and the Chure foothills, which are characterized by erosion-prone sediments and seasonal streams. BNP has a tropical monsoon climate with four distinct seasons: a hot and dry pre-monsoon period, a wet monsoon season with frequent flooding, a post-monsoon period, and a cool, dry winter. Mean annual rainfall is approximately 2,300 mm, with around 80% falling during the monsoon, while dry-season conditions are associated with high fire risk. The park is designated as an IUCN Category II protected area with a strictly protected core zone and an actively managed buffer zone (BNPO, 2022). BNP supports diverse bird and mammal communities, including carnivores, mesoherbivores, and megaherbivores, making it a suitable study area for community-level wildlife monitoring and density-estimation studies (BNPO, 2022; DNPWC & DFSC, 2022; He et al., 2025).

3.2.2 Camera-trap deployment and data storage

We deployed 36 paired vertical and horizontal PIR-triggered camera traps (see Table S3.5 for models) in a 1.4 × 1.4 km grid. Vertical cameras were mounted at 4.5-8.4 m by field staff with ladders, elephant-back, or climbing, and horizontal cameras (all Reconyx HF2X, Reconyx Inc., Holmen, USA) were mounted at 50 cm above ground, in such a manner that the two cameras had overlapping detection zones. Vertical camera traps operate from May 2018 to August 2024, and horizontal camera traps from late April to late August 2024, covering both dry and monsoon seasons (June–September; (Thapa et al., 2021). Only observations from late April to late August were used in the analysis to ensure survey overlap. Images were uploaded to Agouti, a web-based platform for processing and archiving camera-trap data (Casaer et al., 2019). Vertical camera images were pre-processed using a trained AI model developed specifically for this deployment and subsequently manually verified. For horizontal cameras, blank captures were filtered out, and the remaining images were then manually verified and annotated. Observations less than 2 minutes apart were merged into a single record.

3.2.3 Detection zone digitisation and animal tracking

Seven terrestrial mammal species had sufficient observations for density estimation: chital (*Axis axis*), Indian hog deer (*Axis porcinus*), Asian elephant (*Elephas maximus*), barking deer (*Muntiacus muntjak*), tiger (*Panthera tigris*), Indian rhinoceros (*Rhinoceros unicornis*), and sambar (*Rusa unicolor*). Domestic elephants were included because the study focuses on methodological comparisons rather than density estimation, and most individuals could not be distinguished from wild elephants in horizontal images when only parts of the body were visible. In vertical setups, detection zones were estimated from

camera height and field of view (FOV) using photogrammetry. The real-world width of the FOV was first calculated from camera geometry using trigonometric relationships. Pixel distance within image was then converted to real-world distance based on the known FOV (Fig. 3.1, He et al., 2025).

In horizontal setups, estimation of animal positions relative to camera, and hence speeds of movement, used the methods described in Wearn et al. (2022, Appendix 2). Calibration was performed in the field using a 1-m pole with alternating 10-cm black–white bands. The pole was held perpendicular to the camera's line of sight, placed every 2 m along the midline up to 14 m, and randomly within ±20° for at least 30 placements. Calibration pole images were digitized in Agouti by marking the highest and lowest visible band boundaries on poles to parameterise a model mapping image pixels to real world ground positions for each deployment. Animal locations within images were then digitised and these locations converted to real-world ground positions using the relevant deployment calibration model. Animal movement paths were tracked by digitising the same frontmost foot across all images of a group observation and converting pixel positions to real-world coordinates. The first individual triggering the camera in each group was tracked. When the front foot was obscured, its position was estimated if an accurate guess was possible. This procedure was consistent for both horizontal and vertical setups, except for large species such as Indian rhinoceros and Asian elephant, for which the central visible body point in the first image was used (He et al., 2025). All processing and visualization were done in R 4.4.0 (R Core Team, 2024). Calibration and digitizing of horizontal setups followed ENETWILD et al. (2023).

3.2.4 Parameter and density estimation

Detection zone profile estimation (the effective path width averaged across all approach angles) followed Rowcliffe et al. (2011) for horizontal cameras and He et al. (2025) for vertical cameras. Profiles for vertical setups were estimated assuming a rectangular detection zone varying by species (body mass), camera height, and camera type using maximum likelihood. Parametric bootstrap (1,000 resamples) with the *boot* package was used to quantify profile uncertainty (Canty & Ripley, 2022). For both orientations, the harmonic mean of speed observations was calculated using the *hmean* function in the *sbd* package (Rowcliffe, 2024), which reduces the influence of faster speeds because animals are more likely to be detected while moving quickly (Rowcliffe et al., 2016). We derived activity level estimates from circular kernel density distribution functions fitted to the times of day of animal records (Rowcliffe et al. 2014). We estimated detection zone profile, speed and activity level parameters using only observations from locations at which both cameras successfully operated

simultaneously in both orientations, but used all available data for capture rate estimation. Except for movement speed and detection zone profile for the vertical orientation, we estimated all other parameters for both orientations using *camtrapDensity* (Rowcliffe, 2025) and *camtraptor* (Oldoni et al. 2025). Density estimation and uncertainty followed Rowcliffe et al. (2008) and He et al. (2025) for horizontal and vertical cameras respectively, with uncertainty in trap rate estimated using non-parametric bootstrapping (1,000 resamples of deployments with replacement), and 95% confidence intervals given by the 2.5% and 97.5% quantiles of the resulting trap rates.

3.3 RESULTS

Thirty-one species were recorded, including nine bird, one amphibian, and 21 mammal species (Table S3.4). Chital was the most recorded species in both orientations, with 1,197 horizontal and 665 vertical detections from paired cameras.

Of the 36 horizontal cameras, seven were damaged by animals (2 lost) and 1 was destroyed by fire. Eight of the 36 vertical deployments failed due to camera malfunction. In total, we had 25 successful pairs that represented a sampling effort of 1,695 days during the focal period. Only these pairs were used for parameter estimation. Captures rates were calculated for all cameras, based on a total effort of 3,071 and 2,594 effort days in horizontal and vertical orientations respectively (Figs. 3.2 and 3.3).

3.3.1 Capture rates

Horizontal cameras recorded nearly two-fold higher capture rates than vertical cameras on average, with differences more pronounced for smaller species (Fig. 3.4 and Table 3.1).

3.3.2 Comparison of detection parameters

Speed estimates were broadly consistent between orientations (Fig. 3.5A and Table 3.1), except for rhinoceros (55 km day^{-1} in horizontal and 29 km day^{-1} in vertical setups). Group size estimates were also comparable except for chital (1.71 in vertical and 2.97 in horizontal setups; Fig. 3.5D and Table 3.1). Activity level was more variable (Fig. 3.5C and Table 3.1). Detection profiles from vertical setups tended to be larger than those from horizontal setups, ranging from 4.01 to 6.41 in vertical and 2.84 to 4.77 in horizontal setups, except for chital and sambar, which show similar values. In vertical setups, detection profile size increased with body mass (Fig. 3.5B and Table 3.1), while in horizontal setups it did not.

3.3.3 Comparison of density estimates

Density estimates were consistently higher for hREM than for vREM across all species, with a nearly three-fold difference on average. Only for rhinoceros and elephant were density estimates close to comparable (Fig. 3.6; Table 3.1).

3.4 DISCUSSION

This study compared REM outcomes from horizontally and vertically oriented cameras (respectively hREM and vREM) under identical field conditions to assess the consistency of their results. The comparison included detection parameters, capture rates, and density estimates for seven mammal species in Bardiya National Park, Nepal, spanning four orders of magnitude in body mass which allowed us to explore differences in species detectability. Eight of the 36 horizontal camera traps were damaged by wildlife or fire, showing the benefit of vertical deployments for minimizing equipment loss (Figs. 3.2 and 3.3). However, vREM yielded lower density estimates than REM, primarily due to lower capture rates, whereas most detection parameters remained comparable between orientations. Lower capture rates were likely caused by missed detections at higher mounting positions.

Two of the three REM parameters were largely consistent between orientations. Movement speed was similar across species except for rhinoceros (Fig. 3.5A; Table 3.1). Rhinoceros appeared particularly sensitive to the presence of horizontal cameras, as several instances were recorded where individuals fled after noticing the devices, which likely contributed to the higher speed estimates derived from the 2024 horizontal camera-trap data (Fig. S3.2). Such species- or individual-specific responses to camera traps have also been shown to influence detection probability (Meek et al., 2016b). However, no clear evidence of comparable responses was observed for other species in this study. Group size estimates were also consistent across most species, except for chital (Fig. 3.5D; Table 3.1), a gregarious species that can form herds of hundreds of individuals (De & Spilt, 1966). Because group size was derived directly from the number of individuals visible in the field of view rather than from the effective detection zone, counting from horizontal setups likely overestimated group size. Adjustments to correct this detection bias are needed. In contrast, estimates of the third parameter, activity level, were less consistent between orientations (Fig. 3.5C; Table 3.1), even though the calculation itself is independent of camera setup. This variability most likely reflects limited sample sizes rather than methodological differences, as activity-level estimation generally requires larger datasets to achieve stable results (Lashley et al., 2018; Rowcliffe et al., 2014b).

Detection profiles showed substantial variation between the two orientations. Larger detection zones were expected in horizontal setups. However, vertical deployments yielded larger estimated detection profiles than horizontal deployments, despite the wider and more distant field of view associated with horizontal cameras (Fig. 3.5B; Table 3.1). At the same time, detection distance did not increase with body mass as expectated (Rowcliffe et al., 2011). In contrast, detection profiles in vertical deployments were consistently larger and showed a clear increase with body mass. These profiles were derived from maximum likelihood estimation, with body mass included as a covariate, and therefore resulting in an increasing pattern between detection profile and body mass in vertical deployments (Table S3.3). Several factors may explain the absence of a clear body-mass pattern in horizontal setups. First, local environmental conditions, including high ambient temperatures during the dry season and dense vegetation structure, may have constrained effective detection distances in horizontal deployments (Hofmeester et al., 2017; Kelly and Holub, 2008; Rowcliffe et al., 2011). In addition, several cameras were placed along animal trails, which may have biased detection distances if animals entered the field of view at short range. Finally, limited sample sizes for some species may also have contributed to imprecise parameter estimation, resulting in smaller estimated effective detection areas.

The component that contributed most to the observed density differences was capture rate. Capture rates were consistently higher in horizontal deployments than in vertical deployments, and this difference decreased with body mass among herbivores (Fig. 3.4; Table 3.1). This pattern is consistent with previous studies reporting higher detection probabilities for horizontally oriented camera traps, particularly for smaller-bodied species (Taylor et al., 2014; Meek et al., 2016a; Moore et al., 2020; Thomas et al., 2018). A primary factor underlying this pattern is the third dimension of deployment: camera mounting height. Estimated effective detection radii for horizontally oriented cameras ranged from 3.44 m (tiger) to 5.55 m (chital) (Table 3.1), whereas most vertical cameras were mounted at heights of 7–8 m (Table S3.6). At these heights, a substantial proportion of animal movements likely occurred outside the effective detection range of the sensors, resulting in missed detections. Under such conditions, recorded detections represent only a subset of individuals passing beneath the camera. Another non-negligible factor lies in the detection mechanism of PIR sensors, the Fresnel lens. In PIR-based camera traps, the Fresnel lens array defines the spatial arrangement of detection zones by focusing infrared radiation from different directions (Welbourne et al., 2016; He et al., 2025; Meek et al., 2024). In most commercially available camera-trap models, Fresnel lenses are designed such that terrestrial animals are most likely to be detected when entering the

field of view from the lower to middle margin of the image. Although animals can still pass through the field of view without triggering the sensor, this design partly explains why appropriate deployment height and angle according to your targeted species are critical for horizontal setups (Meek et al., 2024). Under vertical ("bird's-eye") deployments, animals may pass through gaps between detection zones more frequently, increasing the likelihood of missed detections and reducing overall detection probability.

Because of the differences, particularly in capture rates, density estimates from horizontal setups were higher than those from vertical setups. Two approaches can be considered to correct this bias. First, camera traps should be installed not higher than the effective detection distance (EDD) reported in previous studies, while still minimizing the risk of elephant damage. Such heights should fall within the EDD range of the target species but remain beyond the reach of elephants. Considering the reach of elephants and the detection range of large mammals, mounting heights around 5 m appear optimal for balancing visibility and protection. Second, a general correction framework could be developed using data collected at standardized camera heights across mammal communities with broad and overlapping body-mass ranges. Such data could then be used to adjust for detection biases related to camera height and body mass, which were not available in this study.

3.5 CONCLUSION AND RECOMMENDATIONS

Our study illustrates how vertical camera setups help protect both equipment and data from fire and vandalism. Also, compared with horizontal setups, they offer advantages for species tracking and identification. For instance, in horizontal setups, animals sometimes trigger cameras without entering the field of view, making tracking difficult, whereas such cases occur less frequently in vertical setups. Vertical orientation also improves species identification when medium- to large-bodied animals are too close to the camera for their entire body to be visible, as partial images can still be informative. However, due to missed detections, vertical setups require longer sampling periods than horizontal setups to obtain sufficient observations for parameter estimation. This issue may be mitigated by choosing camera height within the effective detection distance of the target species yet still out of reach from elephants or other agents of camera destruction. The key challenge for wider application of vertical setups remains compensating for missed detections, either through general correction models or optimized deployment heights. At the same time, capture rate is the key empirical input for many camera-trap–based density estimation

methods. Clarifying how deployment decisions influence capture rate allows vertical camera-trap setups to be more effectively integrated into survey design and methodological choice. This provides a broader basis for adapting existing density-estimation frameworks to vertical deployments and supports wider application of this alternative deployment strategy.

3.6 ACKNOWLEDGEMENTS

We thank Bardiya National Park (BNP), National Trust for Nature Conservation (NTNC), and Department of National Parks and Wildlife Conservation (DNPWC) for their help and support; Wildlife Ecology and Conservation group, Wageningen University & Research, and the Himalayan Tiger Foundation for funding the Bardiya survey; the Chinese Scholarship Council (CSC) for funding the PhD project; NTNC field technicians, who diligently maintained the camera trap network in BNP, in particular Ram Raj Chaudhary, Khusiram Chaudhary, Phirulala Tharu, Tikaram Tharu, and Kararu Tharu, and Santigali, the elephant field technician of NTNC; Hanzhe Lin for making Fig. 3.1.

3.7 DATA AND METHODS AVAILABILITY

Codes and methods for horizontal density estimation are available at https://github.com/MarcusRowcliffe. Codes and data for vertical density estimation are available at https://github.com/Shuiqinghe.

TABLES

Table 3.1 Summary of REM and vREM density estimates (individuals km^{-2}) and associated parameters for seven mammal species in Bardiya National Park, Nepal. Parameters including detection radius (m) and angle (radians) from horizontal setups, group size, movement speed (km day^{-1}), and activity level. Body mass (BM) data are sourced from PHYLACINE 1.2 (Faurby et al., 2018a).

Species	BM (kg)	Orientation	RAI (n/100d)	Group size	Radius (m)	Angle (radian)	Profile (m)	Speed (km/d)	Activity level	Density (n/km2)
Chital	66	V	39.23	1.71 ±0.1	-	-	4.1 ±0.07	15.54 ±2.06	0.22 ±0.01	51.8 ±19.3
		H	70.62	2.97 ±0.23	5.55 ±0.6	0.69 ±0.05	4.77 ±0.53	13.2 ±1.89	0.25 ±0.01	131 ±26
Barking deer	16	V	2.54	1.06 ±0.02	-	-	4.01 ±0.07	20.15 ±2.94	0.37 ±0.04	1.01 ±0.72
		H	6.9	1.06 ±0.03	3.45 ±0.28	0.72 ±0.08	2.99 ±0.27	10.53 ±1.75	0.34 ±0.03	7.17 ±1.58
Sambar	180	V	0.94	1.15 ±0.07	-	-	4.25 ±0.07	17 ±3.52	0.58 ±0.07	0.28 ±0.09
		H	2.01	1.35 ±0.14	4.9 ±0.71	0.86 ±0.13	4.45 ±0.68	16.99 ±8.07	0.51 ±0.07	0.7 ±0.37
Tiger	163	V	0.94	1 ±0	-	-	4.22 ±0.07	40.2 ±9.09	0.67 ±0.08	0.07 ±0.03
		H	2.95	1 ±0	3.44 ±0.34	0.6 ±0.07	2.84 ±0.29	41.6 ±15.47	0.53 ±0.09	0.47 ±0.19
Rhinoc-eros	1,602	V	0.59	1.14 ±0.05	-	-	5.38 ±0.11	28.45 ±8.41	0.46 ±0.07	0.1 ±0.06
		H	0.83	1.17 ±0.05	3.97 ±0.48	0.68 ±0.09	3.37 ±0.43	55.27 ±6.88	0.3 ±0.05	0.17 ±0.04
Hog deer	34	V	1.36	1.17 ±0.05	-	-	4.05 ±0.07	12.12 ±2.99	0.59 ±0.08	0.61 ±0.31
		H	2.89	1.33 ±0.09	3.63 ±0.3	0.71 ±0.07	3.13 ±0.26	16.81 ±2.79	0.39 ±0.04	1.82 ±0.41
Elephant	3,160	V	2.54	1.87 ±0.18	-	-	6.41 ±0.17	31.02 ±6.06	0.27 ±0.04	0.95 ±0.5
		H	2.77	1.71 ±0.22	3.49 ±0.38	1.12 ±0.15	3.45 ±0.43	31.06 ±7.54	0.31 ±0.05	1.42 ±0.48

FIGURES

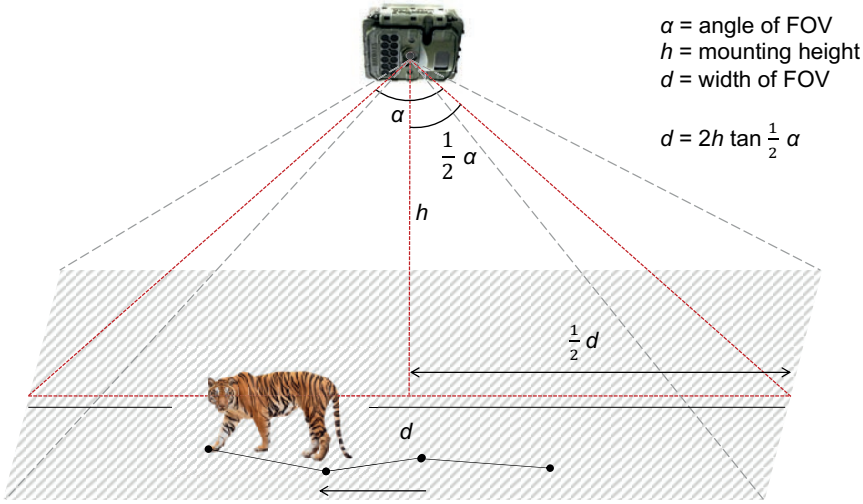


Figure 3.1 Estimation of the detection zone using photogrammetry and trigonometric relationships. The angle and width of FOV are defined by α and *d, h* represents the camera mounting height.

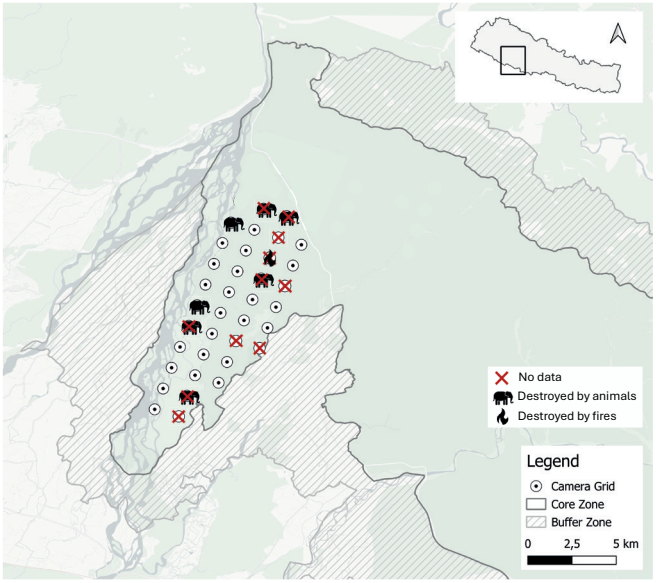


Figure 3.2 Map of camera-trap deployments in western Bardiya National Park, Nepal. White dots indicate paired deployments used for trap rate estimation. Animal and fire icons mark sites at which horizontal cameras were destroyed by wildlife and fire respectively, while red crosses indicate broken or missing cameras, mainly from vertical setups. The inset map (top right) shows the location of Bardiya National Park within Nepal.



Figure 3.3 (A) Elephant pulling down and inspecting a camera trap; (B) destroyed camera trap found in the field; (C) elephant pushing the camera trap with its trunk; (D) camera tilted toward the ground after elephant attack; (E) field of view during fire; (F) field of view after fire.

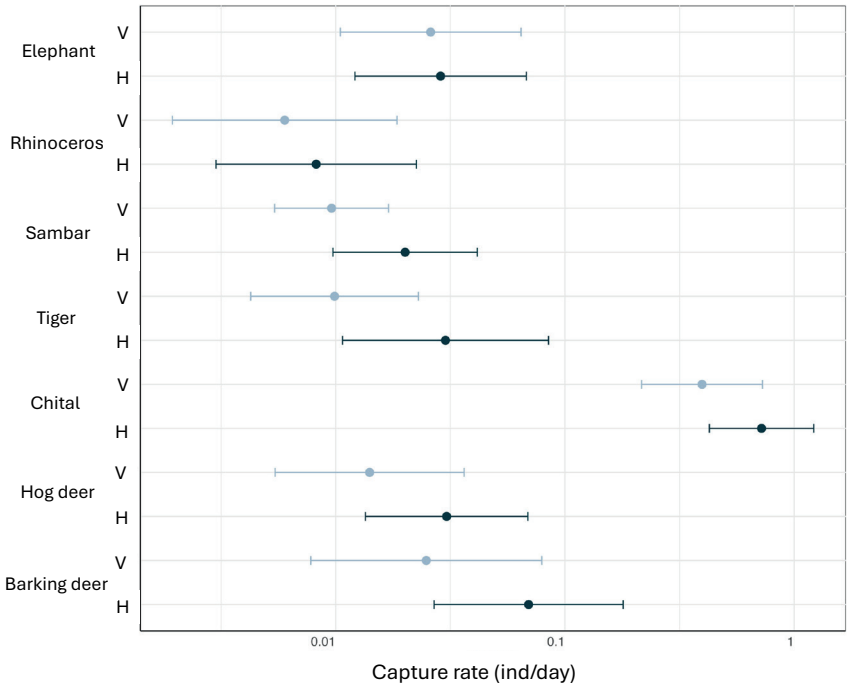


Figure 3.4 Capture rates estimated from paired sites using horizontal and vertical camera-trap data for seven mammal species in Bardiya National Park, Nepal, arranged by body mass from low to high. Letters "H" and "V" indicate parameters from horizontal and vertical setups respectively. Uncertainty is represented by 95% ln-transformed confidence intervals.

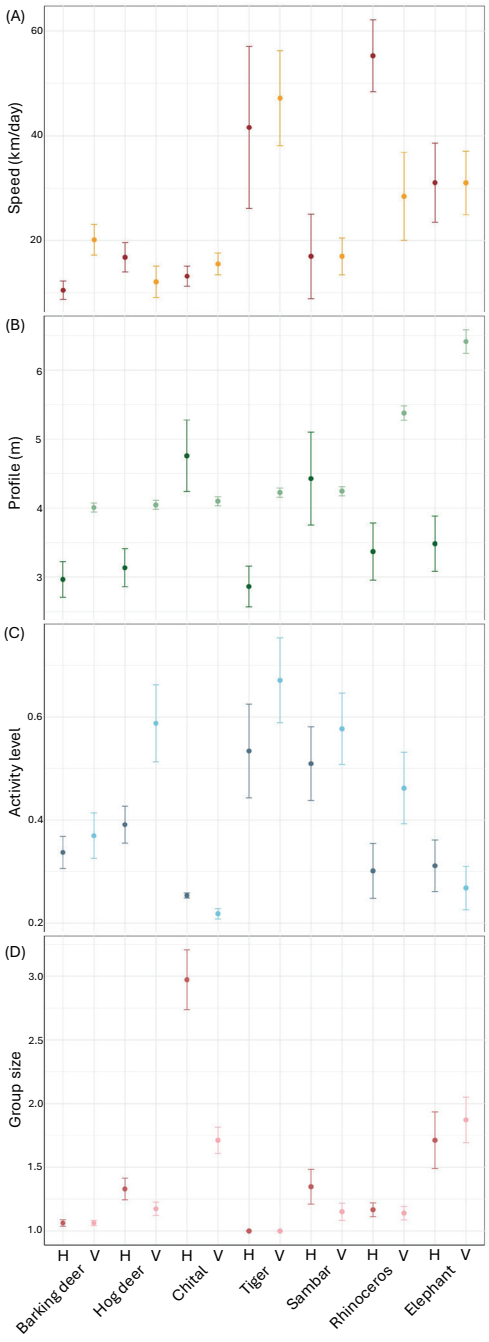


Figure 3.5 Parameter estimates from horizontal and vertical camera-trap data for seven mammal species in Bardiya National Park, Nepal, arranged by body mass from low to high: (A) movement speed (km day^{-1}); (B) detection zone profiles (m), with vertical profiles representing mean values across sites with different camera models and heights; (D) activity levels; (D) group size.

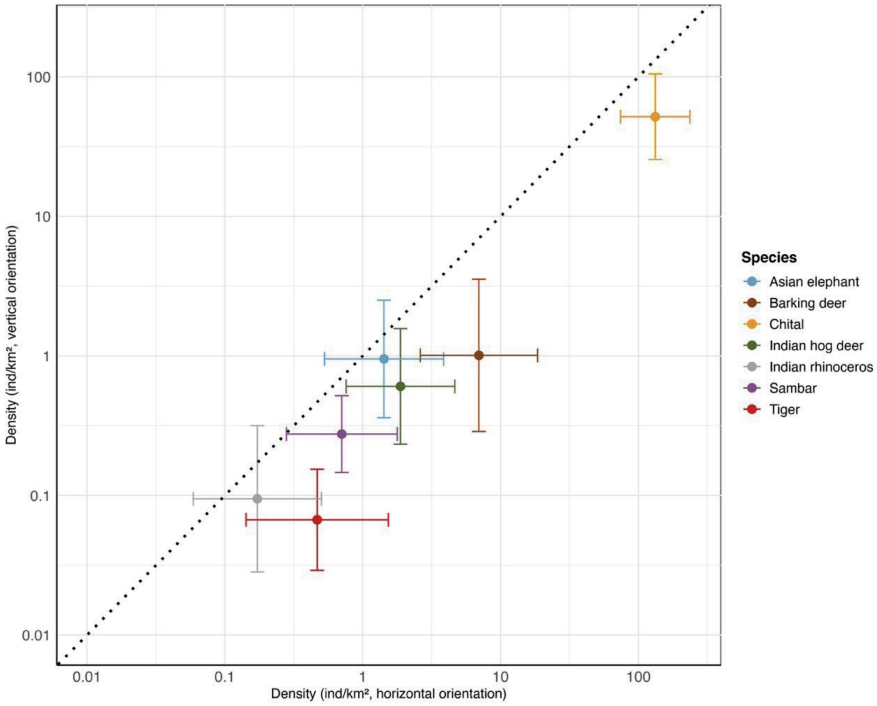


Figure 3.6 Comparison of density estimates from REM analysis of data from vertically (y axis) versus horizontal (x axis) camera trap orientations for seven mammal species in Bardiya National Park, Nepal. The black dotted line is the identity line (y = x). The closer the point is to this line, the more similar the two estimates are. Axes are $\log_{10}$-transformed. Error bars show 95% ln-transformed confidence intervals.

SUPPORTING INFORMATION

Table S3.1 Observations from simultaneous and full deployments used to estimate trapping rates and model parameters during the study period.

Orientation	Common Name	Simultaneous	All
Vertical	Chital	665	785
Vertical	Barking deer	43	53
Vertical	Sambar deer	16	31
Vertical	Tiger	16	28
Vertical	Indian rhinoceros	10	12
Vertical	Indian hog deer	23	25
Vertical	Asian elephant	43	55
Horizontal	Chital	1,197	2,910
Horizontal	Barking deer	117	190
Horizontal	Sambar deer	34	58
Horizontal	Tiger	50	85
Horizontal	Indian rhinoceros	14	56
Horizontal	Indian hog deer	49	297
Horizontal	Asian elephant	47	82

Table S3.2 Sample size for parameter estimation.

Orientation	Common Name	Radius	Angle	speed	Activity level	Group size
Vertical	Chital	-	-	318	930	361
Vertical	Barking deer	-	-	129	146	142
Vertical	Sambar deer	-	-	51	53	53
Vertical	Tiger	-	-	77	84	84
Vertical	Indian rhinoceros	-	-	54	59	57
Vertical	Indian hog deer	-	-	76	90	86
Vertical	Asian elephant	-	-	83	100	86
Horizontal	Chital	100	179	159	2,914	182
Horizontal	Barking deer	102	113	107	185	112
Horizontal	Sambar deer	29	46	40	58	46
Horizontal	Tiger	55	65	47	85	65
Horizontal	Indian rhinoceros	35	48	37	56	48
Horizontal	Indian hog deer	107	128	110	296	124
Horizontal	Asian elephant	40	65	45	82	66

Table S3.3 Coefficients from the summary result of the best fit model using *mle2* function: 0.5*width ~ height + body mass + camera type; ratio ~ camera type. 0.5*width was ln-transformed and body mass was power-transformed with an exponent of 2/3 (Schmidt-Nielsen, 1984). The ratio (height/width) defines the shape of the detection zone from different types of camera traps.

Response	Estimate	Std. Error	Z value	Pr(z)
0.5*width intercept: Browning	-0.5609	0.1256	-4.4663	***
0.5*width height (m):	0.1548	0.0167	9.2790	***
0.5*width body mass (kg)	0.0023	0.0001	18.4080	***
0.5*width intercept: Reconyx HC500	-0.3878	0.0923	-4.2004	***
0.5*width intercept: Reconyx Hyperfire 2	-0.2980	0.0236	-12.6307	***
Ratio: Browning	0.3523	0.0085	41.3668	***
Ratio: Reconyx HC500	0.2141	0.0734	2.9172	**
Ratio: Reconyx Hyperfire 2	0.0086	0.0119	0.7272	

Table S3.4 List of all captured species.

Class	Order	Scientific name	Common name
Aves	Accipitriformes	*Circus pygargus*	Montagu's harrier
	Columbiformes	*Spilopelia chinensis*	spotted turtledove
		Chalcophaps indica	emerald dove
		Gallus gallus	Red junglefowl
		Pavo cristatus	Indian peafowl
		Pavo muticus	Green peafowl
	Perissodactyla	*Rhinoceros unicornis*	Greater one-horned rhinoceros
	Pholidota	*Manis pentadactyla*	Chinese pangolin
	Proboscidea	*Elephas maximus*	Asian elephant
Mammalia	Artiodactyla	*Axis axis*	Chital
		Axis porcinus	Indian hog deer
		Muntiacus muntjak	Barking deer
		Rucervus duvaucelii	Barasingha
		Rusa unicolor	Sambar deer
		Sus scrofa	Wild boar
	Carnivora	*Arctictis binturong*	Binturong
		Canis aureus	Golden jackal
		Herpestes edwardsi	Indian grey mongoose
		Herpestes javanicus	Javan mongoose
		Leopardus pardalis	Ocelot
		Mellivora capensis	Honey badger
		Panthera pardus	Leopard
		Panthera tigris	Tiger

Table S3.4 Continued

Class	Order	Scientific name	Common name
		Paradoxurus hermaphroditus	Asian palm civet
		Viverra zibetha	Large Indian civet
		Viverricula indica	Small Indian civet
	Lagomorpha	*Caprolagus hispidus*	Hispid hare
	Primates	*Macaca mulatta*	Rhesus macaque
		Semnopithecus schistaceus	Nepal gray langur
	Rodentia	*Hystrix indica*	Indian crested porcupine
Reptilia	Squamata	*Varanus bengalensis*	Bengal monitor

Table S3.5 Camera types used in the survey.

Camera type	FOV (°)	Source
Browning BTC-5HDPX	55	Instruction manual
Reconyx HYPERFIRE 2	38	Official support manager
Reconyx HC500 (HYPERFIRE)	42	Official support manager

Table S3.6 Vertical deployments and their mounting heights in Bardia National Park, Nepal.

Location	Height
BNP-01	4.5
BNP-02	7.25
BNP-03	7.5
BNP-04	8.1
BNP-05	7.35
BNP-06	7.1
BNP-07	7.15
BNP-08	7.6
BNP-09	7.5
BNP-10	7.3
BNP-11	7.5
BNP-12	8.4
BNP-13	7.5
BNP-14	7.16
BNP-15	7.1
BNP-16	8.2
BNP-17	7.5
BNP-18	7.08
BNP-19	7.5

Table S3.6 Continued

Location	Height
BNP-20	7.75
BNP-21	7.8
BNP-22	7.35
BNP-23	7.35
BNP-24	7.5
BNP-25	7
BNP-26	7.4
BNP-27	7.2
BNP-28	7.4
BNP-29	8.1
BNP-30	7.25
BNP-31	7.7
BNP-32	7.1
BNP-33	7
BNP-34	7.1
BNP-36	7.7
BNP-37	7.4

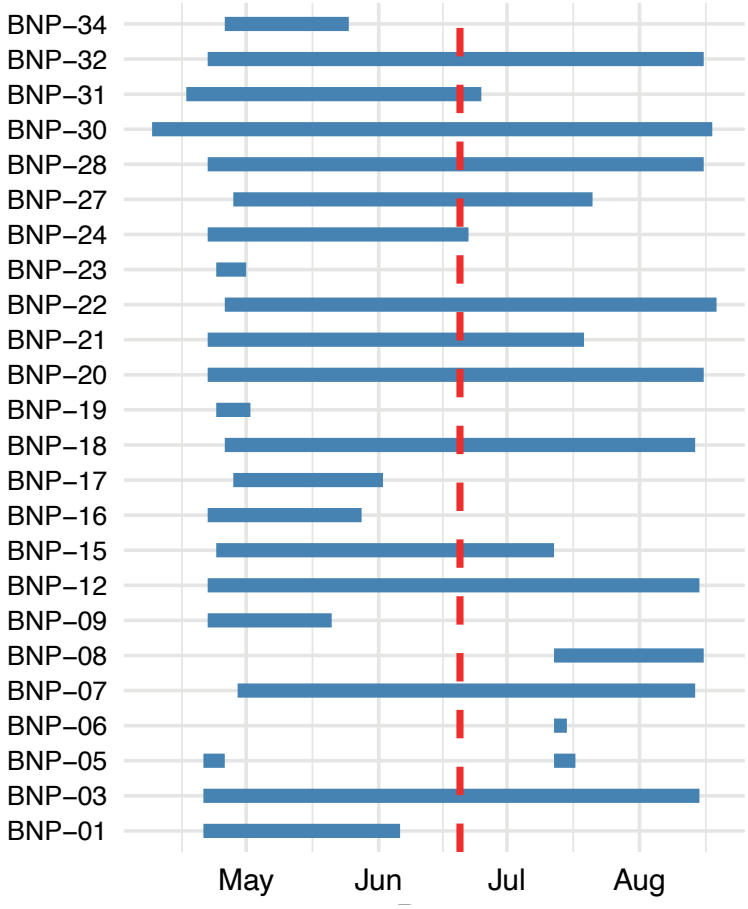


Figure S3.1 Deployment duration at paired sites with both horizontal and vertical camera trapping setups during the study period in Bardiya National Park, Nepal. Red line indicates the start of the monsoon season.



Figure S3.2 Rhinoceros fled after noticing horizontal camera traps in Bardiya National Park, Nepal.


024-08-16 12:46:22
M 1/10
28°C
NP-19H
RECONYX

4

Does controlling for body size and diet improve relative abundance estimates for macroecological studies using camera-trap data?

Abstract

Background: Camera trapping offers a convenient opportunity for assessing the species composition of terrestrial mammal communities. The estimation of relative abundance index (RAI), however, is hampered by interspecific differences in detectability by camera traps and can therefore be unsuitable for interspecific comparisons.

Aim: This study explores whether body-mass scaling relationships based on Random Encounter Model can be used to minimise the bias in RAI to better represent variation in true abundance within terrestrial mammal communities.

Methodology: We first estimated scaling relationships for various determinants of animal detectability by camera traps with contrasting body mass and diet. We then combined these relationships with Random Encounter Model (REM) into a macro-corrected RAI (mRAI). Finally, camera-trap data from studies with known animal densities were used to determine whether mRAI represented the relative abundance of species better than the ordinary RAI.

Principal findings: Day range, effective detection distance (EDD), and effective detection angle (EDA) showed significant scaling with body mass, with day range differing between faunivores and herbivores. The range of mRAI density estimates were on similar scales to independent estimates with improved fits to independent density estimates in most communities.

Innovation: Derived from the Random Encounter Model, mRAI serves as a valuable proxy for animal abundance in large-scale macroecological studies as a simple and practical means of extracting meaningful ecological insights from extensive existing camera-trap datasets.

Main conclusions: While there were significant relationships between RAI and density, mRAI estimates on the whole provided a better fit in slope and fit. Its consistency, however, can be improved, as detectability likely depends on factors beyond body mass and diet. Nevertheless, these results indicate that mRAI provides a valuable proxy for animal abundance in large-scale macroecological studies. It provides a simple and practical alternative for extracting valuable ecological information from large amounts of existing camera-trapping data.

Keywords: abundance estimation; bias improving; camera trapping; body mass scaling; mammal community; detectability

4.1 INTRODUCTION

Animal abundance is a key variable in many important questions in ecology and conservation biology (Andrewartha & Birch, 1954; Damuth, 1981). Camera trapping provides a practical, non-invasive method for estimating the abundance of terrestrial mammals, and has been extensively used in wildlife and biodiversity research and conservation worldwide over the past decades (Burton et al., 2015b). However, the ability to estimate the abundance of individually unmarked species (the majority of mammals) has been severely limited. Previous studies have used relative abundance indices (RAIs) as a proxy for abundance (Carbone et al., 2001; O'Brien et al., 2003), but RAIs have been criticized for potential bias due to differences in detection probability between species, environment, and camera deployments (Carbone et al., 2001; MacKenzie et al., 2002; Sollmann et al., 2013). Nearly all camera traps use passive infrared sensors (PIR) to detect heat being emitted from the surfaces of objects in motion (Welbourne et al., 2016). Larger animals passing in front of camera traps are thus more likely to be detected as they emit more heat (Rowcliffe et al., 2011; McNab, 1980). Moreover, longer daily travel distances make larger species more likely to pass in front of camera traps (Carbone et al., 2005). As a result, RAIs may not accurately reflect the relative abundance across species within communities or even across populations within a species.

In contrast, the Random Encounter Model (REM), camera trap distance sampling (CT-DS), Time to Event (TTE), Random Encounter and Staying Time (REST), and related methods do represent robust and comprehensive methods to estimate the density of unmarked species (Howe et al., 2017; Moeller et al., 2018b; Nakashima et al., 2018b; Rowcliffe et al., 2008a). The REM, for example, uses estimates of speed, activity, and camera detection parameters to estimate density from camera trap data, which is based on a theoretical framework known as gas models (Hutchinson and Waser, 2007). However, this method involves a number of additional steps including the need to track animal positions within the photographic record, and while automated methods are in development, currently this approach is time-consuming, potentially limiting its wider use.

Body mass appears to be a key factor underlying interspecific differences in individual detectability within mammal communities. Scaling relationships between body mass and several determinants of detectability have been found in prior studies. Specifically, effective detection distance (EDD), effective detection angle (EDA), movement speed, activity level or day range (the product of movement speed and activity level) all scale with body mass to some degree (Carbone et al., 2005; Rowcliffe et al., 2011, 2014, & 2016). For day range, these

relationships also differ with diet, in faunivores and herbivores (Carbone et al., 2005; Rowcliffe et al., 2016). This raises the question of whether these scaling relationships due to body mass and diet can be incorporated into RAI estimates to produce a macro-corrected RAI (mRAI) that better reflects the relative abundance of species within communities.

This study explores whether body-mass scaling relationships can be used to alleviate the bias in RAI based on REM to better represent relative abundance for multiple species within terrestrial mammal communities. We first estimated scaling relationships for three determinants of animal detectability by camera traps, using existing data from species with contrasting body mass and diet. We then combined these relationships within an REM framework to produce mRAI. Finally, camera-trap data from studies with known animal densities were used to determine whether this mRAI indeed represented the relative abundance of species within communities better than the ordinary RAI through comparing regression fits (R square), the ranges of mRAI and independently estimated density, as well as the slopes of the relationships between RAI, mRAI, and density.

4.2 METHODS

4.2.1 Data collection

Data from two types of camera-trap studies were compiled. The first type includes three determinants of detectability of mammal species: day range, EDD and EDA, which vary in body mass and diet (Carbone et al., 2005; BCI team, unpublished; He et al., 2025; N. Heida, unpublished; Wearn et al., 2022; Véliz Rosas, unpublished; Rowcliffe et al., 2011; Hofmeester et al., 2017). The second included studies with both RAI and independently estimated density estimate (BCI team, unpublished; Wearn et al., 2022; O'Brien et al., 2003; He et al., 2025). Three of these studies used horizontal oriented camera traps (BCI team, unpublished; Wearn et al., 2022; O'Brien et al., 2003) and one of them used vertical oriented camera traps (He et al., 2025). Body mass data of all mammal species in these studies were obtained from PHYLACINE 1.2 . Dietary classification — animalivore, herbivore, omnivore, and frugivore— was done using the method outlined by Lintulaakso et al. (2023), which categorizes species based on the taxonomy of consumed food items and plant parts. These four diets were further classified into faunivore and herbivore.

4.2.2 Mass-corrected RAI

REM for wildlife density estimation, derived from the ideal gas model, reasons that the likelihood of an animal being detected by a randomly placed camera

traps is determined by four species-specific factors: (1) the effective detection angle of the camera, (2) the effective detection distance of the camera, (3) activity level of the animal, and (4) movement speed of the animal while active. Day range was applied to represent activity level and movement speed of the animal in this study (Carbone et al., 2005). EDD was used as a proxy for the sensitivity of camera trap sensors, following previous studies (Hofmeester et al., 2017; Rowcliffe et al., 2011). For day range and body mass, we conducted power regressions fitting to the $\log_{10}$-transformed values. Camera-based estimates of effective distance to detection (EDD) are limited in the literature due to the relatively recent use of the latter versions of the REM Model (Rowcliffe et al. 2011). Therefore, we used published estimates of EDD, but with a slope constrained by the following theoretical derivation. For detection distance, we assumed that in the real world, area coverage of an animal scales with the body mass $M^{2/3}$ (Schmidt-Nielsen, 1984). Additionally, we assume a camera trap requires a fixed minimum warm-bodied area or 2D profile, to trigger the camera. According to the pinhole camera model (Hartley & Zisserman, 2004), the perceived linear size of an object scales with distance as d^{-1}, and thus the profile in 2D area scales as d^{-2}. Among mammals, the side profile area in 2D is proportional to $M^{2/3}$ which when multiplied by size in image with distance, we expect maximum detection distance d is proportional to $M^{1/3}$. Based on this theoretical relationship, we fixed the exponent for effective detection distance (EDD) to 0.33, and used the resulting regression model to estimated the intercept.

We first estimated the scaling relationships between day range, EDD, EDA, and body mass (Equation 1-3). Day range was represented by *r*, which scales to the body mass *M* to the exponent *q* with constant *k*, both derived from day range scaling. EDD, represented by *d*, scales to *M* to the 0.33 power to estimate the fitted constant. EDA, represented by ø, which scales to the *M* to the exponent *h* with constant *g*, both derived from EDA scaling. Constants *k*, *c*, and *g*, as well as exponent *q* and *h*, were estimated as the intercepts and slope of $\log_{10}$-transformed regressions. The exponents and constants estimated from scaling relationships were then incorporated with REM to adjust RAI into mRAI with density (*D*), and body mass into a new metric, the mRAI (Equation 4). Both day range and EDD were measured in kilometers for consistency, q in radians, body mass *M* in kilograms, and mRAI in individuals/km^2. We also used data from an REM study using vertically placed cameras. For this study we have adapted the equation to account for the limited effect of size on detection area (He et al., 2025).

$$r = k * M^{q} \quad \textit{Equation 1}$$

$$d = c * M^{0.33} \quad \textit{Equation 2}$$

$$\mathrm{q} = g * M^{h} \quad \textit{Equation 3}$$

$$mRAI = RAI * \pi / kc * M^{q+0.33} * (2 + gM^{h})) \quad \textit{Equation 4}$$

4.2.3 Model evaluation

We considered the modification valid if the scale of mRAIs aligned more closely with independently estimated densities than did the ordinary RAIs. Specifically, we assessed (1) whether the numerical ranges of mRAIs better matched that of the independent density estimates; (2) whether the fits (R square) of the $\log_{10}$-transformed relationships between mRAIs and densities improved relative to RAIs. (3) whether the relationships between the logarithm of mRAIs and densities had a slope closer to 1, i.e., mRAIs would be more proportional to actual densities than RAIs. The model was evaluated across all species, as well as within dietary groups. One-sample t-tests were performed in R to assess whether the slope estimates differed significantly from 1 (Lenth, 1989).

4.3 RESULTS

4.3.1 Scaling of detectability

Day range was positively associated with body mass in both faunivores and herbivores, with estimated slopes of 0.45 and 0.28, respectively (Fig. 4.1; Table 4.1). The relationship was stronger in faunivores, indicating a steeper increase in day range with body mass compared to herbivores. For EDD in relation to body mass, the best-fitted intercept given a slope of 0.33 was calculated based on the minimum residual sum of squares. EDA was positively associated with body mass across all species, with an estimated slope of 0.03.

Based on equation 4, substituting the values from respective scaling relationships, we got the separate equations for mRAI for faunivores and herbivores separately:

$$\textit{Faunivore: } mRAI_{f} = RAI * \pi / (0.004 * M^{0.779} * (2 + 0.561 * M^{0.032})) \quad \textit{Equation 5}$$

$$\textit{Herbivore: } mRAI_{h} = RAI * \pi / (0.002 * M^{0.607} * (2 + 0.561 * M^{0.032})) \quad \textit{Equation 6}$$

4.3.2 Evaluation

Studies of mammal communities that included both camera-trap capture rates and independently estimated densities were used to evaluate the performance of mRAI. Across all communities, mRAIs showed strong alignment in range with independently estimated densities (Table 4.3; Fig. 4.2). A closer fit to 1:1 and an increased R square were found in 3 out of 5 communities compared to RAI. The fits of the other two communities (Wearn et al., 2022) remained comparable (Table 4.2; Fig. 4.2). These findings mean that, body mass-based adjustments improved the accuracy of relative abundance estimates and shows promising consistency in scaling with actual density values.

4.4 DISCUSSION

There has been considerable debate about the validity of using capture rates in camera trap studies as a method for estimating relative abundance because these rates may be confounded by factors influencing detectability. This study investigated whether general scaling relationships could be used to account for variation in detectability related to body mass and diet. We found that a mass-corrected relative abundance index, mRAI, effectively improved animal density estimation and value ranges of mRAI robustly aligned with independently estimated densities. While there is room for improved estimates which are currently limited by the amount of available data derived from REM camera-trap studies, mRAI presents a robust approach for estimating animal densities.

Strong power relationships between day range and body mass varying in different diets were observed, aligning with findings from previous studies (e.g., Carbone et al., 2005; Rowcliffe et al., 2011, 2014, & 2016; Ramesh et al., 2015). Larger mammal species generally display higher activity levels, likely due to the increased time required to meet their greater energetic demands. For example, large herbivores often spend extended periods foraging, reflecting the low nutritional quality of their generalist diets, while carnivores typically travel longer distances to locate prey (McNab, 1963; Weckerly, 2013). Additionally, the positive relationship observed between EDD, EDA, and body mass in this study is consistent with earlier studies finding that larger species are detected from greater distances and wider angles by passive infrared (PIR) camera sensors (Rowcliffe et al., 2011; Hofmeester et al., 2017; Welbourne et al., 2016). While the estimated slopes from the earlier studies were lower than the expected theoretical value of 0.33, this discrepancy may be due to the limited range of body sizes among sampled species (species with extreme body sizes were underrepresented).

Therefore, we believe that the use of a theoretically derived exponent of 0.33 is justified until data on a wider body mass range of species becomes available.

Robust fits and aligned ranges were observed between mRAI and independently estimated densities. This finding highlights the potential of using camera trap capture rates alone to estimate mammal density and, by extension, to infer additional ecological information e.g., total population size, biomass, energy flow, and ecosystem health. Density estimates provide critical insights into mammal communities (Andrewartha & Birch, 1954; Damuth, 1981). Many existing methods offer more robust and comprehensive approaches for estimating the density of animals, particularly unmarked species (Howe et al., 2017; Moeller et al., 2018; Nakashima et al., 2018; Rowcliffe et al., 2008). However, these approaches often require intensive fieldwork and detailed parameter measurements at the community level, while the mRAI method presents a comparatively efficient and cost-effective alternative. It presents an important opportunity to make broader use of existing RAIs, particularly from historical studies where density estimates are no longer obtainable, or in regions and species where density estimation can be challenging. With large amounts of camera-trapping data collected and accumulated over the past decades (Burton et al., 2015), greater value can be realized if useful ecological information can be extracted using comparatively robust and accessible methods with existing data.

Although improved fits and aligned ranges between mRAIs and independently estimated densities were observed, this approach would be further improved by having a wider collection of camera-trap data with which to estimate how size and diet influence detectability. In addition, in future, we may develop ways of incorporating habitat factors in these estimates. One such factor may be the variability in scaling relationships across different environments. For instance, the EOW study (ENETWILD et al., 2023) found that body mass-related parameters in herbivores vary substantially across European sites. To better understand such variability, it may be useful to categorize the determinants of detectability into two perspectives: animal-based factors (e.g., movement speed and activity level) and camera trap-based factors (e.g., effective detection distance, EDD). Our results suggests that while mRAI has the potential to reflect true species density across diverse communities.

Many factors affect the movement and activity strategies of mammals. For instance, vegetation density has been shown to affect animal movement speeds, with animals moving faster in open areas compared to densely vegetated regions with more food resources (De Knegt et al., 2011). Additionally, animal speed and activity levels differ between urban and non-urban environments

and across regions with varying degrees of anthropogenic pressure (Lovell et al., 2022; Tucker et al., 2021). For faunivores, activity timing appears to be more closely related to prey size than to the predator's own body mass (Rizzuto et al., 2018). Group behavior further influences estimates of movement speed, as highlighted by Palencia et al. (2022). Together, these findings illustrate why body mass alone can be insufficient to fully explain the movement and activity patterns of mammals.

Likewise, the detection distance of camera traps may be influenced by other factors in addition to body mass. Passive Infrared (PIR) sensors in camera traps are triggered by differences in emitted heat between the animal and its environment (Welbourne et al., 2016). Consequently, even individuals or species of similar body mass may exhibit differing detection distances. For instance, the thickness of an animal's fur can influence the amount of heat emitted and affect detection (Montanholi et al., 2008). Seasonal or temperature variations can also impact camera trap effectiveness (Newey et al., 2015). Furthermore, landscape features, particularly uneven terrain within the camera's field of view, can alter detection probabilities (Sultaire et al., 2023). Dense vegetation can influence both animal movement speed and detection distance (Hofmeester et al., 2017). Thus, factors other than body mass and density can be responsible for the determinants of day range and detection distance.

4.5 CONCLUSION

While species- and community-specific parameterization is generally a more accurate method for animal density estimation, the mRAI, derived from the Random Encounter Model (REM), provides a simple and practical alternative, particularly in difficult-to-access areas or for elusive species. mRAI also enables the extraction of valuable insights into mammal communities from large existing camera-trap datasets. Although there is potential for improvement in the consistency of mRAI's performance, this suggests that interspecific differences in detectability during camera-trap surveys are influenced by factors such as body shape, posture, thermal characteristics, and behavioral variations, in addition to body mass scaling. Given species specific characteristics and site-based differences in vegetation structure, where possible, we would recommend adopting an REM approach allowing for species-specific and site-specific estimates for speed, detection distance and angle. However, the results highlight mRAI's strong potential as a proxy for animal abundance, offering a practical tool for large-scale macroecological studies and the extraction of ecological information from extensive camera-trap datasets.

TABLES

Table 4.1 Scaling coefficients of the log_{10}-transformed power relationships between day range, EDD (slope fixed at 0.33), EDA, and body mass.

Response		Slope	Intercept	Std.Error	DF	t value	Pr(>|t|)	R square
Day range	Faunivore	0.45	0.28	0.05	281	9.88	***	0.37
	Herbivore	0.28	-0.03	0.07	281	3.70	**	0.37
EDD	All species	0.33	-2.67	-	-	-	-	0.48
EDA	All species	0.03	-0.25	0.01	108	4.57	***	0.33

Table 4.2 Coefficients of the linear regressions between RAI, mRAI, and independently estimated densities.

		Slope	Std.Error	DF	t value (compared with 1)	Pr(>|t|)	R^2
O'Brien et al., 2003	RAI	0.44	0.17	4	3.41	*	0.55
	mRAI	1.02	0.26	4	0.07	-	0.75
Wearn et al., 2022	RAI	0.99	0.07	28	0.21	-	0.88
(old grownth forest)	mRAI	0.97	0.09	28	0.37	-	0.82
Wearn et al., 2022	RAI	0.98	0.05	26	0.46	-	0.93
(logged forest)	mRAI	0.87	0.10	26	1.28	-	0.74
BCI team, unpublished	RAI	0.81	0.18	7	1.06	-	0.72
	mRAI	1.04	0.13	7	0.30	-	0.89
He et al., 2025	RAI	0.76	0.09	10	2.83	*	0.88
	mRAI	1.03	0.07	10	0.41	-	0.95

Table 4.3 Range of mRAIs and independently estimated densities in communities. The unit of mRAI and density is individuals per square kilometer. Values in the square brackets refer to minimum and maximum values within the category.

	mRAI range	Density range
O'brien et al., 2003	[0.0144, 15.7746]	[0.0156, 5.0200]
Wearn et al., 2022 (old grownth forest)	[0.0203, 24.5891]	[0.0100, 17.1900]
Wearn et al., 2022 (logged forest)	[0.0059, 10.1254]	[0.0100, 6.7400]
BCI team, unpublished	[1.3299, 205.3423]	[0.7376, 86.7240]
He et al., 2025	[0.2893, 236.4419]	[0.2200, 154.8800]

FIGURES

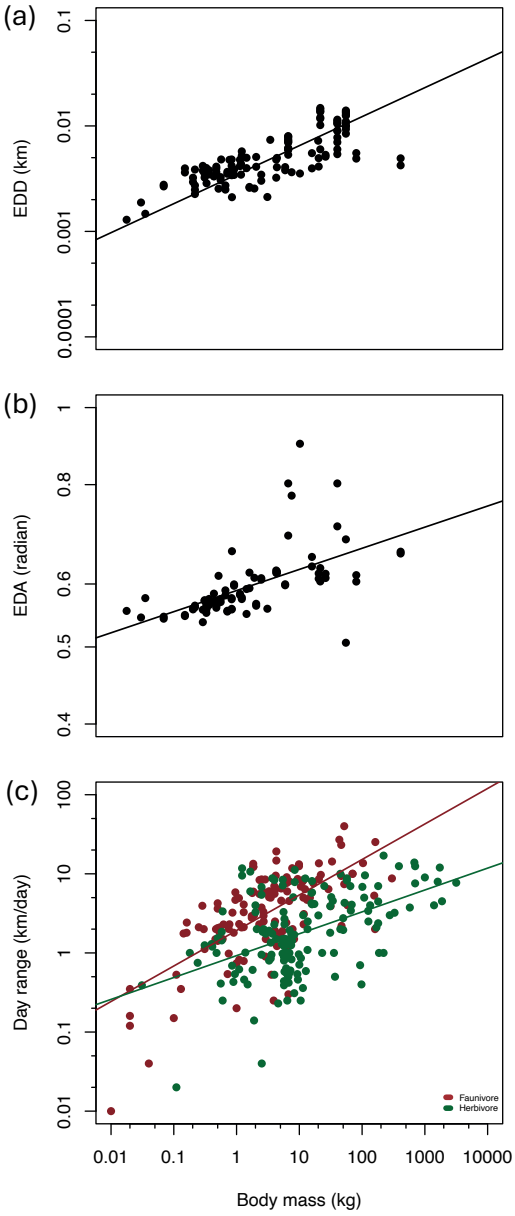


Figure 4.1 Scaling relationships between (A) Effective Detection Distance EDD (km) and body mass (kg); (B) Effective Detection Angle EDA (radian) and body mass (kg); (C) day range (km/day) and body mass with diet used as a covariate. Axes are log10-scaled.

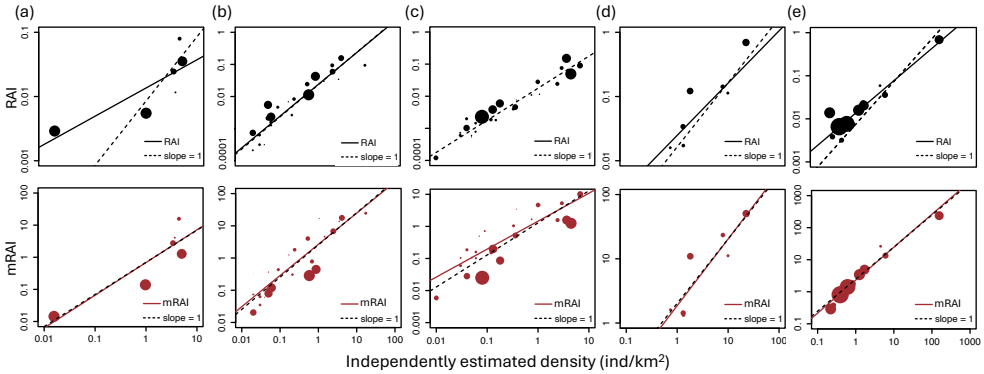


Figure 4.2 Fits to 1:1 between relative abundance index (RAI, y axis, first row), macro-corrected relative abundance index (mRAI, y axis, second row), and independently estimated density (x axis) among 4 communities. Black lines are fits before *improvement*. Red lines are fits after *improvement.* Dotted lines indicate 1:1 slopes passing through the points of pre- or post-improvement fits when the x-axis equals the mean value of the independent estimated density range. The dot sizes are proportional to the body mass of the species (log_{10}-scaled). A to F display community data from O'Brien et al., 2003, Wearn et al., 2022 (B, old growth forest & C, logged forest), BCI team, unpublished, and He et al., 2025, respectively.

4.6 DATA ACCESSIBILITY STATEMENT

Part of the code and data for scaling relationships and verifying the model are available on Dryad: http://datadryad.org/share/V2vuP-I8tfE1y6a0z-Rp-s3k69rt9uYs0XRyuSuGFAyk.

4.7 AUTHORSHIP

CC, MR, and PJ conceived the ideas and designed the methods; CC, and SH built the model and analysed the data; CC and SH collected the data; SH, PJ, MR, and CC did the writing.

SUPPORTING INFORMATION

From scaling relationships to mRAI

The power regressions from equations 1-3 were $\log_{10}$-transformed. The coefficients were then obtained from linear regression models and applied in equation 4 to calculate the mRAI. Day range was represented by r, which scales to the body mass M to the exponent q with constant k, both derived from day range scaling (see below). Effective detection distance (EDD), represented by d, scales to M to the 0.33 power derived theoretically with constant derived below. Effective detection angle (EDA), represented by q, scales to the M to the exponent g with constant h, both derived from EDA scaling (see below). Constants k, c, and g, as well as exponent q, were estimated as the intercepts and slope of $\log_{10}$-transformed regressions. Both day range and EDD were measured in kilometers for consistency, q in radians, body mass M in kilograms, and density in individuals per square kilometers.

$$\log_{10} r = \log_{10} M^{q} + \log_{10} k \qquad \log_{10} d = \log_{10} M^{0.33} + \log_{10} c \qquad \log_{10} \theta = \log_{10} M^{h} + \log_{10} g$$

$$y = \beta_q x + C_k \qquad y = 0.33x + C_c \qquad y = \beta_h x + C_g$$

$$k = 10^{Ck} \qquad c = 10^{Cc} \qquad g = 10^{Cg}$$

$$q = \beta_q \qquad b = 0.33 \qquad h = \beta_h$$

$$mRAI = RAI * \pi / (kc * M^{q+0.33} * (2 + gM^{h})) = RAI * \pi / (10^{Ck + Cc} * M^{\beta q + 0.33} * (2 + 10^{Cg} M^{\beta h}))$$


024-07-14 07:09:46
M 3/10
27°C
NP-31H
RECONYX

5

Synthesis

Camera traps are now widely used as a non-invasive tool for monitoring terrestrial mammals and supporting population density estimation, particularly for species that are nocturnal, elusive, or difficult to observe directly (Burton et al., 2015; O'Connell et al., 2011; Tobler et al., 2008; Steenweg et al., 2017). Most camera-trap systems used in wildlife monitoring rely on passive infrared (PIR) sensors, which trigger in response to changes in infrared radiation generated by warm-blooded animals moving through a defined detection zone (Welbourne et al., 2016). Previous studies have shown that larger animals are more likely to be detected because they emit stronger thermal signals (McNab, 1980; Rowcliffe et al., 2011), while species with longer daily movement distances or larger home ranges have a higher probability of encountering cameras (Carbone et al., 2005; Sollmann et al., 2013). Consequently, detection probability depends not only on animal presence but also on the interaction between sensor characteristics, detection geometry, animal body size, movement behaviour, and environmental conditions (Carbone et al., 2005; MacKenzie et al., 2002; Rowcliffe et al., 2008; McNab, 1980; Sollmann et al., 2013). Capture rates therefore reflect not only animal density but also variation in detectability across species and environments, limiting the reliability of relative abundance indices for unmarked species (Burton et al., 2015; Nakashima et al., 2017; Rowcliffe et al., 2008; Sollmann et al., 2013). The variability in detection seems to be "the Achilles' heel" of camera trapping (personal discussion with Patrick Jansen).

Although several analytical approaches have been developed to estimate wildlife density of unmarked species from camera-trap data, they typically require additional parameters or study designs that are unavailable for most datasets. (Rowcliffe et al., 2008; Chandler & Royle, 2013; Nakashima et al., 2018; Sollmann et al., 2013). At the same time, conventional horizontal deployments are often vulnerable to vandalism, fire, and damage by wildlife, leading to data loss and incomplete surveys (Smith & Coulson, 2012; Meek et al., 2016; He et al., 2025). Together, these constraints define two unresolved challenges: how wildlife abundance can be inferred robustly from camera-trap data when only relative abundance indices are available, and how density estimation can be adapted when deployment decisions modify the detection process.

Based on these background questions and challenges this thesis adopts the Random Encounter Model (REM) as an analytical framework to address them. Across the chapters, REM was used to (i) adapt density estimation to an alternative camera orientation, (ii) quantify how deployment orientation influences detection processes and density estimates, and (iii) develop approaches that allow capture rates, which constitute the majority of existing camera-trap data, to better reflect underlying wildlife density. The thesis

progresses from methodological development, through empirical evaluation, to macroecological application, with a focus on understanding detection and detectability in camera-trap surveys.

5.1 FROM HORIZONTAL TO VERTICAL CAMERA-TRAP DEPLOYMENTS

The need to protect camera traps and the data they collect from damage and vandalism by humans, wildlife, and extreme weather conditions such as floods and fire has motivated alternative deployment strategies (Meek et al., 2016; Grassman et al., 2005; Wearn & Glover-Kapfer, 2019). These pressures highlight that deployment design is not merely a fixed strategy but a choice. Using the Random Encounter Model (REM) as a framework, Chapter 2 develops a vertical Random Encounter Model (vREM) to enable density estimation from vertically oriented camera traps. In conventional REM applications, the effective detection zone is represented as a fan-shaped sector corresponding to a forward-facing field of view. In contrast, vertically oriented cameras produce a detection zone that differs in both shape and orientation, which makes the standard geometry inappropriate. Chapter 2 modifies REM to accommodate a vertical field of view and represents the effective detection area as a rectangle, with dimensions determined by camera sensor properties, camera height, and species body mass.

Two broader messages emerge from this chapter. First, the vREM formulation demonstrates that vertical deployment can be applied with density estimation, provided that orientation-specific paramters, especially detection zone are adapted accordingly. Validation results conducted in Bardiya National Park, Nepal (BNP) show that vREM produces density estimates that broadly align with independent density estimates across multiple species spanning a wide range of body mass. This indicates that vertical camera traps need not be restricted to basic capture rates, but can support formal density estimation. However, the degree of agreement between vREM and reference densities varies among species. Such variation may reflect temporal and spatial mismatches between reference studies, as well as additional factors influencing detectability. This variation highlights the importance of identifying the conditions under which vertical deployments perform reliably and where further refinement is needed.

5.2 TRADE-OFFS BETWEEN PROTECTION AND DETECTABILITY

If vertical deployment offers protection, it also raises a critical question: what is gained, and what is lost, in terms of detectability and encounter processes? After establishing the theoretical basis of vREM, Chapter 3 addresses how comparable and reliable parameter estimates and density outputs are under vertical and horizontal deployments. Horizontal camera traps were therefore deployed simultaneously with vertical cameras at the same locations, allowing direct comparison between deployment orientations under matched environmental conditions.

The paired-deployment study in Bardiya National Park implemented vertical and horizontal camera traps at 36 locations, enabling direct comparison of capture rates, core REM parameters, and resulting density estimates for seven species with sufficient detections. In parallel, practical constraints were also documented associated with horizontal deployments, including camera damage by wildlife and fire (8 out of 36 horizontal camera traps), reinforcing the practical motivation for protected deployment strategies.

Across species, three consistent patterns emerged. First, several core REM parameters were broadly comparable between orientations, particularly movement speed for most species. Second, capture rates were consistently lower in vertical deployments, with differences becoming more pronounced for smaller-bodied herbivores. Third, these reduced capture rates propagated into lower density estimates under vREM relative to REM. Crucially, this pattern was not driven by geometry alone, but more by the interaction between mounting height and species-specific effective detection distance.

These results reveal a fundamental trade-off: vertical deployment improves protection but can reduce encounter probability if mounting height exceeds effective detection distance. vREM therefore performs most reliably when deployment heights remain within the detection range of target species while still minimizing the risk of damage and vandalism. This reframes deployment height as a key design parameter rather than a secondary field constraint. Alternatively, correction approaches based on standardized deployment heights across communities could be developed to account for capture-rate loss associated with height and body mass, although such approaches would require comparable surveys across multiple study areas. Together, these findings give explicit, testable guidance for vertical camera-trap survey design.

5.3 RECOVERING DENSITY INFORMATION FROM CAPTURE RATES

While site-level density estimation provides detailed inference, it is not always achievable. Chapters 2 and 3 rely on site-level parameter estimation using vREM, which can yield robust density estimates but requires substantial field effort and additional data collection, including tracking-based movement information and explicit estimation of detection zones. In contrast, most camera-trap datasets accumulated over past decades lack this information and consist primarily of capture-rate summaries.

This mismatch between methodological requirements and available data motivates a complementary contribution of this thesis: improving the interpretability of capture rates when formal density estimation is not feasible and thereby enabling better use of the global archive of camera-trap data. Chapter 4 develops the macro-corrected RAI (mRAI) based on the premise that detectability differs systematically among species and that a substantial proportion of capture-rate variation can be explained by predictable scaling relationships with body mass and diet. Larger-bodied species emit more heat and typically travel longer distances, making them more likely to trigger passive infrared sensors and resulting in higher detectability (Welbourne et al., 2016; Carbone et al., 2005; Rowcliffe et al., 2011). Building on the REM framework, this chapter derives scaling relationships for REM parameters using data from formal studies that include both independent density estimates and camera-trap capture data (BCI team, unpublished; O'Brien et al., 2003; Wearn et al., 2022; He et al., 2025). These relationships are integrated into a corrected abundance index designed to better align capture rates with independently estimated densities.

Evaluation results show that mRAI improves correspondence with independent density estimates relative to uncorrected RAI, both in absolute magnitude and model fit across several mammal communities. This demonstrates that capture-rate data, often dismissed as weak proxies, can recover meaningful density-related information when corrected using biologically grounded principles. Consistent with the broader contributions of this thesis, Chapter 4 extends REM-based thinking beyond site-specific density estimation by providing a practical framework for macroecological analyses when only capture-rate data are available.

5.4 CONTRIBUTIONS AND PRACTICAL GUIDANCE

Together, the three chapters show that density estimation from camera traps depends as much on deployment decisions and data structure, through their effects on detection and detectability, as on statistical formulation. First, under field conditions where camera traps are exposed to high risks of damage, alternative deployment strategies can maintain equipment and data integrity (Smith & Coulson, 2012; Meek et al., 2016). By adapting parameters and detection-zone estimation, REM can be extended to vertically oriented camera traps, explicitly redefining the detection process and enabling density estimation for unmarked species from a protected deployment orientation.

Second, although vertical deployment improves protection, it introduces systematic detectability trade-offs by altering detection geometry. Matched deployments show that capture rates decrease with decreasing body mass under vertical placement, consistent with established links between detection distance, body size, and encounter processes. Reliable density estimation therefore requires explicit consideration of mounting height relative to species-specific effective detection distance, which directly governs detection probability. Deployment design thus becomes a central component of inference rather than a purely logistical constraint. Third, when only capture-rate data are available, mRAI provides a principled correction that improves interpretability and comparability across species and communities by accounting for systematic differences in detectability, addressing long-standing limitations of RAI (Carbone et al., 2001; Rowcliffe et al., 2011; Sollmann et al., 2013).

A central practical message emerging from this thesis is that explicitly accounting for detection processes allows camera-trap data to be used more robustly under field and data constraints that have previously limited inference (Steenweg et al., 2017; Wearn & Glover-Kapfer, 2019). Together, these contributions do not resolve all detectability-related limitations of camera trapping, but they provide concrete, tested approaches that extend the conditions under which density information can be inferred, reduce data loss, and improve the effective use of existing camera-trap data.

5.5 LIMITATIONS AND UNCERTAINTIES

Several limitations and uncertainties emerge across this thesis. These reflect trade-offs between deployment choice, field feasibility, and data availability, rather than fundamental weaknesses of the approaches developed. Identifying

these constraints helps clarify the conditions under which the proposed methods perform best and highlights priorities for future research.

5.5.1 Field validation of optimal mounting height

Chapter 3 demonstrates that the mismatch between camera mounting height and species-specific effective detection distance is a primary determinant of capture-rate loss in vertical deployments. Direct empirical validation of this relationship would benefit from data collected at optimally selected heights. However, among the 36 paired locations, only one vertical camera was mounted close to the theoretically recommended height (approximately 4.5–5.5 m), which lies within the effective detection distance of focal species while remaining beyond the reach of elephants in Bardiya National Park. As a result, empirical evaluation of capture rates under optimal vertical mounting heights was limited. Additional field experiments using paired camera traps deployed at heights that simultaneously satisfy detectability and protection constraints would allow more direct testing of the proposed deployment strategy.

5.5.2 Feasibility of generalized correction for capture-rate loss

Chapter 3 also discusses an alternative strategy in which capture-rate loss associated with mounting height and body mass could be addressed using generalized correction models derived from standardized deployments across multiple study areas. Developing such transferable corrections would reduce reliance on site-specific deployment decisions driven by local detection distances, species assemblages, and sources of camera damage. However, establishing general correction rules requires data collected across a wide range of ecological contexts. Ecological theory shows that patterns inferred from limited spatial or taxonomic scope may not generalize beyond the conditions under which they were derived, as ecological processes and their observable outcomes are strongly scale-dependent (Levin, 1992). Similarly, robust general patterns typically emerge only through the synthesis of data across multiple communities and regions, rather than from isolated case studies (McGill, 2003). Coordinated multi-site datasets with comparable paired deployments and overlapping body-mass distributions would therefore be necessary to support broadly applicable correction models. The logistical and financial effort required to generate such datasets is substantial, which may limit the feasibility of this approach in the short term.

5.5.3 Parameter estimation effort and sampling sufficiency

Both REM and vREM rely on reliable estimates of movement speed, activity level, group size, and detection parameters, all of which directly determine density estimates and propagate uncertainty through the model (Rowcliffe

et al., 2008). In Chapter 2, five years of accumulated data provided sufficient detections to support stable parameter estimation, with at least 100 observations per species, consistent with empirical suggestions of minimum sample sizes required for reliable estimates of movement speed and activity patterns (Rowcliffe et al., 2008; Lashley et al., 2016). In contrast, the shorter deployment period in Chapter 3 limited detections for some species, resulting in reduced precision of parameter estimates. This pattern reflects a general constraint in ecological modelling, whereby parameter uncertainty increases rapidly as sample size declines relative to model complexity (Kelly, 2007; Maxwell et al., 2008). Where vertical deployment reduces capture rates, longer sampling durations or adjusted mounting heights are therefore required to achieve comparable parameter precision. At the same time, the large sample sizes required for reliable parameter estimation highlight the importance of approaches that reduce manual processing effort, such as automated extraction of movement paths to support estimation of movement speed and detection zones, and automated species identification from camera-trap data. These developments motivate increasing interest in the application of artificial intelligence in camera-trap studies.

5.5.4 Reliability and limitations of artificial intelligence applications

Artificial intelligence is increasingly used in wildlife monitoring to automatically give species identification and image annotation from camera-trap data, substantially reducing manual processing effort (Christin et al., 2019; Norouzzadeh et al., 2018; Tabak et al., 2019). While deep learning models can achieve high classification accuracy for common and well-represented species, their performance varies across species, environments, and image conditions. Classification accuracy typically declines for rare or new species, morphologically similar taxa, and images affected by low light or motion blur (Beery et al., 2019; Tabak et al., 2019; Whytock et al., 2021). These limitations are relevant for large-scale or long-term monitoring programmes, where data heterogeneity is unavoidable. As a result, AI-derived labels should not be treated as error-free observations (Christin et al., 2019). Examples from this thesis reflect these broader patterns. In Bardiya National Park, chital were occasionally misclassified as other sympatric deer species under low-light or adverse weather conditions, despite models being trained on multi-year datasets. While manual verification was feasible for the datasets analysed here, such validation becomes impractical for larger or longer-term studies. Overall, artificial intelligence improves the efficiency of camera-trap data processing but risk of observation error should not be ignored. Its outputs should therefore be viewed as part of the detection process rather than a replacement for it. Without explicit consideration of classification

uncertainty, AI-assisted workflows risk introducing new sources of bias into camera-trap analyses (Schindler and Steinhage, 2021).

5.5.5 Environmental drivers of detectability beyond body mass and diet

The mRAI framework demonstrates that body mass and diet explain a substantial proportion of interspecific variation in detectability. Detectability, however, is also influenced by environmental and behavioural factors, including thermal contrast, posture, movement behaviour, and vegetation structure (De Knegt et al., 2011; ENETWILD-consortium et al., 2023; Lovell et al., 2022; Palencia et al., 2021; Rizzuto et al., 2018). One way to incorporate such effects is through hierarchical models, where environmental covariates enter at the observation level. Many of these covariates, however, act indirectly by shaping core mechanistic parameters rather than detection itself. Environmental conditions such as habitat structure, resource availability, climate, and anthropogenic disturbance are known to modify animal movement speed and activity patterns (Delisle et al., 2024; Gaynor et al., 2018; Rowcliffe et al., 2014c; Tucker et al., 2021), which in turn determine encounter rates and effective detection distance as well. This highlights a key modelling distinction between representing environmental drivers explicitly as covariates in hierarchical modelling and capturing their effects implicitly through parameters in mechanistic modelling. The central question is therefore not how many additional covariates should be included, but to what extent existing parameters already integrate environmental influences on detectability.

5.5.6 Group size and detectability in gregarious species

Results from Chapter 3 highlight challenges in estimating group size for highly gregarious species such as chital, which can form groups exceeding 100 individuals (De & Spillett, 1966). Estimated group size differed systematically between vertical and horizontal deployments, reflecting differences in field of view and detectability. In vertical deployments, group size was inferred from individuals visible within the vertical detection zone, typically representing only a subset of a larger group. In contrast, horizontal deployments often recorded a greater number of individuals within the field of view. However, individuals observed at greater distances may not trigger the camera and therefore do not necessarily contribute equally to encounter processes. These results indicate that observed group size does not directly correspond to the effective group size relevant for density estimation. Developing standardized criteria for defining and estimating group size, particularly for horizontal deployments, remains to be explored (Rowcliffe, in preparation).

5.6 FUTURE DIRECTIONS: APPLYING VERTICAL CAMERA TRAPS FOR INTEGRATED MONITORING

With the development and evaluation of vREM, a natural next step is to consider how vertical camera traps can be more broadly applied in ecological monitoring. Rather than focusing solely on density estimation, vertical deployments open opportunities for integrated monitoring of wildlife and environmental disturbance, particularly in seasonal, fire-prone landscapes.

One promising application highlighted by this thesis is the simultaneous monitoring of wildlife dynamics and fire-related processes using the same camera-trap network. Mounting cameras above ground not only reduces vulnerability to fire damage, but also allows cameras to remain operational during and after fire events, thereby preserving temporal continuity in data collection. This makes it possible for fire-related variables to be derived directly from camera-trap imagery, for example through pixel- or colour-based proxies indicating burning, smoke, ash cover, or post-fire ground conditions. These variables can then be incorporated as covariates influencing animal abundance or detection processes.

Density estimation methods can be broadly grouped into hierarchical models and mechanistic (non-hierarchical) models. Hierarchical models explicitly separate the ecological state process (true abundance or density) from the observation process that generates imperfect data, which include occupancy models, spatial capture–recapture models, and N-mixture models (MacKenzie et al., 2002; Royle et al., 2014; Chandler & Royle, 2014). These approaches rely on likelihood-based or Bayesian inference and can incorporate spatial structure, covariates, and repeated sampling to account for imperfect detection (Royle & Dorazio, 2008). In contrast, mechanistic models such as REM and REST estimate density by linking encounter rates to animal movement and detection processes through analytical relationships (Rowcliffe et al., 2008; Nakashima et al., 2017). Having demonstrated that vertically oriented camera traps can support density estimation within a mechanistic framework, a natural next step is to further apply vertical deployments to hierarchical modelling approaches that incorporate environmental covariates, allowing broader sources of variation in detectability and abundance to be accounted for.

Existing camera-trap networks provide a good chance for this extension, because fire events and their immediate effects are often visible in camera imagery while the same cameras record wildlife activity before, during, and after disturbance. In this context, fire-related image-derived variables can be

incorporated into hierarchical models as covariates affecting both abundance and detection probability. For example, short-term responses of multiple mammal species to fire severity can be analysed using multispecies N-mixture models (Yamaura et al., 2012), with abundance linked to fire occurrence, time since fire, and severity, and detection allowed to vary with post-fire vegetation structure and ground conditions.

This fire-focused application complements the core contributions of the thesis in two key ways. First, it emphasize a principal advantage of vertical deployments, which is reducing equipment loss and improving sampling continuity. Second, it extends the role of vertical camera traps beyond mechanistic density estimation by enabling integration with hierarchical models that accommodate additional ecological drivers of abundance and detectability.

Finally, this framework is not restricted to fire-resilient systems such as Bardiya National Park or tropical savannas (Bond and Keeley, 2005; Van Langevelde et al., 2003). Fire-driven ecosystem change is a major conservation concern globally, particularly in tropical regions such as the Amazon, where recurrent fires have caused widespread habitat degradation with limited recovery (Brando et al., 2014; Cochrane and Barber, 2009). While research in these systems has largely focused on vegetation responses, wildlife responses to fire remain comparatively understudied (Driscoll et al., 2010). Insights gained from a seasonal, fire-resilient system demonstrate how the integration of protected vertical camera deployments with mechanistic and hierarchical inference can be used to quantify disturbance dynamics and wildlife responses in ecosystems that are less resilient to fire, especially where long-term monitoring is difficult to maintain.

5.7 CONCLUSION

This thesis shows that the central limitation of camera-trap–based density estimation lies in how detection processes are represented and constrained by deployment design and data structure. By treating detection geometry and detectability as integral components of inference, this work demonstrates that density estimation for unmarked species can be adapted to alternative deployment strategies and extended to detection-limited datasets. The results indicate that deployment decisions, particularly camera orientation and mounting height, directly shape detection probability and therefore inference on density. Vertical deployments reduce equipment damage and data loss in high-risk field conditions, but introduce changes in detectability that must be accounted

for accordingly. When these changes are incorporated, deployment height becomes an inferential parameter rather than a purely logistical choice. More broadly, this thesis demonstrates that capture-rate data, which dominate existing camera-trap datasets, can support more informative inference on wildlife abundance when systematic variation in detectability is addressed. By correcting capture rates for biologically driven differences in detection, density-related information can be extracted without extra parameter estimations and study designs. Taken together, these findings highlight that variability in detection is the fundamental constraint on camera-trap inference. By explicitly accounting for this "Achilles' heel" of camera trapping, a clearer basis is provided for integrating deployment design, mechanistic modelling frameworks, and large-scale datasets in ecological research and conservation practice.



Appendix

Summary
Acknowledgement
Biography
Publication list
Overview of Completed Training Activities
Colophon

SUMMARY

Reliable estimates of wildlife abundance are fundamental to ecological research and conservation, yet remain difficult to obtain for many species that are nocturnal, elusive, or unmarked species. Over the past decades, camera traps have become a central tool for wildlife monitoring because they provide non-invasive observations across broad spatial and temporal scales. However, camera-trap data do not directly reflect animal density. Instead, observed capture rates are shaped by detection processes that depend on biotic and abiotic factors including sensor properties, deployment geometry, animal movement, body size, and environmental conditions. As a result, variation in detectability represents a key limitation for inference from camera-trap data and can therefore be seen as "the Achilles' heel" of camera trapping.

This thesis addresses how wildlife density estimation from camera-trap data can be improved by explicitly accounting for detection processes and detectability, with a focus on unmarked terrestrial mammals that cannot be individually identified. Using the Random Encounter Model (REM) as a analytical framework, the thesis examines how deployment decisions, detection geometry, and data structure jointly shape what can be inferred from camera-trap encounters. Rather than treating camera deployment as a fixed design choice, the work views deployment orientation and detectability as integral components of density inference.

At the site level, this thesis extends the REM to vertically oriented camera traps. Vertical deployments can substantially reduce camera damage, theft, and data loss in high-risk field conditions, but they alter detection geometry relative to conventional horizontal setups. By reformulating detection-zone geometry and associated parameters, this work demonstrates that density estimation for unmarked species can be maintained under vertical deployment when changes in detectability are explicitly incorporated. Empirical comparisons between vertical and horizontal deployments show that protection and detectability are linked through a measurable trade-off, governed primarily by the relationship between mounting height and species-specific effective detection distance. Deployment height therefore emerges as a parameter that directly influences detection probability and density inference, rather than a purely logistical decision.

Beyond site-level estimation, this thesis addresses the challenge that most existing camera-trap datasets consist capture-rate information only and lack the additional parameters or specific study design required for full density estima-

tion designed for unmarked species these years. To improve the interpretability of such data, the thesis develops a mass-relative abundance index (mRAI) that accounts for systematic differences in detectability among species. By incorporating scaling relationships between body mass, movement behaviour, and detection processes, mRAI improves correspondence between capture rates and independently estimated density across species. This provides a practical approach for comparative and macroecological analyses where direct density estimation is not feasible.

Taken together, the chapters demonstrate that variation in detection processes underlies both methodological and practical limitations of camera-trap–based inference. By adapting detection geometry to alternative deployments and correcting capture-rate indices for detectability, this thesis extends the conditions under which camera-trap data can be used to reflect animal abundance in a more robust way. These contributions do not eliminate all sources of bias in camera-trap data, nor do they resolve all camera-trap–based limitations. Rather, they provide concrete and tested approaches that reduce data and equipment loss, improve inferential robustness, and enable more effective use of the exisiting camera-trap datasets.

More broadly, this work highlights that future progress in camera-trap ecology depends on recognising the detection process as the link between animal density and observed data. As camera traps continue to expand in number, spatial extent, and application, their scientific value will increasingly depend on deployment strategies and analytical frameworks that explicitly address variation in detectability. By linking deployment design, detection geometry, and scalable inference, this thesis contributes a coherent framework for improving wildlife density estimation from camera-trap data across local, regional, and macroecological scales.

REFERENCE

Ahumada, J.A., Silva, C.E.F., Gajapersad, K., Hallam, C., Hurtado, J., Martin, E., McWilliam, A., Mugerwa, B., O'Brien, T., Rovero, F., Sheil, D., Spironello, W.R., Winarni, N., Andelman, S.J., 2011. Community structure and diversity of tropical forest mammals: data from a global camera trap network. Phil. Trans. R. Soc. B 366, 2703–2711. https://doi.org/10.1098/rstb.2011.0115

Becker, M., Huggard, D.J., Dickie, M., Warbington, C., Schieck, J., Herdman, E., Serrouya, R., Boutin, S., 2022. Applying and testing a novel method to estimate animal density from motion-triggered cameras. Ecosphere 13, e4005. https://doi.org/10.1002/ecs2.4005

Beery, S., Morris, D., Yang, S., 2019. Efficient Pipeline for Camera Trap Image Review. https://doi.org/10.48550/arXiv.1907.06772

Bond, W., Keeley, J., 2005. Fire as a global 'herbivore': the ecology and evolution of flammable ecosystems. Trends in Ecology & Evolution 20, 387–394. https://doi.org/10.1016/j.tree.2005.04.025

Buckland, S.T., Magurran, A.E., Green, R.E., Fewster, R.M., 2005. Monitoring change in biodiversity through composite indices. Phil. Trans. R. Soc. B 360, 243–254. https://doi.org/10.1098/rstb.2004.1589

Burton, A.C., Neilson, E., Moreira, D., Ladle, A., Steenweg, R., Fisher, J.T., Bayne, E., Boutin, S., 2015a. REVIEW: Wildlife camera trapping: a review and recommendations for linking surveys to ecological processes. J Appl Ecol 52, 675–685. https://doi.org/10.1111/1365-2664.12432

Burton, A.C., Neilson, E., Moreira, D., Ladle, A., Steenweg, R., Fisher, J.T., Bayne, E., Boutin, S., 2015b. REVIEW: Wildlife camera trapping: a review and recommendations for linking surveys to ecological processes. J Appl Ecol 52, 675–685. https://doi.org/10.1111/1365-2664.12432

Carbone, C., Christie, S., Conforti, K., Coulson, T., Franklin, N., Ginsberg, J.R., Griffiths, M., Holden, J., Kawanishi, K., Kinnaird, M., Laidlaw, R., Lynam, A., Macdonald, D.W., Martyr, D., McDougal, C., Nath, L., O'Brien, T., Seidensticker, J., Smith, D.J.L., Sunquist, M., Tilson, R., Shahruddin, W.N., 2001. The use of photographic rates to estimate densities of tigers and other cryptic mammals. Animal Conservation 4, 75–79. https://doi.org/10.1017/S1367943001001081

Carbone, C., Cowlishaw, G., Isaac, N.J.B., Rowcliffe, J.M., 2005. How Far Do Animals Go? Determinants of Day Range in Mammals. The American Naturalist 165, 290–297. https://doi.org/10.1086/426790

Casaer, J., Milotic, T., Liefting, Y., Desmet, P., Jansen, P., 2019. Agouti: A platform for processing and archiving of camera trap images. BISS 3, e46690. https://doi.org/10.3897/biss.3.46690

Chandler, R.B., Royle, J.A., 2013. Spatially explicit models for inference about density in unmarked or partially marked populations. Ann. Appl. Stat. 7. https://doi.org/10.1214/12-AOAS610

Christin, S., Hervet, É., Lecomte, N., 2019. Applications for deep learning in ecology. Methods Ecol Evol 10, 1632–1644. https://doi.org/10.1111/2041-210X.13256

De Bondi, N., White, J.G., Stevens, M., Cooke, R., 2010. A comparison of the effectiveness of camera trapping and live trapping for sampling terrestrial small-mammal communities. Wildl. Res. 37, 456. https://doi.org/10.1071/WR10046

De Knegt, H.J., Van Langevelde, F., Skidmore, A.K., Delsink, A., Slotow, R., Henley, S., Bucini, G., De Boer, W.F., Coughenour, M.B., Grant, C.C., Heitkönig, I.M.A., Henley, M., Knox, N.M., Kohi, E.M., Mwakiwa, E., Page, B.R., Peel, M., Pretorius, Y., Van Wieren, S.E., Prins, H.H.T., 2011. The spatial scaling of habitat selection by African elephants: Scaling habitat selection by elephants. Journal of Animal Ecology 80, 270–281. https://doi.org/10.1111/j.1365-2656.2010.01764.x

Delisle, Z.J., Sample, R.D., Caudell, J.N., Swihart, R.K., 2024. Deer activity levels and patterns vary along gradients of food availability and anthropogenic development. Sci Rep 14, 10223. https://doi.org/10.1038/s41598-024-60079-6

Dinerstein, E., 1980. An ecological survey of the Royal Karnali-Bardia Wildlife Reserve, Nepal. Biological Conservation 18, 5–37. https://doi.org/10.1016/0006-3207(80)90063-4

Dinerstein, E., 1979a. An ecological survey of the royal Karnali-Bardia Wildlife Reserve, Nepal. Part I: Vegetation, modifying factors, and successional relationships. Biological Conservation 15, 127–150. https://doi.org/10.1016/0006-3207(79)90030-2

Dinerstein, E., 1979b. An ecological survey of the Royal Karnali-Bardia Wildlife Reserve, Nepal. Part II: Habitat/animal interactions. Biological Conservation 16, 265–300. https://doi.org/10.1016/0006-3207(79)90055-7

ENETWILD-consortium, Guerrasio, T., Pelayo Acevedo, P., Apollonio, M., Arnon, A., Barroqueiro, C., Belova, O., Berdión, O., Blanco-Aguiar, J.A., Bijl, H., Bleier, N., Bučko, J., Elena Bužan, E., Carniato, D., Carro, F., Casaer, J., Carvalho, J., Csányi, S., Lucía del Rio, L., Aliaga, H.D.V., Ertürk, A., Escribano, F., Duniš, L., Fernández-Lopez, J., Ferroglio, E., Fonseca, C., Gačić, D., Gavashelishvili, A., Giannakopoulos, A., Gómez-Molina, A., Gómez-Peris, C., Gruychev, G., Gutiérrez, I., Veith Häberlein, V., Hasan, S.M., Hillström, L., Hoxha, B., Iranzo, M., Mihael Janječić, M., Jansen, P., Illanas, S., Kashyap, B., Keuling, O., Laguna, E., Lefranc, H., Licoppe, A., Liefting, Y., Martínez-Carrasco, C., Mrđenović, D., Nezaj, M., Xosé Pardavila, X., Palencia, P., Pereira, G., Pereira, P., Pinto, N., Plhal, R., Plis, K., Podgórski, T., Pokorny, B., Preite, L., Radonjic, M., Marcus Rowcliffe, M., Ruiz-Rodríguez, C., Santos, J., Rodríguez, O., Scandura, M., Sebastián, M., Sereno, J., Šestovic, B., Shyti, I., Somoza, E., Soriguer, R., de la Torre, J.S., Soyumert, A., Šprem, N., Stoyanov, S., Smith, G.C., Sulce, M., Torres, R.T., Trajçe, A., Urbaitis, G., Urbani, N., Uguzashvili, T., Vada, R., Zanet, S., Vicente, J., 2023. Wild ungulate density data generated by camera trapping in 37 European areas: first output of the European Observatory of Wildlife (EOW). EFS3 20. https://doi.org/10.2903/sp.efsa.2023.EN-7892

Faurby, S., Davis, M., Pedersen, R.Ø., Schowanek, S.D., Antonelli1, A., Svenning, J., 2018a. PHYLACINE 1.2: The Phylogenetic Atlas of Mammal Macroecology. Ecology 99, 2626–2626. https://doi.org/10.1002/ecy.2443

Faurby, S., Davis, M., Pedersen, R.Ø., Schowanek, S.D., Antonelli1, A., Svenning, J.-C., 2018b. PHYLACINE 1.2: The Phylogenetic Atlas of Mammal Macroecology. Ecology 99, 2626–2626. https://doi.org/10.1002/ecy.2443

Gaynor, K.M., Hojnowski, C.E., Carter, N.H., Brashares, J.S., 2018. The influence of human disturbance on wildlife nocturnality. Science 360, 1232–1235. https://doi.org/10.1126/science.aar7121

Gilbert, N.A., Clare, J.D.J., Stenglein, J.L., Zuckerberg, B., 2021. Abundance estimation of unmarked animals based on camera-trap data. Conservation Biology 35, 88–100. https://doi.org/10.1111/cobi.13517

Gopalaswamy, A.M., Royle, J.A., Delampady, M., Nichols, J.D., Karanth, K.U., Macdonald, D.W., 2012. Density estimation in tiger populations: combining information for strong inference. Ecology 93, 1741–1751. https://doi.org/10.1890/11-2110.1

Grassman, L.I., Tewes, M.E., Silvy, N.J., 2005. Armoring the Camtrakker® camera-trap in a tropical Asian forest. Wildlife Society Bulletin 33, 349–352. https://doi.org/10.2193/0091-7648(2005)33%255B349:FTFATC%255D2.0.CO;2

He, S., Rowcliffe, J.M., Lin, H., Carbone, C., Liefting, Y., Thapa, S.K., Shrestha, B.P., Jansen, P.A., 2025. A random encounter model for wildlife density estimation with vertically oriented camera traps. Remote Sens Ecol Conserv 11, 327–338. https://doi.org/10.1002/rse2.427

He, S., Rowcliffe, J.M., Lin, H., Carbone, C., Liefting, Y., Thapa, S.K., Shrestha, B.P., Jansen, P.A., 2024. A random encounter model for wildlife density estimation with vertically oriented camera traps. Remote Sens Ecol Conserv rse2.427. https://doi.org/10.1002/rse2.427

Hofmeester, T.R., Rowcliffe, J.M., Jansen, P.A., 2017. A simple method for estimating the effective detection distance of camera traps. Remote Sens Ecol Conserv 3, 81–89. https://doi.org/10.1002/rse2.25

Howe, E.J., Buckland, S.T., Després-Einspenner, M., Kühl, H.S., 2017. Distance sampling with camera traps. Methods Ecol Evol 8, 1558–1565. https://doi.org/10.1111/2041-210X.12790

Hsing, P., Hill, R.A., Smith, G.C., Bradley, S., Green, S.E., Kent, V.T., Mason, S.S., Rees, J., Whittingham, M.J., Cokill, J., MammalWeb Citizen Scientists, Stephens, P.A., 2022. Large-scale mammal monitoring: The potential of a citizen science camera-trapping project in the United Kingdom. Ecol Sol and Evidence 3, e12180. https://doi.org/10.1002/2688-8319.12180

Hutchinson, J.M.C., Waser, P.M., 2007. Use, misuse and extensions of "ideal gas" models of animal encounter. Biological Reviews 82, 335–359. https://doi.org/10.1111/j.1469-185X.2007.00014.x

Jarman, P.J., n.d. IN RELATION TO THEIR ECOLOGY 53.

Kaplan, A., Maehr, M.L., 2007. The Contributions and Prospects of Goal Orientation Theory. Educ Psychol Rev 19, 141–184. https://doi.org/10.1007/s10648-006-9012-5

Karanth, K.U., Nichols, J.D., n.d. ESTIMATION OF TIGER DENSITIES IN INDIA USING PHOTOGRAPHIC CAPTURES AND RECAPTURES.

Kelly, M.J., Holub, E.L., 2008. Camera Trapping of Carnivores: Trap Success Among Camera Types and Across Species, and Habitat Selection by Species, on Salt Pond Mountain, Giles County, Virginia. Northeastern Naturalist 15, 249–262. https://doi.org/10.1656/1092-6194(2008)15%255B249:CTOCTS%255D2.0.CO;2

Kral, M.J.C., van Lunenburg, M., 2017. The spatial distribution of ungulates and primates across the vegetation gradient in Bardiya National Park, West Nepal 6.

Lashley, M.A., Cove, M.V., Chitwood, M.C., Penido, G., Gardner, B., DePerno, C.S., Moorman, C.E., 2018. Estimating wildlife activity curves: comparison of methods and sample size. Sci Rep 8, 4173. https://doi.org/10.1038/s41598-018-22638-6

Lenth, R.V., 1989. Algorithm AS 243: Cumulative Distribution Function of the Non-Central t Distribution. Applied Statistics 38, 185. https://doi.org/10.2307/2347693

Levin, S.A., 1992. The Problem of Pattern and Scale in Ecology: The Robert H. MacArthur Award Lecture. Ecology 73, 1943–1967. https://doi.org/10.2307/1941447

Lintulaakso, K., Tatti, N., Žliobaitė, I., 2023. Quantifying mammalian diets. Mamm Biol 103, 53–67. https://doi.org/10.1007/s42991-022-00323-6

Lovell, C., Li, S., Turner, J., Carbone, C., 2022. The effect of habitat and human disturbance on the spatiotemporal activity of two urban carnivores: The results of an intensive camera trap study. Ecology and Evolution 12. https://doi.org/10.1002/ece3.8746

MacKenzie, D.I., Nichols, J.D., Lachman, G.B., Droege, S., Andrew Royle, J., Langtimm, C.A., 2002. ESTIMATING SITE OCCUPANCY RATES WHEN DETECTION PROBABILITIES ARE LESS THAN ONE. Ecology 83, 2248–2255. https://doi.org/10.1890/0012-9658(2002)083%255B2248:ESORWD%255D2.0.CO;2

Marcus Rowcliffe, J., Carbone, C., Jansen, P.A., Kays, R., Kranstauber, B., 2011. Quantifying the sensitivity of camera traps: an adapted distance sampling approach: *Quantifying camera trap sensitivity*. Methods in Ecology and Evolution 2, 464–476. https://doi.org/10.1111/j.2041-210X.2011.00094.x

McGill, B., 2003. Strong and weak tests of macroecological theory. Oikos 102, 679–685. https://doi.org/10.1034/j.1600-0706.2003.12617.x

McNab, B.K., 1980a. On Estimating Thermal Conductance in Endotherms. Physiological Zoology 53, 145–156. https://doi.org/10.1086/physzool.53.2.30152577

McNab, B.K., 1980b. On Estimating Thermal Conductance in Endotherms. Physiological Zoology 53, 145–156. https://doi.org/10.1086/physzool.53.2.30152577

McNab, B.K., 1963. Bioenergetics and the Determination of Home Range Size. The American Naturalist 97, 133–140. https://doi.org/10.1086/282264

McShea, W.J., Forrester, T., Costello, R., He, Z., Kays, R., 2016. Volunteer-run cameras as distributed sensors for macrosystem mammal research. Landscape Ecol 31, 55–66. https://doi.org/10.1007/s10980-015-0262-9

Meek, P., Ballard, G., Fleming, P., Falzon, G., 2016. Are we getting the full picture? Animal responses to camera traps and implications for predator studies. Ecology and Evolution 6, 3216–3225. https://doi.org/10.1002/ece3.2111

Meek, P.D., Ballard, G.A., Falzon, G., 2016a. The higher you go the less you will know: placing camera traps high to avoid theft will affect detection. Remote Sens Ecol Conserv 2, 204–211. https://doi.org/10.1002/rse2.28

Meek, P.D., Ballard, G.A., Falzon, G., 2016b. The higher you go the less you will know: placing camera traps high to avoid theft will affect detection. Remote Sensing in Ecology and Conservation 2, 204–211. https://doi.org/10.1002/rse2.28

Meek, P.D., Ballard, G.A., Sparkes, J., Robinson, M., Nesbitt, B., Fleming, P.J.S., 2019a. Camera trap theft and vandalism: occurrence, cost, prevention and implications for wildlife research and management. Remote Sens Ecol Conserv 5, 160–168. https://doi.org/10.1002/rse2.96

Meek, P.D., Ballard, G.A., Sparkes, J., Robinson, M., Nesbitt, B., Fleming, P.J.S., 2019b. Camera trap theft and vandalism: occurrence, cost, prevention and implications for wildlife research and management. Remote Sensing in Ecology and Conservation 5, 160–168. https://doi.org/10.1002/rse2.96

Moe, S.R., Wegge, P., 1994. Spacing behaviour and habitat use of axis deer (*Axis axis*) in lowland Nepal. Can. J. Zool. 72, 1735–1744. https://doi.org/10.1139/z94-234

Moeller, A.K., Lukacs, P.M., Horne, J.S., 2018a. Three novel methods to estimate abundance of unmarked animals using remote cameras. Ecosphere 9, e02331. https://doi.org/10.1002/ecs2.2331

Moeller, A.K., Lukacs, P.M., Horne, J.S., 2018b. Three novel methods to estimate abundance of unmarked animals using remote cameras. Ecosphere 9, e02331. https://doi.org/10.1002/ecs2.2331

Montanholi, Y.R., Odongo, N.E., Swanson, K.C., Schenkel, F.S., McBride, B.W., Miller, S.P., 2008. Application of infrared thermography as an indicator of heat and methane production and its use in the study of skin temperature in response to physiological events in dairy cattle (Bos taurus). Journal of Thermal Biology 33, 468–475. https://doi.org/10.1016/j.jtherbio.2008.09.001

Nakashima, Y., Fukasawa, K., Samejima, H., 2018a. Estimating animal density without individual recognition using information derivable exclusively from camera traps. Journal of Applied Ecology 55, 735–744. https://doi.org/10.1111/1365-2664.13059

Nakashima, Y., Fukasawa, K., Samejima, H., 2018b. Estimating animal density without individual recognition using information derivable exclusively from camera traps. Journal of Applied Ecology 55, 735–744. https://doi.org/10.1111/1365-2664.13059

Newey, S., Davidson, P., Nazir, S., Fairhurst, G., Verdicchio, F., Irvine, R.J., Van Der Wal, R., 2015. Limitations of recreational camera traps for wildlife management and conservation research: A practitioner's perspective. Ambio 44, 624–635. https://doi.org/10.1007/s13280-015-0713-1

Norouzzadeh, M.S., Nguyen, A., Kosmala, M., Swanson, A., Palmer, M.S., Packer, C., Clune, J., 2018. Automatically identifying, counting, and describing wild animals in camera-trap images with deep learning. Proc. Natl. Acad. Sci. U.S.A. 115. https://doi.org/10.1073/pnas.1719367115

O'Brien, T.G., Kinnaird, M.F., Wibisono, H.T., 2003. Crouching tigers, hidden prey: Sumatran tiger and prey populations in a tropical forest landscape. Animal Conservation 6, 131–139. https://doi.org/10.1017/S1367943003003172

O'Connell, A.F., Nichols, J.D., Karanth, K.U. (Eds.), 2011. Camera traps in animal ecology: methods and analyses / Allan F. O'Connell, James D. Nichols, K. Ullas Karanth, editors. Presented at the International Mammalogical Conference, Springer, Tokyo ; New York.

Palencia, P., Barroso, P., Vicente, J., Hofmeester, T.R., Ferreres, J., Acevedo, P., 2022. Random encounter model is a reliable method for estimating population density of multiple species using camera traps. Remote Sens Ecol Conserv 8, 670–682. https://doi.org/10.1002/rse2.269

Palencia, P., Fernández-López, J., Vicente, J., Acevedo, P., 2021. Innovations in movement and behavioural ecology from camera traps: Day range as model parameter. Methods Ecol Evol 12, 1201–1212. https://doi.org/10.1111/2041-210X.13609

Pd, M., 2024. A Calibration Method for Optimizing Detection of Species Using Camera Traps. JOJWB 5. https://doi.org/10.19080/jojwb.2024.05.555656

Pettigrew, P., Sigouin, D., St-Laurent, M., 2021. Testing the precision and sensitivity of density estimates obtained with a camera-trap method revealed limitations and opportunities. Ecology and Evolution 11, 7879–7889. https://doi.org/10.1002/ece3.7619

Pfeffer, S.E., Spitzer, R., Allen, A.M., Hofmeester, T.R., Ericsson, G., Widemo, F., Singh, N.J., Cromsigt, J.P.G.M., 2018. Pictures or pellets? Comparing camera trapping and dung counts as methods for estimating population densities of ungulates. Remote Sens Ecol Conserv 4, 173–183. https://doi.org/10.1002/rse2.67

Pollock, K.H., Nichols, J.D., Simons, T.R., Farnsworth, G.L., Bailey, L.L., Sauer, J.R., 2002. Large scale wildlife monitoring studies: statistical methods for design and analysis. Environmetrics 13, 105–119. https://doi.org/10.1002/env.514

Ramesh, T., Kalle, R., Sankar, K., Qureshi, Q., 2015. Role of body size in activity budgets of mammals in the Western Ghats of India. J. Trop. Ecol. 31, 315–323. https://doi.org/10.1017/S0266467415000188

Rizzuto, M., Carbone, C., Pawar, S., 2018. Foraging constraints reverse the scaling of activity time in carnivores. Nat Ecol Evol 2, 247–253. https://doi.org/10.1038/s41559-017-0386-1

Rowcliffe, J.M., Field, J., Turvey, S.T., Carbone, C., 2008a. Estimating animal density using camera traps without the need for individual recognition. Journal of Applied Ecology 45, 1228–1236. https://doi.org/10.1111/j.1365-2664.2008.01473.x

Rowcliffe, J.M., Field, J., Turvey, S.T., Carbone, C., 2008b. Estimating animal density using camera traps without the need for individual recognition. Journal of Applied Ecology 45, 1228–1236. https://doi.org/10.1111/j.1365-2664.2008.01473.x

Rowcliffe, J.M., Jansen, P.A., Kays, R., Kranstauber, B., Carbone, C., 2016a. Wildlife speed cameras: measuring animal travel speed and day range using camera traps. Remote Sensing in Ecology and Conservation 2, 84–94. https://doi.org/10.1002/rse2.17

Rowcliffe, J.M., Jansen, P.A., Kays, R., Kranstauber, B., Carbone, C., 2016b. Wildlife speed cameras: measuring animal travel speed and day range using camera traps. Remote Sens Ecol Conserv 2, 84–94. https://doi.org/10.1002/rse2.17

Rowcliffe, J.M., Jansen, P.A., Kays, R., Kranstauber, B., Carbone, C., 2016c. Wildlife speed cameras: measuring animal travel speed and day range using camera traps. Remote Sens Ecol Conserv 2, 84–94. https://doi.org/10.1002/rse2.17

Rowcliffe, J.M., Kays, R., Kranstauber, B., Carbone, C., Jansen, P.A., 2014a. Quantifying levels of animal activity using camera trap data. Methods in Ecology and Evolution 5, 1170–1179. https://doi.org/10.1111/2041-210X.12278

Rowcliffe, J.M., Kays, R., Kranstauber, B., Carbone, C., Jansen, P.A., 2014b. Quantifying levels of animal activity using camera trap data. Methods Ecol Evol 5, 1170–1179. https://doi.org/10.1111/2041-210X.12278

Rowcliffe, J.M., Kays, R., Kranstauber, B., Carbone, C., Jansen, P.A., 2014c. Quantifying levels of animal activity using camera trap data. Methods Ecol Evol 5, 1170–1179. https://doi.org/10.1111/2041-210X.12278

Sanderson, J.G., Trolle, M., 2005. Monitoring Elusive Mammals.

Schaus, J., Uzal, A., Gentle, L.K., Baker, P.J., Bearman-Brown, L., Bullion, S., Gazzard, A., Lockwood, H., North, A., Reader, T., Scott, D.M., Sutherland, C.S., Yarnell, R.W., 2020. Application of the Random Encounter Model in citizen science projects to monitor animal densities. Remote Sens Ecol Conserv 6, 514–528. https://doi.org/10.1002/rse2.153

Schindler, F., Steinhage, V., 2021. Identification of animals and recognition of their actions in wildlife videos using deep learning techniques. Ecological Informatics 61, 101215. https://doi.org/10.1016/j.ecoinf.2021.101215

Schmidt-Nielsen, K., 1984. Scaling, why is animal size so important? Cambridge University Press, Cambridge ; New York.

Shamon, H., Maor, R., Cove, M.V., Kays, R., Adley, J., Alexander, P.D., Allen, D.N., Allen, M.L., Appel, C.L., Barr, E., Barthelmess, E.L., Baruzzi, C., Bashaw, K., Bastille-Rousseau, G., Baugh, M.E., Belant, J., Benson, J.F., Bespoyasny, B.A., Bird, T., Bogan, D.A., Brandt, L.S.E., Bresnan, C.E., Brooke, J.M., Buderman, F.E., Buzzell, S.G., Cheeseman, A.E., Chitwood, M.C., Chrysafis, P., Collins, M.K., Collins, D.P., Compton, J.A., Conner, L.M., Cosby, O.G., Coster, S.S., Crawford, B., Crupi, A.P., Darracq, A.K., Davis, M.L., DeGregorio, B.A., Denningmann, K.L., Dougherty, K.D., Driver, A., Edelman, A.J., Ellington, E.H., Ellis-Felege, S.N., Ellison, C.N., Fantle-Lepczyk, J.E., Farris, Z.J., Favreau, J., Fernandez, P., Fisher-Reid, M.C., Fitzpatrick, M.C., Flaherty, E.A., Forrester, T.D., Fritts, S.R., Gallo, T., Gerber, B.D., Giery, S.T., Glasscock, J.L., Gonatas, A.D., Grady, A.C., Green, A.M., Gregory, T., Griffin, N., Hagen, R.H., Hansen, C.P., Hansen, L.P., Hasstedt, S.C., Hernández-Yáñez, H., Herrera, D.J., Horan, R.V., Jackson, V.L., Johnson, L., Jordan, M.J., Kahano, W., Kiser, J., Knowles, T.W., Koeck, M.M., Koroly, C., Kuhn, K.M., Kuprewicz, E.K., Lafferty, D.J.R., LaPoint, S.D., Lashley, M., Lathrop, R.G., Lee, T.E., Lepczyk, C.A., Lesmeister, D.B., Lombardi, J.V., Long, R.A., Lonsinger, R.C., MacKay, P., Maher, S.P., Mason, D.S., Millspaugh, J.J., Moll, R.J., Moon, J.B., Mortelliti, A., Mychajliw, A.M., Nagy, C.M., Neiswenter, S.A., Nelson, D.L., Nemes, C.E., Nielsen, C.K., Olson, E., O'Mara, M.T., O'Neill, B.J., Page, B.R., Parsons, E., Pease, B.S., Pendergast, M.E., Proctor, M., Quick, H., Rega-Brodsky, C.C., Rentz, M.S., Rezendes, K., Rich, D., Risch, D.R., Romero, A., Rooney, B.R., Rota, C.T., Samples, C.A., Schalk, C.M., Sekercioğlu, Ç.H., Sergeyev, M., Smith, A.B., Smith, D.S., Sperry, J.H., Stenglein, J.L., Stokes, M.K., Stutzman, J.S., Todd, K.R., Vanek, J.P., Varga, W., Wardle, Z.M., Webb, S.L., Wehr, N.H., Whipple, L.S., Whittier, C.A., Widness, J.S., Williamson, J., Wilson, A.M., Wolf, A.J., Zimova, M., Zorn, A.S., McShea, W.J., 2024. SNAPSHOT USA 2021: A third coordinated national camera trap survey of the U nited S tates. Ecology 105, e4318. https://doi.org/10.1002/ecy.4318

Sheng L., Dajun W., Zhishu X., Xinhai L., Tianming W., Limin F., Yun W., 2014. Camera-trapping in wildlife research and conservation in China: review and outlook. Biodiversity Science 22, 685. https://doi.org/10.3724/SP.J.1003.2014.14203

Silveira, L., Jácomo, A.T.A., Diniz-Filho, J.A.F., 2003. Camera trap, line transect census and track surveys: a comparative evaluation. Biological Conservation 114, 351–355. https://doi.org/10.1016/S0006-3207(03)00063-6

Smith, F.A., Lyons, S.K., Ernest, S.K.M., Jones, K.E., Kaufman, D.M., Dayan, T., Marquet, P.A., Brown, J.H., Haskell, J.P., 2003. BODY MASS OF LATE QUATERNARY MAMMALS: *Ecological Archives E084-094*. Ecology 84, 3403–3403. https://doi.org/10.1890/02-9003

Smith, J.K., Coulson, G., 2012. A comparison of vertical and horizontal camera trap orientations for detection of potoroos and bandicoots. Aust. Mammalogy 34, 196. https://doi.org/10.1071/AM11034

Sollmann, R., Mohamed, A., Samejima, H., Wilting, A., 2013a. Risky business or simple solution – Relative abundance indices from camera-trapping. Biological Conservation 159, 405–412. https://doi.org/10.1016/j.biocon.2012.12.025

Sollmann, R., Mohamed, A., Samejima, H., Wilting, A., 2013b. Risky business or simple solution – Relative abundance indices from camera-trapping. Biological Conservation 159, 405–412. https://doi.org/10.1016/j.biocon.2012.12.025

Steenweg, R., Hebblewhite, M., Kays, R., Ahumada, J., Fisher, J.T., Burton, C., Townsend, S.E., Carbone, C., Rowcliffe, J.M., Whittington, J., Brodie, J., Royle, J.A., Switalski, A., Clevenger, A.P., Heim, N., Rich, L.N., 2017. Scaling-up camera traps: monitoring the planet's biodiversity with networks of remote sensors. Frontiers in Ecol & Environ 15, 26–34. https://doi.org/10.1002/fee.1448

Sultaire, S.M., Millspaugh, J.J., Jackson, P.J., Montgomery, R.A., 2023. The influence of fine-scale topography on detection of a mammal assemblage at camera traps in a mountainous landscape. Wildlife Biology 2023, e01026. https://doi.org/10.1002/wlb3.01026

Tabak, M.A., Norouzzadeh, M.S., Wolfson, D.W., Sweeney, S.J., Vercauteren, K.C., Snow, N.P., Halseth, J.M., Di Salvo, P.A., Lewis, J.S., White, M.D., Teton, B., Beasley, J.C., Schlichting, P.E., Boughton, R.K., Wight, B., Newkirk, E.S., Ivan, J.S., Odell, E.A., Brook, R.K., Lukacs, P.M., Moeller, A.K., Mandeville, E.G., Clune, J., Miller, R.S., 2019. Machine learning to classify animal species in camera trap images: Applications in ecology. Methods Ecol Evol 10, 585–590. https://doi.org/10.1111/2041-210X.13120

Taylor, B.D., Goldingay, R.L., Lindsay, J.M., 2014. Horizontal or vertical? Camera trap orientations and recording modes for detecting potoroos, bandicoots and pademelons. Aust. Mammalogy 36, 60. https://doi.org/10.1071/AM13012

Thapa, S.K., De Jong, J.F., Subedi, N., Hof, A.R., Corradini, G., Basnet, S., Prins, H.H.T., 2021. Forage quality in grazing lawns and tall grasslands in the subtropical region of Nepal and implications for wild herbivores. Global Ecology and Conservation 30, e01747. https://doi.org/10.1016/j.gecco.2021.e01747

Tobler, M.W., Carrillo-Percastegui, S.E., Leite Pitman, R., Mares, R., Powell, G., 2008. An evaluation of camera traps for inventorying large- and medium-sized terrestrial rainforest mammals. Animal Conservation 11, 169–178. https://doi.org/10.1111/j.1469-1795.2008.00169.x

Tucker, M.A., Santini, L., Carbone, C., Mueller, T., 2021. Mammal population densities at a global scale are higher in human-modified areas. Ecography 44, 1–13. https://doi.org/10.1111/ecog.05126

Van Langevelde, F., Van De Vijver, C.A.D.M., Kumar, L., Van De Koppel, J., De Ridder, N., Van Andel, J., Skidmore, A.K., Hearne, J.W., Stroosnijder, L., Bond, W.J., Prins, H.H.T., Rietkerk, M., 2003. EFFECTS OF FIRE AND HERBIVORY ON THE STABILITY OF SAVANNA ECOSYSTEMS. Ecology 84, 337–350. https://doi.org/10.1890/0012-9658(2003)084%255B0337:EOFAHO%255D2.0.CO;2

Van Lunenburg, M., Kral, M.J.C., Van Alphen, J.J.M., 2017. Decreased ungulate density in Bardiya National Park, West Nepal, and the implications for increasing tiger populations. A comment on Thapa et al. (2015). Ethology Ecology & Evolution 29, 304–309. https://doi.org/10.1080/03949370.2016.1145147

Vazquez, C., Rowcliffe, J.M., Spoelstra, K., Jansen, P.A., 2019. Comparing diel activity patterns of wildlife across latitudes and seasons: Time transformations using day length. Methods Ecol Evol 10, 2057–2066. https://doi.org/10.1111/2041-210X.13290

Wearn, O.R., Bell, T.E.M., Bolitho, A., Durrant, J., Haysom, J.K., Nijhawan, S., Thorley, J., Rowcliffe, J.M., 2022. Estimating animal density for a community of species using information obtained only from camera-traps. Methods Ecol Evol 13, 2248–2261. https://doi.org/10.1111/2041-210X.13930

Wearn, O.R., Glover-Kapfer, P., 2019. Snap happy: camera traps are an effective sampling tool when compared with alternative methods. R. Soc. open sci. 6, 181748. https://doi.org/10.1098/rsos.181748

Wearn, O.R., Glover-Kapfer, P., n.d. CAMERA-TRAPPING PAGE 2.

Weckerly, F.W., 2013. Conspecific body weight, food intake, and rumination time affect food processing and forage behavior. Journal of Mammalogy 94, 120–126. https://doi.org/10.1644/12-MAMM-A-066.1

Welbourne, D.J., Claridge, A.W., Paull, D.J., Lambert, A., 2016. How do passive infrared triggered camera traps operate and why does it matter? Breaking down common misconceptions. Remote Sens Ecol Conserv 2, 77–83. https://doi.org/10.1002/rse2.20

Whytock, R.C., Świeżewski, J., Zwerts, J.A., Bara-Słupski, T., Koumba Pambo, A.F., Rogala, M., Bahaa-el-din, L., Boekee, K., Brittain, S., Cardoso, A.W., Henschel, P., Lehmann, D., Momboua, B., Kiebou Opepa, C., Orbell, C., Pitman, R.T., Robinson, H.S., Abernethy, K.A., 2021. Robust ecological analysis of camera trap data labelled by a machine learning model. Methods Ecol Evol 12, 1080–1092. https://doi.org/10.1111/2041-210X.13576

Yamaura, Y., Royle, J.A., Shimada, N., Asanuma, S., Sato, T., Taki, H., Makino, S., 2012. Biodiversity of man-made open habitats in an underused country: a class of multispecies abundance models for count data. Biodivers Conserv 21, 1365–1380. https://doi.org/10.1007/s10531-012-0244-z

ACKNOWLEDGEMENT

我在南京的家里有很多佛像，常年受我妈妈的供奉。大大小小，精美华丽，栩栩如生。如果你来我家做客，进门便是令人心安的陈年香火气息。其中有一尊佛像，如果仅从工艺角度去评价，她算不上精美华丽，和佛台上的其他佛像比起来甚至显得有些粗糙。那是一尊30厘米左右高的观音菩萨像。

这尊佛像是家里最早的一尊。是当年小小的我从庙会上套圈套来的。2000年左右版本的我，只有膝盖高度。膝盖高度，对于使用红外相机的人来说是个熟悉的词，那是我们安装红外相机的高度。而就是这样高度的我，在呈倒三角排列的套圈游戏中，在周围大人的“哇”声中，套中了最远处的三角尖尖，也就是这尊佛像。

前些日子我确定了未来几年的工作，于是向妈妈讨要这个佛像。

“哪个？”

“我套圈套到的那个。”

“哦，那是外婆。”

简单的对话勾勒出了碎片般的记忆和过去的影像。那时候，边缘起皮的桌子上，只有这一尊佛像。常年的香火将上方的柜子熏得发黑。佛像面前跪着的是外婆。一个清瘦、朴素的女人，除了在佛像前坐着，就是在给家人打毛衣和做饭。

“乖乖肉啊，你今天要吃什么？”这是从外婆那里听到最多的话。在她那里，好好吃饭是天大的事情。冬天厨房里没有暖气，为了让我能吃到有弹性的黄鳝，她在冰冷的水里一遍遍地揉搓，直到我放学回来开火做饭；为了让我不用剥就能吃到螃蟹肉，她用筷子和牙签将螃蟹肉一点点挑出，做成肉丸，放进青菜汤里；春天的时候，她会用针线把蚕豆穿成串子，挂在我的脖子上，像西游记里的沙和尚，这样我可以一边在外面和其他小朋友玩，一边吃到新鲜的应季蚕豆。“如果外婆有一天死了怎么办？”这是二十年前小小的我心里最大的恐惧。我越想越害怕，干脆低头把嘴塞满，这样心里就不怕了。

可是那一天还是到了。我迷迷糊糊地起床喊外婆：“我早上要吃溏心蛋。”但她安静地躺在那里，再也没有回应我。

外婆没读过什么书。中国的那一辈人，最大的任务就是生存。所以吃饱饭、吃好饭、好好吃饭，是外婆眼里最大的事。妈妈也常抱怨，在大城市打拼的委屈，很难在外婆那里得到开解，在家里等着她的，只有一桌妈妈做的饭。可那饭的味道，我们俩都已经二十二年多没有再吃过了。外婆走后，那尊佛像对妈妈而言，便成了她的妈妈。面对妈妈诉说的委屈，“外婆”依旧沉默。

外婆看不到将来，只在乎当下。在七十到八十年代，她在无数个夜里安静地踩着缝纫机，做着一些裁缝活。多接一些，两个女儿的日子就能过得好一些，明天就有更充足的预算去买菜。她就这样把孩子养大，送去省会，又揽下照顾他们孩子的任务。

妈妈和外婆是截然不同的。妈妈热情、努力、乐观，同时一点也不会做饭。我说不出妈妈的拿手菜，妈妈也说不上来我喜欢吃什么。

“肯德基，心情不好压力大就订点肯德基吃吃，别委屈自己。”

在妈妈眼里，肯德基是我三十年来最喜欢吃的东西，尽管其实我对肯德基的执念已经过去多年了。

但是这样一个不会做饭的妈妈，是我的妈妈，我的心理医生，永远听我说废话的人，永远被我糟糕笑话逗笑的人，我的精神支柱，我的底气，是我坠落时会牢牢接住我的人。我忘不了当年妈妈在谷底时，眼神坚毅地对我说：“想买什么就买什么，我有钱，我一定能让我们过上好日子。”那时的妈妈，年轻，漂亮，眼里有光。并且她做到了。尽管妈妈如今不再年轻，但她依旧漂亮，眼里依旧有光。

妈妈很早就知道，她的未来不属于小镇。她要去更大的地方，她要让她的孩子在更广阔的天地里长大。于是今天的我，在想家的时候，才有南京这座城市让我牵挂。

当大部分人读到这里的时候，我或许已经，或即将取得我的博士学位。我称不上优秀，博士文凭也只是学术圈的敲门砖。但这一步，我走了很久，从1950年开始，从外婆的脚开始。是这两代女性拼尽全力的托举，让我拥有了站在更广阔天地的机会。这让我联想到了去年看的一部电视剧《苦尽柑来》里的台词。“外婆在海里游，妈妈在地上跑，我才能在天上飞。”过去的半个世纪里，她们走的每一步，都算数。

我不善于直接表达情感与言辞。今天能取得一些阶段性的成果，离不开这些年遇到的老师、朋友和家人的帮助。这里我就不多说了，我更倾向于用自己的方式表达。但是有些人，还有狗和猫，却再也听不到了。按照中国人的传统，我将用一种不太环境友好的方式传递我的消息：我会将打印出的论文中的一本烧给他们。因为他们的存在与爱，让我作为一名科研人员，却也期盼有一天能与他们再相见。

我期待与他们相见，也期待明天。我期待我的明天，期待我下一代的明天，也期待行业的明天、动物保护的明天。为此，我会努力把这条路走得更宽，更远。



I grew up in a home in Nanjing filled with Buddhist statues, all carefully tended by my mom over the years. They vary in size, intricate and ornate, lifelike in their expression. If you visit my home, you will notice it immediately upon entering: a sense of calm, carried by the lingering scent of incense accumulated over time.

Among them, there is one statue that, from a purely technical perspective, cannot be considered particularly refined. Compared to the others on the altar, it even appears somewhat rough. It is a statue of Guanyin, about 30 cm tall.

This was the very first statue in our home. I won it as a child at a local festival market, by throwing rings (a popular game on such market). Around the year 2000, I was only as tall as an adult's knees. Knee height, for those who work with camera traps is a familiar reference. It is the height at which we often deploy camera traps. At that similar height, in a ring-toss game arranged in an inverted triangle, and accompanied by "wow" of adults around me, I managed to land a ring on the farthest target—this very statue.

Not long ago, after kind of confirming my next contract for the coming years, I asked mom if I could take this statue with me.

"Which one?"

"The one I won with the ring toss."

"Oh, you mean your grandma."

This simple conversation brought my memories to the past. Back then, on a worn wooden table with peeling edges, there was only this one statue. Years of incense had darkened the cabinet above it. And in front of the statue knelt my grandmother, a slender, modest woman who spent her days either sitting before the statue, knitting for the family, or cooking.

"My little meat ball (young me), what would you like to eat today?" This is the sentence I heard most often from her. To her, eating well was the most important thing in the world. In winter, the kitchen had no heating. To make sure I could eat eel with the right texture, she would wash and massage it again and again in icy water, until I came home from school so she could start cooking. To spare me the trouble of picking crab meat, she would patiently extract it piece by piece with chopsticks and toothpicks, shape it into small meatballs, and cook it in vegetable soup. In spring, she would thread broad beans into a string and hang

it around my neck, like the character Sha Wujing from *Journey to the West*, so that I could play outside with other kids while snacking on fresh seasonal beans.

"What if Grandma dies one day?" This was the greatest fear in my childhood. The more I thought about it, the more afraid I became. So I would lower my head and fill my mouth with food, as if there is no space for fear if my mouth and stomach are full.

But that day still came. One morning, half asleep, I called out to her, "I want a soft-boiled egg for breakfast." She lay there quietly, and never responded again.

My grandma had little formal education. For her generation in China, survival was the primary task. To have enough to eat and eat well were the most important things in her world. Mom told me, back in the days, the complains about the difficulties of surviving in a big city could not be eased by talking to grandma. Grandma wouldn't talk, she just went to her kitchen. What awaited mom at home was simply a table of food. Simple, but nice and unreplacable. However, the taste of that food is something we both have not had for over twenty-two years. After grandma passed away, that statue became, for my mom, her mom. And in the face of my mom's complaints and frustrations, "grandma" remained silent.

Grandma did not think about the distant future. She cared only about the present. In the 1970s and 1980s, she spent countless nights quietly working at her sewing machine. Taking on a little more work meant her two daughters could live a little better, and that there would be a slightly larger budget for food the next day. In this way, she raised her children, sent them to the provincial capital, and later took on the responsibility of caring for their children.

Mom is an entirely different person from grandma. She is warm, hardworking, and optimistic, and cannot cook at all. I cannot name a dish she is known for, and she cannot clearly say what I like to eat.

"Just order KFC when you feel stressed, don't make things hard for yourself."

In her mind, KFC has been my favorite food for the past thirty years, even though that attachment for me has been gruadually faded for years.

However, this woman who cannot cook is my mom, my therapist, the one who listens to all my rambling, who laughs at my terrible jokes, my emotional anchor, the one who will always catch me when I fall. I will never forget the time when she

was at her lowest, looking at me with determination and saying, "Buy whatever you want. I have money. I'm gonna for sure bring us a good life." She was young then, beautiful, with light in her eyes. And she made it. Though no longer that young now, mom is still beautiful, with the light in her eyes.

Mom knew it early in mind that her future did not belong to a small town. She wanted to go further, to a bigger world, and to raise her child in a broader landscape, which brings Nanjing a city I can miss as hometown when I feel homesick today.

By the time most people read this, I will perhaps have already obtained, or be about to obtain, my PhD. I would not call myself outstanding, and a PhD is merely an entry ticket into academia. But this step has taken a long time. It began in 1950, with my grandma. It is through the efforts of these two generations of women, who did everything they could to lift me up, that I have the chance to stand in a wider world. It reminds me of a line from a TV series that I watched last year (<When life gives you tangerines>): "Grandma swam in the sea, mom ran on the land, so I can fly in the sky." Every step they took in the past half centry counts.

I am not good at expressing emotions and appreciations directly. Whatever I have achieved so far would not have been possible without the support of a lot of people: supervisors, colleagues, friends, and family I have met along the way. I prefer not to elaborate here but express gratitude in person in my own way. But there are some people, and also some dogs and cats, who can no longer hear these words. Following Chinese tradition, I will deliver the message in a not very environmental friendly way. I will burn a printed copy of this thesis for them. It is because of their presence and their love that, even as a researcher, I still hope that one day I might see them again.

I look forward to meeting them again. I also look forward to tomorrow, my own tomorrow, the tomorrow of my next generation, and the tomorrow of this industry, of wildlife conservation. For that, I will do my best to walk this path as far and wide as I can.

BIOGRAPHY



Shuiqing He was born in Nanjing, China, in 1996. She obtained her Bachelor's degree in Aquaculture from the Department of Animal Science at Yangzhou University. Along the way, she found that she was more committed to nature conservation than to animal production for human use.

In 2019, she started her Master's degree in Ecology and Evolution at the University of Groningen, the Netherlands. During the second project of her Master's in 2021, she moved to Wageningen, where she later continued her studies as a PhD candidate in spring 2022. Her research focused on wildlife monitoring and improving methods for estimating wildlife population density using camera traps, with a particular focus on the Random Encounter Model (REM) and its extensions. Her work combines meta-analysis and field data from camera-trap deployments in Bardiya National Park, Nepal.

After completing her PhD, Shuiqing will continue working in biodiversity and wildlife conservation.

PUBLICATION LIST

He, S., Rowcliffe, J.M., Lin, H., Carbone, C., Liefting, Y., Thapa, S.K., Shrestha, B.P. and Jansen, P.A. (2025), A random encounter model for wildlife density estimation with vertically oriented camera traps. Remote Sens Ecol Conserv, 11: 327-338. https://doi.org/10.1002/rse2.427

Zhao, Q., Van den Brink, P. J., Xu, C., Wang, S., Clark, A. T., Karakoç, C., Sugihara, G., Widdicombe, C. E., Atkinson, A., Matsuzaki, S.-I. S., Shinohara, R., **He, S.**, Wang, Y. X. G., & De Laender, F. (2023). Relationships of temperature and biodiversity with stability of natural aquatic food webs. Nature Communications, 14, 3507. https://doi.org/10.1038/s41467-023-38977-6

He S, Jansen PA, Rowcliffe JM, Jhala Y, Qureshi Q, Carbone C. Does controlling for body size and diet improve the performance of camera-trap relative abundance indices as proxies for density in macroecological studies? (Submitted)

He S, Jansen PA, Carbone C, Subedi N, Prins HHT, Liefting Y, Thapa SK, Shrestha BP, Rowcliffe JM. Wildlife density estimation using the Random Encounter Model: a comparison between horizontal and vertical camera-trap placements (Submitted)

PE&RC TRAINING AND EDUCATION STATEMENT

With the training and education activities listed below the PhD candidate has complied with the requirements set by the Graduate School for Production Ecology and Resource Conservation (PE&RC) which comprises of a minimum total of 30 ECTS (= 22 weeks of activities)

Review/project proposal

- Human Impacts on Mammal Communities: A Global Macro-ecological Study Using Camera-trap Data | 4.5 ECTS

In-depth / Topical / On-site Postgraduate Courses

- The science of conservation | PE&RC | 2025 | 3.5 ECTS

Methodological / Statistical Postgraduate Courses

- Bayesian statistics | PE&RC | 2025 | 0.6 ECTS
- Multivariate analysis | PE&RC | 2024 | 1.5 ECTS
- GIS in practice | PE&RC | 2022 | 1.5 ECTS

Laboratory training and working visits

- Density estimation for macroecological studies | Zoological Society of London (ZSL) | 2025 | 0.3 ECTS
- Comparisons between horizontal and vertical camera-trap placements | Bardia National Park Office and National Turst for Nature Conservation | 2024 | 0.3 ECTS

Invited review of journal manuscripts

- Global Ecology and Biogeography | Mammal community long-term monitoring project using camera traps | 2025 | 1 ECTS

Competence, skills and career-oriented activities

- Critical thinking and argumentation | WGS | 2025 | 0.3 ECTS
- Reviewing a scientific manuscript | WGS | 2025 | 0.1 ECTS
- Expectation day | WEC | 2023 | 0.3 ECTS
- Effective and efficient communication in academia and beyond | PE&RC | 2024 | 0.9 ECTS
- Apply for making impact: Increasing the relevance of research through science-society interaction | WGS | 2026 | 0.6 ECTS

Scientific Integrity/Ethics in science activities

- Ethics in plant and environmental sciences | WGS | 2025 | 0.3 ECTS

PE&RC Retreat, PE&RC Day, and other PE&RC events

- First year's retreat | 2022 | 0.9 ECTS
- Last Years Meeting | 0.1 ECTS

National/local scientific meetings, seminars, and discussion groups

- Netherlands Annual Ecology Meeting | 2024 | 0.6 ECTS
- Nature First Conference | 2025 | 0.6 ECTS
- Journal Club Behaviour & Ecology | 2023 | 0.5 ECTS
- Wageningen Evolution & Ecology Seminars | 2022-2024 | 0.9 ECTS
- Networking event for scientists working in Nepal | 2025 | 0.1 ECTS
- Netherlands Annual Ecology Meeting | 2026 | 0.6 ECTS
- The 1st International Online Conference on Environments | 2026 | 0.9 ECTS

International symposia, workshops and conferences

- European Conference of Tropical Ecology | Amsterdam | 2024 | 2.2 ECTS
- BES Annual Meeting | Edinburgh | 2025 | 2.2 ECTS

Lecturing/Supervision of practicals/tutorials

- Data science for ecology | 2024-2025 | 30 days | 6 ECTS

BSc/MSc thesis supervision

- Research topic 1: Mammal density estimation using vertical camera trapping and the Random Encounter Model: A test in Bardia National Park, Nepal | 3 ECTS

Colophon

The research described in this thesis was financially supported by China Scholarship Council (CSC), Wildlife Ecology and Conservation Group (WEC), Wageningen University & Research, and Himalayan Tiger Foundation.

Financial support from Wageningen University (Laboratory of Microbiology) for printing this thesis is gratefully acknowledged.

Cover design by Di An.

Printed by ProeschriftMaken, The Netherlands

